

Université de Lille
Laboratoire de Mécanique, Multi-physique, Multi-échelle
Ecole Doctorale Sciences Pour l'Ingénieur

THÈSE

Pour l'obtention du grade de
DOCTEUR DE L'UNIVERSITE DE LILLE
Mention Mécanique

A non-incremental numerical method for quasi-static and dynamic elastoplastic problems by the symplectic Brezis-Ekeland-Nayroles variational principle

Une méthode numérique non-incrémentale pour les problèmes
élastoplastiques quasi-statiques et dynamiques par le principe
variationnel symplectique de Brezis-Ekeland-Nayroles

Présentée par

Xiaodan CAO

Soutenue le 25 Septembre 2020

JURY

Amine Ammar	Professeur, Arts et Métiers ParisTech	Rapporteur
Habibou Maitournam	Professeur, ENSTA Paristech	Rapporteur, Président
Céline Bouby	Maître de Conférences, Polytech Nancy	Examinatrice
Bernd Markert	Professeur, RWTH-Aachen University	Examineur

ENCADREMENT

Géry de Saxcé	Professeur, Université de Lille	Directeur de thèse
Abdelbacet Oueslati	Maître de Conférences, Université de Lille	Co-directeur de thèse

Acknowledgment

This work was performed thanks to the international cooperation project *Dissipative Dynamical Systems by Geometrical and Variational Methods and Application to Viscoplastic Structures Subjected to Shock Waves* (DDGV) supported by the *Agence Nationale de la Recherche* (ANR) and the *Deutsche Forschungsgemeinschaft* (DFG).

I would like to express my gratitude to my supervisors de Saxcé and Oueslati for their guidance over the three years. They support me with advice, patience, trust, and give me this opportunity to learn profoundly numerical simulation in mechanical engineering, to participate in several international conferences, etc. Without their enormous contributions to the papers and this thesis, this research could never be published.

Additionally, I acknowledge especially Ammar, Maitournam, Bouby, and Markert for kindly examining my work.

At last, I appreciate my new friends in Lille and colleagues in the LaMcube laboratory for accompanying this particular moment. I am grateful to my old friends and family in my homeland, as well as in France, for their support as always.

Abstract

Keywords: Numerical simulations · Non-incremental method · Brezis-Ekeland-Nayroles principle · Elastic plastic materials · Quasi-static and dynamic evolutions · Finite strains · Variational principle · Constrained optimization

This thesis is devoted to the numerical application of a non-incremental method based on the Symplectic Brezis-Ekeland-Nayroles (SBEN) principle for the quasi-static and dynamic elastoplastic problems. The principle is based on the dissipation potential and its Fenchel transform as an alternative method to the standard step-by-step technique. It allows a consistent view of the whole evolution by computing the nonlinear response along the whole time history as a solution to a suitable minimization problem.

We show that the SBEN variational formulation yields a time-space minimization problem under constraints. The cost function consists in a 2-field functional, depending on the stress and displacement fields, which leads naturally to a mixed finite element discretization.

Numerical applications are performed by two mechanical models. For the thin- or thick-walled tube model under internal pressure, the SBEN principle's feasibility is confirmed in static and dynamic cases. For another plate model, a circular axisymmetric thin or thick plate subjected to a surface pressure is examined under the Love-Kirchhoff and Mindlin plate theories in statics. Numerical results are compared to the analytical solution or the ones derived by the classical step-by-step finite element procedure. Good accuracy of the SBEN principle is observed. At last, the SBEN principle is theoretically extended in finite strains.

Résumé

Mots-clés: Simulation numérique · Méthode non-incrémentielle · Principe de Brezis-Ekeland-Nayroles · Matériaux élastique plastique · Statique · Dynamique · Grande déformation · Principe variationnel · Optimisation sous contraintes

Cette thèse est consacrée à l'application numérique d'une méthode non incrémentale basée sur le principe Symplectic Brezis-Ekeland-Nayroles (SBEN) pour les problèmes élastoplastiques quasi statiques et dynamiques. Le principe est basé sur le potentiel de dissipation et sa transformation de Fenchel comme méthode alternative à la technique standard pas-à-pas. Il permet une vision cohérente de toute l'évolution en calculant la réponse non linéaire tout au long de l'historique temporel comme solution à un problème de minimisation approprié.

Nous montrons que la formulation variationnelle SBEN génère un problème de minimisation espace-temps sous contraintes. La fonction de coût consiste en une fonction à 2 champs, en fonction des champs de contraintes et de déplacements, ce qui conduit naturellement à une discrétisation par éléments finis mixtes.

Les applications numériques sont réalisées par deux modèles mécaniques. Pour le modèle de tube à paroi mince ou épaisse sous pression interne, la faisabilité du principe SBEN est confirmée dans des cas statiques et dynamiques. Pour un autre modèle de plaque, une plaque asymétrique circulaire mince ou épaisse soumise à une pression de surface est examinée sous les théories de plaques Love-Kirchhoff et Mindlin en statique. Les résultats numériques sont comparés à la solution analytique ou à ceux dérivés par la procédure classique des éléments finis pas-à-pas. On observe une bonne précision du principe SBEN. Enfin, le principe SBEN est théoriquement étendu en grande déformation.

Contents

Acknowledgment	1
Abstract	3
Résumé	5
General introduction	11
1 Modeling of dissipative systems and elastoplasticity : a review	15
1.1 Non-incremental variational formulation for dissipative systems	16
1.1.1 Mielke variational formulation	17
1.1.2 Weighted-Inertia-Dissipation-Energy (WIDE) formulation for dynamic elastoplastic problems	19
1.1.3 The Brezis-Ekeland-Nayroles (BEN) principle	20
1.1.4 The symplectic Brezis-Ekeland-Nayroles (SBEN) principle	21
1.2 Basic notions of Elastoplasticity	24
1.2.1 Basic equations	24
1.2.2 Energetic aspects	27
1.3 Numerical treatment of elastoplastic problems	28
1.3.1 Radial return algorithm	29
1.3.2 LATIN method in elastoplasticity	32
2 A direct method for the quasi-static viscoelastoplastic problems by the Brezis-Ekeland-Nayroles principle	37
2.1 Formulation of the elastoplastic problems within the framework of the the Brezis-Ekeland-Nayroles principle	38

2.2	Application to the pressurized thick-walled tube	40
2.2.1	Basic equations	41
2.2.2	The mixed finite element method for thick tube problem	42
2.2.3	Discretization of the BEN functional	45
2.3	Results and discussion	48
2.3.1	Elastic response	49
2.3.2	Elastoplastic response with von Mises criterion	50
2.3.3	Elastoplastic response with Tresca criterion	53
2.3.4	Computation cost	55
2.3.5	Viscoplastic response with Norton-Odqvist law	58
2.4	Conclusion	60
3	Numerical simulation of quasi-static elastoplastic circular plates by the Brezis-Ekeland-Nayroles principle	63
3.1	The problem statement	64
3.1.1	Love-Kirchhoff plate model	65
3.1.2	The Reissner-Mindlin plate model	68
3.2	Numerical implementation	70
3.2.1	Numerical implementation for the circular Love-Kirchhoff plate	70
3.2.2	Numerical implementation for the circular Reissner-Mindlin plates	76
3.3	Results and discussion	80
3.3.1	The Love-Kirchhoff plates	81
3.3.2	The Reissner-Mindlin plates	83
3.4	Conclusion	86
4	A non-incremental numerical method for dynamic elastoplastic problems by the symplectic Brezis-Ekeland-Nayroles principle	89
4.1	Application to dynamic plasticity	90
4.2	Computational procedure for the pressurized tube	92
4.2.1	Problem statement	92
4.2.2	Discretization of the problem	93
4.2.3	Discretization of the SBEN principle	98
4.3	Results and discussion	102
4.3.1	The thin tube	104
4.3.2	The thick-walled tube	108

4.3.3	Comparison between the methods A and B	112
4.4	Conclusion and outlook	114
5	A symplectic Brezis-Ekeland-Nayroles principle for dynamic plasticity in finite strains	115
5.1	Notations and definitions	116
5.2	Lagrangian formalism	117
5.3	Hamiltonian formalism	120
5.4	Symplectic BEN principle for dynamic plasticity	122
5.5	Conclusion	127
	General conclusion	129
	Bibliography	131

General introduction

Numerical simulations become essential in engineering design involving mechanical sciences, civil engineering, transportation, and energy. In computational sciences, the Finite Element Method (FEM) is the most popular procedure used by researchers and engineers to obtain approximate solutions of boundary values problems. During the last few decades, the FEM has accomplished considerable progress and continues to arouse a renewed interest in order to design more efficient and robust algorithms.

The natural and common solution strategy for nonlinear solids submitted to external loads is the path-following incremental analysis, which computes in a step-by-step manner the mechanical fields (stress, strains, displacement, internal variables rates, etc...) along the loading path (Zienkiewicz et al., 1969; Zienkiewicz, 1971; Oden, 2006; Simo and Hughes, 2000; Belytschko and Velebit, 1972; Cristfield, 1998; Ibrahimbegovic, 2009). Roughly speaking, in the nonlinear FEM, the time interval of interest is divided in a sequence of small sub-intervals $[0, T] = \bigcup_{n=1}^N [t_{n-1}, t_n]$ and one supposes that all the mechanical fields are known up to the time t_{n-1} . The purpose is then to compute the values of these fields at the time t_n . The obtained problem over the time sub-interval $[t_{n-1}, t_n]$ is nonlinear and is solved by the Newton-Raphson-like algorithms.

It is worth noting that the choice of the time-integration schemes is crucial for the accuracy and convergence of the numerical incremental procedures. Moreover, for many nonlinear problems, some simulations cannot be performed entirely by using cumbersome time stepping. The convergence frequently fails before the end of the computation and is difficult to restart. The only solution to overcome this pitfall often lies in reducing the step size but increasing computational time. Another difficulty arises because, in an iterative method, truncation error occurs at each iteration. Therefore, the computation error of the usual step-by-step approach accumulates and grows as the number of steps increases. This error cannot be avoided, and it may strongly affect the whole accuracy of complex simulations.

To overcome the pitfalls in traditional methods, direct methods or non-incremental approaches, enabling a consistent view on the entire evolution, have been proposed in the literature. For quasi-static evolutions, we can mention the method of Large Time INcrement (LATIN) proposed by Ladevèze et al. (Ladevèze, 1985b, 1989, 1991, 2012). This iterative procedure is based on the so-called "radial time-space approximations" to compute the global solution as a finite sum of products of a time function by a space function. Basing upon the LATIN method, Comte et al. (Comte et al., 2006) derived a direct cyclic method for computing the asymptotic behavior of elastoplastic solids undergoing cyclic repetitive loadings. Peigney et al. (Peigney and Stolz, 2001, 2003) proposed an optimal control approach for characterizing the stabilized state of inelastic structures under repetitive external loads. Mielke et al. (Mielke, 2005) proposed a variational formulation characterizing the entire trajectories for quasi-static rate-dependent process resulting in a minimization problem of weighted dissipation-energy functional with rapid decaying weights. The Mielke's approach is interesting since it can be reformulated in a dynamical context as in Buliga (Buliga, 2008) to generalize the Hamiltonian inclusion formalism. Moreover, Davoli et al. (Davoli and Stefanelli, 2019) extended the Mielke formulation in a purely mathematical manner to perfect dynamic plasticity. They developed a variational approach that consists in minimizing a Weighted-Inertia-Dissipation-Energy (WIDE) functional. In the same class on non-incremental methods, Brezis and Ekeland (Brezis and Ekeland, 1976b,a) proposed a variational minimization principle for a class of parabolic evolution equations. Independently, Nayroles (1976) (Nayroles et al., 1976) developed a similar principle for nonlinear mechanics, which gives the existence theorem of solutions for the Cauchy problem associated with the constitutive law of Maxwell model.

Recently, Buliga and de Saxcé (Buliga and de Saxcé, 2017) proposed a symplectic Brezis-Ekeland-Nayroles principle for dynamic irreversible dissipative systems that claims that the natural evolution curve in the phase space minimizes a functional dependent on the dissipation potential, the Hamiltonian and a suitable symplectic form.

The objective of this thesis is to investigate the feasibility of the BEN principle to simulate the quasi-static and dynamic elastoplastic evolution deformable solids with good accuracy. In the present work, the principle has been efficiently used to address the elastoplastic and viscoplastic responses of (i) a thick-walled tube under internal pressure in statics, (ii) a thin- or thick plate under surface pressure in statics (iii) a thin- or thick-walled tube under internal pressure in dynamics in small strains basing upon the Symplectic BEN (SBEN) principle. Moreover, the extension of the principle in finite strains is another ambition.

This thesis is composed of 5 chapters, as follows:

Chapter 1 This chapter is a review of the non-incremental formulations for dissipative systems. Besides the BEN and SBEN principles, which are the main subjects in the thesis, two alternative Mielke and WIDE formulations are presented. In the frame of dissipative systems, the elastoplasticity is detailed. We complete this review with the well-known incremental computation technique, radial return algorithm, and the alternative iterative one, LATIN method.

Chapter 2 This chapter is concerned with the energy-dissipation BEN principle for the numerical study of quasi-static elastoplastic and viscoplastic problems in small strains. The BEN principle is applied to address the elastic perfectly plastic and viscoplastic thick hollow cylinder subjected to internal pressure. We present the detailing of the discretization and the numerical implementation of the minimization problem by using the mixed finite element method, which is more efficient in enforcing the yield condition. Computational accuracy and efficiency of the BEN principle are assessed by comparing the numerical results with the analytical ones and the simulations derived by the classical step-by-step finite element procedure.

Chapter 3 In this chapter, the BEN principle is developed for the numerical simulation of elastoplastic plates under the assumptions of small strains and quasi-static evolution. Love-Kirchhoff and Mindlin plate models under flexural pressure are considered. The elastic and elastic perfectly plastic clamped circular thin or thick plate is numerically solved by the BEN principle within the mixed finite element method. Numerical results derived from the BEN principle are compared to the approximations obtained by an incremental approach.

Chapter 4 This chapter is devoted to the numerical simulation of dynamic elastoplastic problems in small strain by using the non-incremental SBEN principle. The solution algorithm details are illustrated through the numerical study of the elastoplastic response of the thin and thick pressurized tubes, including inertia effects. Moreover, the balance of momentum equation is handled by two approaches. It can be satisfied at Gauss points or in an exact way. The accuracy and efficiency of the SBEN principle are assessed by comparing the SBEN numerical results with the analytical solutions (for the thin tube) and the predictions derived by the classical incremental finite element procedure.

Chapter 5 In this chapter, we generalize the SBEN formalism to dissipative media in finite strains. This aim is reached in three steps. Firstly, we develop a Lagrangian formalism for the reversible media based on the calculus of variation by jet theory. Next, we propose a corresponding Hamiltonian formalism for such media. Finally, we deduce from it a symplectic minimum principle for dissipative media, and we show how to get a minimum principle for plasticity in finite strains.

Modeling of dissipative systems and elastoplasticity : a review

1.1	Non-incremental variational formulation for dissipative systems	16
1.1.1	Mielke variational formulation	17
1.1.2	Weighted-Inertia-Dissipation-Energy (WIDE) formulation for dynamic elastoplastic problems	19
1.1.3	The Brezis-Ekeland-Nayroles (BEN) principle	20
1.1.4	The symplectic Brezis-Ekeland-Nayroles (SBEN) principle	21
1.2	Basic notions of Elastoplasticity	24
1.2.1	Basic equations	24
1.2.2	Energetic aspects	27
1.3	Numerical treatment of elastoplastic problems	28
1.3.1	Radial return algorithm	29
1.3.2	LATIN method in elastoplasticity	32

This chapter reviews some variational formulations for quasi-static and dynamic dissipative systems. First, we present the Mielke formulation, the Brezis-Ekeland-Nayroles (BEN) principle for quasi-static evolutions, Davoli et al., and the symplectic Brezis-Ekeland-Nayroles (SBEN) for a dynamic process. Then, attention is focused on elastoplasticity. We set out the fundamental and basic concepts of this theory, and we address some numerical algorithms for approximation of elastoplastic solutions.

1.1 Non-incremental variational formulation for dissipative systems

Non-smooth dissipation involving frictional contact, plasticity, collision, fracture and so on are encountered in many engineering applications and natural environments.

In the last decades, much research has been devoted to simulating dynamically dissipative models within the framework of non-smooth analysis and convexity/duality models. Many variational formulations and approaches for dissipative material models can be found in the literature. The natural and common solution strategy for dissipative systems is the path-following incremental analysis leading to a sequence of variational problems, which computes in a step-by-step manner the trajectory. These incremental formulations are widely used and studied in the literature (Simo and Hughes, 2000; Hibbett et al., 1998; Cast3M, 2019). Moreover, some variational formulations allowing one to work simultaneously on all time steps contrary to the step-by-step procedure have been proposed. For instance, Mielke and co-workers (Mielke, 2005; Mielke and Stefanelli, 2008) have developed a consistent minimization principle that characterizes the global trajectory of the evolutionary system. Davoli et al. (Davoli and Stefanelli, 2019) have extended the Mielke formulation to formulate the dynamic elastoplastic problems as a convex minimization problem. Aubin et al. (Aubin et al., 1977; Aubin, 2003) and Rockafellar (Rockafellar, 1970a) considered various extensions of Hamiltonian and Lagrangian mechanics. Ghoussoub and Moameni (Ghoussoub and Moameni, 2007) proposed self-dual variational principles to construct solutions for Hamiltonians and other dynamical systems, which satisfy a variety of linear and nonlinear boundary conditions. These principles lead to new variational proofs of the existence of parabolic flows with prescribed initial conditions, as well as periodic, anti-periodic, and skew-periodic orbits of Hamiltonian systems. Maso et al. (Dal Maso and Scala, 2014) have developed mathematical tools to study nonlinear evolution problems, namely plasticity with hardening and softening quasi-static crack growth, and dynamic fracture mechanics. A consistency theorem of a discrete-to-continuum limit in the infinite dimensional case study of a cohesive fracture model

is also presented. Another powerful alternative to bypass the nonlinear step-by-step approaches in the sense that it works on the whole evolution of the system is the Brezis-Ekeland-Nayroles variational principle (in short, the BEN principle) (Brezis and Ekeland, 1976b,a). The BEN principle is based on the dissipation potential and its Fenchel transform over time integration. Buliga and de Saxcé have generalized the BEN principle to the dynamics of dissipative systems by linking two worlds together, the one of smooth functions in symplectic geometry systems and the one of non-smooth functions for dissipative systems (Buliga and de Saxcé, 2017).

In this section, we review some non-incremental variational principles for characterizing the entire trajectories of the evolutionary problem.

1.1.1 Mielke variational formulation

In the context of rate-independent dissipative systems, Mielke et al. (Mielke, 2005) proposed a variational formulation characterizing the entire trajectories by minimizing a suitable weak form of the equations. He considered an evolutionary problem modeling the quasi-static viscoelasticity in small strains, finite-deformation viscoplasticity, heat conduction, viscous solid immersed in a Stokes' flow, etc. The strong form of equations is expressed thanks to differential inclusions as follows:

In a Banach space X , find the trajectory $t \mapsto \mathbf{u}(t)$, with the initial condition $\mathbf{u}(0) = \mathbf{u}_0$, such that

$$0 \in \partial\varphi(\dot{\mathbf{u}}(t)) + D\psi(t, \mathbf{u}(t)) \text{ a.e. } t \in [0, T] \quad (1.1)$$

where the function φ is a convex dissipation potential, ψ is an energy function, $\partial\varphi$ is the sub-differential of φ (Rockafellar, 1970b; Krantz, 2015), $D\psi$ denotes for the Fréchet derivative of ψ .

It is worth noting that (1.1) represents the balance between dissipative forces and conservative ones.

The Mielke weak formulation associated to (1.1) is derived in three steps. First, the evolutionary problem is discretized giving a sequence standard time-discretized incremental functionals. To this main, the time interval is divided in sub-intervals $[0, T] = \bigcup_{n=1}^N [t_{n-1}, t_n]$ and the incremental approximation of solution is:

$$\text{Inf}_{u_{n+1} \in X} F_{n+1}(u_{n+1}; u_n), \quad n = 0, 1, \dots, N - 1 \quad (1.2)$$

where

$$F_{n+1}(u_{n+1}; u_n) = \Delta t \varphi\left(\frac{u_{n+1} - u_n}{\Delta t}\right) + \psi(t_{n+1}, u_{n+1}) - \psi(t_n, u_n) \quad (1.3)$$

Then, within the framework of the Pareto multi-objective optimization (Clarke, 1990), a single objective functional is constructed as the sum a weighted sum of the individual functionals built in the previous step:

$$I(u, \lambda) = \sum_{n=0}^{N-1} \lambda_{n+1} F_{n+1}(u_{n+1}; u_n) \quad (1.4)$$

where $\lambda_1, \dots, \lambda_N$ are positive coefficients which are called Pareto weights (Clarke, 1990).

It is worth noting that the weights applied to a single incremental functional are ordered such that the first incremental problem lays disproportionately higher priority over the second, the second over the third, and so. Therefore $\lambda_1 \gg \lambda_2 \gg \dots$. According to Mielke (Mielke, 2005), this ordering can be achieved by considering a parameterized sequence of weights $\lambda_{\eta,1} > \lambda_{\eta,2} > \dots$ such that

$$\lim_{\eta \rightarrow 0} \frac{\lambda_{\eta,n+1}}{\lambda_{\eta,n}} = 0$$

where η is a positive parameter.

Finally, the trajectory-wise functional is obtained formally by passing to the limit of continuous time. Thus the functional (1.4) appears as a discretization of the following continuous function :

$$I(\mathbf{u}, \lambda_\eta) = \int_0^T \lambda_\eta \left\{ \varphi(\dot{\mathbf{u}}) + \frac{d}{dt} \psi(t, \mathbf{u}) \right\} dt \quad (1.5)$$

Moreover, it is shown in (Mielke, 2005) that an admissible possible choice of λ_η can be taken under the form

$$\lambda_\eta = e^{-\frac{t}{\eta}}$$

For this particular choice and by operating an integration by parts, the functional (1.5) writes:

$$I_\eta(\mathbf{u}) = \int_0^T e^{-\frac{t}{\eta}} \left\{ \varphi(\dot{\mathbf{u}}) + \frac{1}{\eta} \psi(t, \mathbf{u}) \right\} dt + e^{-\frac{T}{\eta}} \psi(T, \mathbf{u}(T)) \quad (1.6)$$

This is the so-called weighted dissipation-energy (WDE) which is considered as a one-parameter family of minimum problems. The trajectory \mathbf{u} realizes the minimum of (1.6).

Mielke has shown that the corresponding Euler-Lagrange equations are given by:

$$-\eta D^2 \varphi(\dot{u})\ddot{u} + D\varphi(\dot{u}) + D\psi(t, u) = 0 \quad (1.7)$$

$$u(0) = u_0 \quad (1.8)$$

$$D\varphi(\dot{u}(T)) + D\varphi(T, u(T)) = 0 \quad (1.9)$$

which is an elliptic-in-time regularization of the original evolutionary problem (1.1).

The Γ -limit of these functionals for $\eta \rightarrow 0$ is degenerate and provides limited information regarding the limiting trajectories of the system (Mielke, 2005). However for rate-independent dissipation problems, it is possible to derive bounds which are independent of the regularizing parameter η . The mathematical details and proofs are provided in (Mielke, 2005).

1.1.2 Weighted-Inertia-Dissipation-Energy (WIDE) formulation for dynamic elastoplastic problems

Davoli et al. (Davoli and Stefanelli, 2019) extended the Mielke formulation presented in subsection 1.1.1 in a pure mathematical manner to dynamic perfect plasticity. They developed a variational approach which consists in minimizing a Weighted-Inertia-Dissipation-Energy (WIDE) functional.

The authors considered the following elastic perfect plastic problem involving inertia effects:

$$\operatorname{div} \boldsymbol{\sigma} = \rho \ddot{\mathbf{u}} \quad (1.10)$$

$$\boldsymbol{\sigma} = \mathbb{C} : (\boldsymbol{\varepsilon} - \boldsymbol{\varepsilon}^p) \quad (1.11)$$

$$\boldsymbol{\sigma} \in \partial\varphi(\boldsymbol{\varepsilon}^p) \quad (1.12)$$

where $\boldsymbol{\sigma}$ is the Cauchy stress tensor, \mathbf{u} is the displacement field, \mathbb{C} is the fourth-order elastic tensor, $\boldsymbol{\varepsilon}$ denotes for the linearized strain matrix, $\boldsymbol{\varepsilon}^p$ is the irreversible plastic strains and φ is the dissipation potential. The energy potential reads $\psi(\boldsymbol{\varepsilon}, \boldsymbol{\varepsilon}^p) = \frac{1}{2} (\boldsymbol{\varepsilon} - \boldsymbol{\varepsilon}^p) : \mathbb{C} : (\boldsymbol{\varepsilon} - \boldsymbol{\varepsilon}^p)$.

It is important to underline that modeling of elastoplasticity will be detailed in the next section of this chapter.

The variational formulation (WIDE) proposed in (Davoli and Stefanelli, 2019) writes:

$$I_\eta(\mathbf{u}, \boldsymbol{\varepsilon}^p) = \int_0^T \int_\Omega e^{-\frac{t}{\eta}} \left(\frac{\rho\eta^2}{2} |\ddot{\mathbf{u}}|^2 + \eta\varphi(\dot{\boldsymbol{\varepsilon}}^p) + \frac{1}{2} (\boldsymbol{\varepsilon} - \boldsymbol{\varepsilon}^p) : \mathbb{C} : (\boldsymbol{\varepsilon} - \boldsymbol{\varepsilon}^p) \right) d\Omega dt \quad (1.13)$$

The corresponding Euler-Lagrange are given by the following set of equations:

$$\eta^2 \rho \ddot{\mathbf{u}}^\eta - 2\eta^2 \rho \dot{\mathbf{u}}^\eta + \rho \ddot{\mathbf{u}}^\eta - \operatorname{div} \boldsymbol{\sigma}^\eta = 0 \quad (1.14)$$

$$\boldsymbol{\sigma}^\eta = \mathbb{C} : (\boldsymbol{\varepsilon}^\eta - \boldsymbol{\varepsilon}^{\eta p}) \quad (1.15)$$

$$\boldsymbol{\sigma}^\eta \in -\eta(\partial\varphi(\dot{\boldsymbol{\varepsilon}}^{\eta p})) + \partial\varphi(\dot{\boldsymbol{\varepsilon}}^{\eta p}) \quad (1.16)$$

Davoli et al. (Davoli and Stefanelli, 2019) have proved rigorously that the dynamic elastoplastic (1.10-1.12) is recovered by taking $\eta \rightarrow 0$. Therefore, a numerical procedure for numerical simulation of dynamic elastoplastic problems can be developed basing upon the Weighted-Inertia-Dissipation-Energy (WIDE) formulation. To our knowledge, numerical investigations testing the feasibility and the accuracy of the proposed variational formulation are not yet proposed in the literature.

1.1.3 The Brezis-Ekeland-Nayroles (BEN) principle

In 1976, Brezis and Ekeland (Brezis and Ekeland, 1976b,a) proposed a variational minimization principle for a class of parabolic evolution equations. Independently, Nayroles (1976) (Nayroles et al., 1976) developed a similar principle for nonlinear mechanics, which gives the existence theorem of solutions for the Cauchy problem associated with the constitutive law of Maxwell model. It is worth noting that the Brezis-Ekeland-Nayroles (BEN) principle is similar to that of De Giorgi (De Giorgi et al., 1980). Hereafter, we briefly recall the BEN variational formulation and its extensions to dynamical dissipative systems derived by Buliga and de Saxcé (Buliga and de Saxcé, 2017) within the framework of the symplectic convex analysis.

Consider a time interval $[0, T]$, a convex, proper and lower semicontinuous function (or potential) φ in a Hilbert space V , and a function $f \in L^2(0, T; V)$. The purpose is to solve the following parabolic evolution inclusion:

Find the trajectory $t \mapsto u(t) \in V$ such that:

$$\frac{du}{dt} + \partial\varphi(u) \in f \text{ a.e. } t \in [0, T] \quad (1.17)$$

where $\partial\varphi(u)$ is the subdifferential operator of φ . The problem (1.17) models many physical problems such as the heat conduction, the Stefan problem, the Hele-Shaw cell, certain nonlinear transport equations, etc.

Brezis et al. (Brezis and Ekeland, 1976b,a) demonstrated that the trajectory $u(t)$, the unique

solution of (1.17), achieves the minimum of the convex and non-negative functional j :

$$j(v) = \int_0^T \{\varphi(v) + \varphi^*(f - v') - \langle f, v \rangle\} dt + \frac{1}{2} |v(T)|^2 \quad (1.18)$$

where φ^* is the conjugate function of φ (Rockafellar, 1970b; Krantz, 2015) and $\langle \cdot, \cdot \rangle$ denotes for the scalar product in V . More precisely, the solution function $u(t)$ satisfies $j(u) = 0$. This minimization problem is the so-called Brezis-Ekeland-Nayroles (BEN) principle.

Intriguingly, this variational principle is not very popular in the literature, even if it allows a consistent view of the whole evolution of a dissipative system at once. From the numerical point of view, instead of computing the trajectory in a step-by-step way and facing the convergence problem, the BEN principle allows working simultaneously overall steps.

Consider now the evolution problem (1.17) under periodic conditions:

$$\frac{du}{dt} + \partial\varphi(u) \in f \text{ a.e. } t \in [0, T] \text{ such that } u(0) = u(T) \quad (1.19)$$

As mentioned in (Brézis and Ekeland, 1976b), although the existence and uniqueness of solutions of (1.19) are not guaranteed, the authors showed that a solution minimizes the following functional :

$$j'(v) = \int_0^T \{\varphi(v) + \varphi^*(f - v') - \langle f, v \rangle\} dt + \frac{1}{2} |v(T)|^2 \quad (1.20)$$

Moreover, if a solution u exists then $j'(u) = 0$.

1.1.4 The symplectic Brezis-Ekeland-Nayroles (SBEN) principle

Recently, Buliga and de Saxcé (Buliga and de Saxcé, 2017) developed a symplectic version of the BEN principle by extending the Hamiltonian formalism for dynamical dissipative systems.

Consider two topological, locally convex, real vector spaces X and Y and a lower semicontinuous dissipation potential φ . A symplectic form is a bilinear and antisymmetric form defined on $(X \times Y)^2 \rightarrow \mathbb{R}$. The natural symplectic form (or the Lagrange brackets) ω is defined for any $z = (x, y)$ and $z' = (x', y')$ in $X \times Y$ by:

$$\omega(z, z') = \langle x, y' \rangle - \langle x', y \rangle \quad (1.21)$$

where $\langle \cdot, \cdot \rangle$ is a duality product.

By definition, the symplectic subdifferential $\partial^\omega \varphi(z)$ of the dissipation potential is given by:

$$\partial^\omega \varphi(z) = \{z' \in X \times Y \text{ such as } \forall z'' \in X \times Y, \varphi(z + z'') \geq \varphi(z) + \omega(z', z'')\} \quad (1.22)$$

Moreover, it is natural to introduce the symplectic Fenchel polar function $\varphi^{*\omega}$ as follows:

$$\varphi^{*\omega}(\dot{z}_I) = \sup_z \{\omega(\dot{z}_I, \dot{z}) - \varphi(\dot{z})\} \quad (1.23)$$

According to Buliga et al. (Buliga and de Saxcé, 2017), if the potential φ is lower semicontinuous then, for any $(z, z') \in X \times Y$ one has:

$$\varphi(z) + \varphi^{*\omega}(z') \geq \omega(z', z) \quad (1.24)$$

and the equality is obtained if and only if $z' \in \partial^\omega(z)$

Let now F be a function defined on $X \times Y \rightarrow \mathbb{R} \cup \{+\infty\}$. F has a symplectic gradient at a given $z = (x, y)$, if $F(z) < +\infty$ and there exists $XF(x, y) = (u, v) \in X \times Y$, called the symplectic gradient of F , such that

- for all $y' \in Y$ we have

$$\lim_{\delta \rightarrow 0} \frac{1}{\delta} [F(x, y + \delta y') - F(x, y)] = \langle u, y' \rangle \quad (1.25)$$

- item for all $x' \in X$ we have

$$\lim_{\delta \rightarrow 0} \frac{1}{\delta} [F(x + \delta x', y) - F(x, y)] = \langle -x', v \rangle \quad (1.26)$$

The attention is focused now on the evolution curve $t : [0, T] \mapsto z(t) \in X \times Y$ satisfying the following relation:

$$\dot{z}(t) = XH(t, z(t)) \quad (1.27)$$

where the function $H = H(t, x, y) = H(t, z)$ is called the Hamiltonian and defining the motion and $XH = (\text{grad}_y H, -\text{grad}_x H)$ is the symplectic gradient of the Hamiltonian (see Buliga and de Saxcé (2017)), also called Hamiltonian vector field in the literature.

The extension of the BEN principle for the evolution curve $t \mapsto z(t)$ relies on the additive decomposition of the time rate \dot{z} into a reversible part $\dot{z}_R = XH(z)$ (the symplectic gradient, see (Buliga and de Saxcé, 2017)) and a dissipative or irreversible one $\dot{z}_I = \dot{z} - \dot{z}_R$, and the use of symplectic subdifferential $\partial^\omega \varphi(z)$ of the dissipation potential.

According to the authors, an evolution curve $z(t)$ satisfies the symplectic Brezis-Ekeland-Nayroles principle for the Hamiltonian H and dissipation potential φ if for almost any $t \mapsto [0, T]$ has:

$$\varphi(\dot{z}(t)) + \varphi^{*\omega}(\dot{z}_I(t)) = \omega(\dot{z}_I(t), \dot{z}(t)) \quad (1.28)$$

Basing upon these assumptions, Buliga and de Saxcé (Buliga and de Saxcé, 2017) announced and proved the following symplectic BEN principle:

An evolution curve $t \in [0, T] \mapsto z(t) \in X \times Y$ satisfies the symplectic BEN principle for the Hamiltonian H and dissipation potential φ if and only if it satisfies one of the following:

- *for almost every $t \in [0, T]$*

$$\dot{z}(t) - XH(t, z(t)) \in \partial^w \varphi(\dot{z}) \quad (1.29)$$

- *the evolution curve minimizes the functional*

$$\Pi(z') = \int_0^T \{ \varphi(\dot{z}') + \varphi^{*w}(\dot{z}' - XH) - \omega(\dot{z}' - XH, \dot{z}') \} dt \quad (1.30)$$

among all curves $z'(t) : [0, T] \mapsto X \times Y$ such that $z'(0) = z(0)$ and the minimum is zero.

One of the advantages of this symplectic Brezis-Ekeland-Nayroles principle of minimizing the functional Π with the initial condition is to generate variational inequalities associated to any function $f(t, z)$:

$$\begin{aligned} & \int_0^T [\varphi(\dot{z}(t) - Xf(t, Z)) - \varphi(\dot{z})] \\ & \geq f(T, z(T)) - f(0, z(0)) + \int_0^T [H, f(t, z(t)) - D_t f(t, z(t))] dt \end{aligned} \quad (1.31)$$

where $\{\cdot, \cdot\}$ is Poisson's bracket. These inequalities could be very helpful considering in particular the Hamiltonian and (exact or approximated) integrals of the motion. In this formalism, the energy balance writes:

$$H(T, z(T)) + D_{iss}(z, [0, T]) = H(0, z_0) + \int_0^T D_t H(t, z) dt \quad (1.32)$$

The BEN principle and its symplectic version are the core of this thesis.

1.2 Basic notions of Elastoplasticity

Elastoplastic problems of deformable bodies are among the oldest ones in the field of nonlinear mechanics. With the significant advances in mathematics and material sciences, elastoplasticity has accomplished increasing progress and has reached a certain maturity. Since the pioneering work of Hill (Hill, 1998), two dates related to the development of this theory deserve to be mentioned. The first one dates back to Halphen and Son (Halphen and Nguyen, 1975), who proposed a rigorous framework called the generalized standard materials, which allows the built thermodynamic admissible models. This framework relies on a dissipation potential and an energy function under the assumption of normal flow rule. The second date is related to the work of Suquet (Suquet, 1981), who studied the existence of solutions for the quasi-static problems within suitable spaces.

Without loss of generality and for seek of shortness, the present survey reviews some basic concepts of the elastic perfect plastic problems at the macroscopic scale. Hardening plasticity is easily formulated within the framework of standard plasticity (Halphen and Nguyen, 1975; Nguyen, 2000). The reader can refer with great interest to the monographs (Nguyen, 2000; Temam, 2018; Lubliner, 2008). Micromechanical aspects of elastoplasticity are out of the scope of the present work.

1.2.1 Basic equations

Consider an elastic plastic solid occupying an open volume Ω with a sufficiently regular boundary $\Gamma = \partial\Omega$. The later is divided into two disjoint parts Γ_T and Γ_u . The solid is subjected to body forces \mathbf{f}_v , prescribed surface tractions \mathbf{T}^d on Γ_T and imposed displacement \mathbf{u}^d on Γ_u . These actions depend on the position $x \in \Omega$ and the time $t \in [0, T]$ and they define the so-called history loading or path loading. In the sequel, space and time dependence of the loadings and the mechanical fields are not mentioned explicitly.

We assume small strains, elastic linear under small loads, and rate-independent plasticity. The quasi-static elastoplastic problem consists in finding the mechanical fields $\boldsymbol{\sigma}, \mathbf{u}$ satisfying the following boundary value problem:

$$\operatorname{div}\boldsymbol{\sigma} + \mathbf{f}_v = 0 \quad \text{in}\Omega \tag{1.33}$$

$$\text{elastoplastic constitutive law} \tag{1.34}$$

$$\boldsymbol{\sigma} \cdot \mathbf{n} = \mathbf{T}^d \quad \text{on}\Gamma_T \tag{1.35}$$

$$\mathbf{u} = \mathbf{u}^d \quad \text{on}\Gamma_u \tag{1.36}$$

where \mathbf{n} is normal outward vector to the surface Γ .

Let K be the elastic domain which is defined by:

$$k = \{\boldsymbol{\sigma} \text{ such that } f(\boldsymbol{\sigma}) \leq 0\}$$

Experimental have shown that the set K is convex and non empty (Bui, 1969).

For isotropic metals, the Tresca and von Mises criteria are the most widely used (Tresca, 1864; von Mises, 1928). These models are dependent on the second invariant J_2 of the deviatoric part of the stress tensor. For compressible materials like geomaterials and polymers, yield criteria must include the first invariant I_1 .

For instance, Tresca yield domain is defined as follows: $\sigma_{eq,T}$:

$$f(\boldsymbol{\sigma}) = \sup(|\sigma_I - \sigma_{II}|, |\sigma_{II} - \sigma_{III}|, |\sigma_{III} - \sigma_I|) - \sigma_Y \leq 0 \quad (1.37)$$

where are $\sigma_I, \sigma_{II}, \sigma_{III}$ the principle stresses of the stress tensor and σ_Y denotes the yield stress.

The von Mises plastic criterion is stated as:

$$f(\boldsymbol{\sigma}) = \sqrt{\frac{3}{2} \mathbf{s} : \mathbf{s}} - \sigma_Y \leq 0 \quad (1.38)$$

with \mathbf{s} is deviatoric part of the stress field stress $\boldsymbol{\sigma}$.

Let us recall that a displacement field \mathbf{u}^* is said to be kinematically admissible (K.A.) if $\mathbf{u}^* = \mathbf{u}^d$ on Γ_u . A stress field $\boldsymbol{\sigma}^*$ is statically admissible (S.A.) if $\text{div } \boldsymbol{\sigma}^* + \mathbf{f}_v = 0$ within Ω and $\boldsymbol{\sigma}^* \mathbf{n} = \mathbf{T}^d$ on Γ_T . Furthermore, $\boldsymbol{\sigma}^*$ is said to be plastically admissible (P.A.) if $\boldsymbol{\sigma}^*$ is S.A and $\boldsymbol{\sigma}^* \in K$.

The total strain tensor splits additively into its elastic part and its plastic one:

$$\boldsymbol{\varepsilon} = \boldsymbol{\varepsilon}^e + \boldsymbol{\varepsilon}^p \quad (1.39)$$

The elastic part is related to the stress field through the Hooke law:

$$\boldsymbol{\varepsilon}^e = \mathbf{S} : \boldsymbol{\sigma}$$

in which \mathbf{S} is the forth order stiffness tensor.

For the variation of the plastic strain tensor, we limit ourselves to the associated plasticity

which means that the normal flow rule is adopted:

$$\dot{\boldsymbol{\varepsilon}}^p = \lambda \frac{\partial f}{\partial \boldsymbol{\sigma}}(\boldsymbol{\sigma}) \quad (1.40)$$

where $\lambda > 0$ is called the plastic multiplier. Moreover, the consistency equation $\lambda \cdot \dot{f} = 0$ must be considered also. This equation allows the determination of the plastic multiplier as follows (Nguyen, 2000; Maitournam, 2013):

It is important to underline that the normality law is equivalent to the following inequality:

$$\forall \boldsymbol{\sigma}^* \in K, (\boldsymbol{\sigma} - \boldsymbol{\sigma}^*) : \dot{\boldsymbol{\varepsilon}}^p \geq 0 \quad (1.41)$$

This is the so-called Hill's maximum power principle (Nguyen, 2000; Maitournam, 2013).

Basing upon this principle (1.41), one introduces the dissipation potential:

$$\varphi(\dot{\boldsymbol{\varepsilon}}^p) = \text{Sup} \{ \boldsymbol{\sigma}^* : \dot{\boldsymbol{\varepsilon}}^p; \quad \boldsymbol{\sigma}^* \in K \} \quad (1.42)$$

It has been shown that φ is convex, lower semi-continuous and a positively homogeneous of order one (Halphen and Nguyen, 1975; Nguyen, 2000; Maitournam, 2013). Within the framework of convex analysis, it can be easily established that

$$\boldsymbol{\sigma} \in \partial\varphi(\dot{\boldsymbol{\varepsilon}}^p) \quad (1.43)$$

where $\partial\varphi$ is the subdifferential of the dissipation function (Rockafellar, 1970b).

The Legendre-Fenchel transform allows to derive the converse constitutive law thanks to the conjugate function χ of φ :

$$\varphi^*(\boldsymbol{\sigma}) = \text{Sup} \{ \boldsymbol{\sigma} : \dot{\boldsymbol{\varepsilon}}^{*p} - \varphi(\dot{\boldsymbol{\varepsilon}}^{*p}), \quad \dot{\boldsymbol{\varepsilon}}^{*p} \in V \} \quad (1.44)$$

where V is a topological vector space of plastic strain rate field. The potentials φ and φ^* satisfy Fenchel's inequality:

$$\varphi(\dot{\boldsymbol{\varepsilon}}^{*p}) + \varphi^*(\boldsymbol{\sigma}) \geq \boldsymbol{\sigma} : \dot{\boldsymbol{\varepsilon}}^p \quad (1.45)$$

For the plasticity, φ^* is the indicatory function of the convex elastic domain K and subsequently φ^* is convex. Thus

$$\dot{\boldsymbol{\varepsilon}}^p \in \partial\varphi^*(\boldsymbol{\sigma}) \quad (1.46)$$

Equivalently, the couple $(\dot{\boldsymbol{\varepsilon}}^p, \boldsymbol{\sigma})$ is extremal in the sense that the equality is reached in (1.45):

$$\varphi(\dot{\boldsymbol{\varepsilon}}^p) + \varphi^*(\boldsymbol{\sigma}) = \boldsymbol{\sigma} : \dot{\boldsymbol{\varepsilon}}^p \quad (1.47)$$

if $\boldsymbol{\sigma} \in K$, the stress potential φ^* vanishes and we recover the meaning of φ as the dissipation:

$$\varphi(\dot{\boldsymbol{\varepsilon}}^p) = \boldsymbol{\sigma} : \dot{\boldsymbol{\varepsilon}}^p$$

Eventually, it is interesting to underline that an incremental relationship between the strain and stress rates can be written as follows (Son, 1977):

$$\dot{\boldsymbol{\varepsilon}} \in \mathbb{S}\dot{\boldsymbol{\sigma}} + \partial\varphi^*(\boldsymbol{\sigma}) \quad (1.48)$$

$$\boldsymbol{\sigma}(0) = \boldsymbol{\sigma}_0 \quad (1.49)$$

1.2.2 Energetic aspects

Similar to elasticity, two minimum principles of the potential energy and the complementary one can be formulated for elastoplasticity.

Let us consider the elastic perfectly plastic boundary value problem (BVP) as described in section 1.2. It can be proven that one has:

- The Greenberg minimum principle

The displacement rate $\dot{\mathbf{u}}$ minimizes the following functional:

$$F(\dot{\mathbf{u}}^*) = \int_{\Omega} \varphi(\dot{\boldsymbol{\varepsilon}}^*) d\Omega - \int_{\Omega} \dot{\mathbf{f}}_v \dot{\mathbf{u}}^* d\Omega - \int_{\Gamma_T} \dot{\mathbf{T}}^d \dot{\mathbf{u}}^* d\Gamma \quad (1.50)$$

Among all kinematically admissible displacement rate, i.e. $\dot{\mathbf{u}}^ = \dot{\mathbf{u}}^d$ on Γ_u .*

The proof is provided in (Greenberg, 1949; Lubliner, 2008).

- The Hodge-Prager minimum principle

The stress tensor rate $\dot{\boldsymbol{\sigma}}$ minimizes the following functional:

$$G(\dot{\boldsymbol{\sigma}}^*) = \int_{\Omega} \frac{1}{2} \dot{\boldsymbol{\sigma}}^* : \mathbb{S} : \dot{\boldsymbol{\sigma}}^* d\Omega - \int_{\Gamma_u} \dot{\boldsymbol{\sigma}}^* \dot{\mathbf{u}} \mathbf{n} d\Gamma \quad (1.51)$$

Among all statically and plastically admissible stress rate field $\dot{\boldsymbol{\sigma}}$.

The reader can refer to (Prager and Hodge, 1968; Lubliner, 2008) for details of the proof.

Furthermore, the existence and uniqueness of the solution for perfect plasticity can be announced as follows (Nguyen, 2000; Lubliner, 2008):

Theorem

For quasi-static evolution, the stress solution is unique. The displacement solution is unique for dynamic problems.

Proof

Following Son (Nguyen, 2000), let $(\boldsymbol{\sigma}, \mathbf{u})$ and $(\hat{\boldsymbol{\sigma}}, \hat{\mathbf{u}})$ be 2 solutions of (BVP) in terms of the stress and displacement fields. The virtual work equation writes:

$$\int_{\Omega} \boldsymbol{\sigma} : \delta \boldsymbol{\varepsilon} d\Omega - \int_{\Omega} (\mathbf{f}_v - \rho \ddot{\mathbf{u}}) \cdot \delta \mathbf{u} d\Omega - \int_{\Gamma_T} \mathbf{T}^d \cdot \delta \mathbf{u} d\Gamma = 0 \quad (1.52)$$

for $\delta u = 0$ on Γ_u .

The virtual work equation (1.52) holds also for the couple $(\hat{\boldsymbol{\sigma}}, \hat{\mathbf{u}})$. It follows

$$\int_{\Omega} (\boldsymbol{\sigma} - \hat{\boldsymbol{\sigma}}) : (\dot{\boldsymbol{\varepsilon}} - \dot{\hat{\boldsymbol{\varepsilon}}}) d\Omega + \int_{\Omega} \rho(\ddot{\mathbf{u}} - \ddot{\hat{\mathbf{u}}})(\dot{\mathbf{u}} - \dot{\hat{\mathbf{u}}}) d\Omega = 0 \quad (1.53)$$

By taking into account the relationship $\dot{\boldsymbol{\varepsilon}} = \dot{\boldsymbol{\varepsilon}}^e + \dot{\boldsymbol{\varepsilon}}^p$ in eq. (1.53), one gets:

$$\int_{\Omega} (\boldsymbol{\sigma} - \hat{\boldsymbol{\sigma}}) : (\dot{\boldsymbol{\varepsilon}}^p - \dot{\hat{\boldsymbol{\varepsilon}}}^p) d\Omega + \int_{\Omega} (\boldsymbol{\sigma} - \hat{\boldsymbol{\sigma}}) : \mathbf{S} : (\dot{\boldsymbol{\sigma}} - \dot{\hat{\boldsymbol{\sigma}}}) d\Omega + \int_{\Omega} \rho(\ddot{\mathbf{u}} - \ddot{\hat{\mathbf{u}}})(\dot{\mathbf{u}} - \dot{\hat{\mathbf{u}}}) d\Omega = 0 \quad (1.54)$$

On the other hand $(\boldsymbol{\sigma} - \hat{\boldsymbol{\sigma}}) : (\dot{\boldsymbol{\varepsilon}}^p - \dot{\hat{\boldsymbol{\varepsilon}}}^p) \geq 0$ which yields:

$$\frac{d}{dt} \frac{1}{2} \left(\int_V (\boldsymbol{\sigma} - \hat{\boldsymbol{\sigma}}) : \mathbf{S} : (\boldsymbol{\sigma} - \hat{\boldsymbol{\sigma}}) dV + \int_V \rho(\dot{\mathbf{u}} - \dot{\hat{\mathbf{u}}})^2 dV \right) \leq 0 \quad (1.55)$$

Subsequently, the positive functional

$$I(t) = \frac{1}{2} \left(\int_V (\boldsymbol{\sigma} - \hat{\boldsymbol{\sigma}}) : \mathbf{S} : (\boldsymbol{\sigma} - \hat{\boldsymbol{\sigma}}) dV + \int_V \rho(\dot{\mathbf{u}} - \dot{\hat{\mathbf{u}}})^2 dV \right)$$

is decreasing. Moreover, this function is vanishing initially, thus it remains equal to zero for all time t , which leads to $\boldsymbol{\sigma} = \hat{\boldsymbol{\sigma}}$ and $\mathbf{u} = \hat{\mathbf{u}}$.

1.3 Numerical treatment of elastoplastic problems

The natural and common solution strategy for nonlinear problems is the path-following incremental analysis, which computes in a step-by-step manner the system response along the loading history (Zienkiewicz et al., 1969; Zienkiewicz, 1971; Oden, 2006; Simo and Hughes, 2000; Be-

lytschko and Velebit, 1972; Cristfield, 1998; Ibrahimbegovic, 2009).

Regarding the elastoplastic problems, undoubtedly, the radial return algorithm, initially proposed by Nguyen (Son, 1977) is the most popular method. It belongs to the family of trial-and-error algorithms and is widely implemented in many commercial codes such as Abaqus, Cast3m, Adina, etc...

A different non-incremental numerical algorithm, namely the LARge Time INcrement method (LATIN) (Ladevèze, 1985a,b) has been proposed in order to compute an approximation solution for the whole time history.

1.3.1 Radial return algorithm

The radial return is a predictor-corrector scheme that allows to determine the stress at the end of the increment from the strain increment and the stress at the beginning of the increment. To this end, loading history into many successive small time increments and to solve the non linear equilibrium equations at each end of the increment.

An initial equilibrium state at t and the variables at $t + \Delta t$ are noted respectively as:

$$\{\boldsymbol{\sigma}(t), \boldsymbol{\varepsilon}(t), \boldsymbol{\varepsilon}_e(t), \boldsymbol{\varepsilon}_p(t), p(t)\} = \{\boldsymbol{\sigma}^n, \boldsymbol{\varepsilon}^n, \boldsymbol{\varepsilon}_e^n, \boldsymbol{\varepsilon}_p^n, p^n\}$$

$$\{\boldsymbol{\sigma}(t + \Delta t), \boldsymbol{\varepsilon}(t + \Delta t), \boldsymbol{\varepsilon}_e(t + \Delta t), \boldsymbol{\varepsilon}_p(t + \Delta t), p(t + \Delta t)\} = \{\boldsymbol{\sigma}^{n+1}, \boldsymbol{\varepsilon}^{n+1}, \boldsymbol{\varepsilon}_e^{n+1}, \boldsymbol{\varepsilon}_p^{n+1}, p^{n+1}\}$$

For each time increment, the final state at $t + \Delta t$ is computed from the initial state at t by applying the radial return algorithm (fig. 1.1). Hence in this incremental method, the increment size determines computation precision. Within a complex loading history, one needs to impose many tiny time increments to obtain an accurate simulation, that increases the computation time. A flaw of the method is the accumulation of the computational error. In each step, computation provides an approximation result with a small computational error. While in the next time step, the integration is executed based on the error produced in the previous one, etc. This accumulation of errors may lead to the failure of the whole simulation. The only possibility is to start again from the beginning with a smaller time increment.

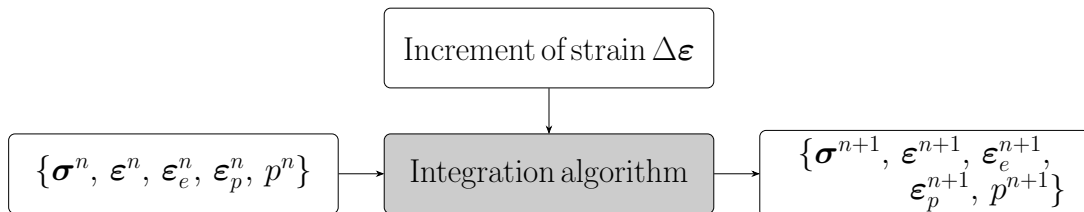


Figure 1.1: Function of elastoplastic return mapping algorithm enter variables at t and $t + \Delta t$

In discretization form, the constitutive equations reads:

$$\Delta \boldsymbol{\varepsilon} = \Delta \boldsymbol{\varepsilon}_e + \Delta \boldsymbol{\varepsilon}_p \quad (1.56a)$$

$$\Delta \boldsymbol{\sigma} = 2\mu \Delta \boldsymbol{\varepsilon}_e + \lambda \text{tr}(\Delta \boldsymbol{\varepsilon}_e) \mathbf{1} \quad (1.56b)$$

$$f_{vm/T}^{n+1}(\boldsymbol{\sigma}) = \sigma_{eq}^{n+1} - \sigma_Y \leq 0 \quad (1.56c)$$

$$\Delta \boldsymbol{\varepsilon}_p = \Delta \lambda \frac{3\boldsymbol{s}^{n+1}}{2\sigma_Y} \quad (1.56d)$$

$$\Delta \lambda \geq 0 \quad (1.56e)$$

There are two steps in the radial return algorithm: (i) Elastic prediction (ii) Elastoplastic correction (if necessary).

(i) Elastic prediction Imposing a null plastic deformation, one has:

$$\Delta \boldsymbol{\varepsilon}_p = \mathbf{0} \quad \Rightarrow \quad \Delta \boldsymbol{\varepsilon} = \Delta \boldsymbol{\varepsilon}_e + \Delta \boldsymbol{\varepsilon}_p = \Delta \boldsymbol{\varepsilon}_e$$

thus the constitutive model in elastic prediction is:

$$\boldsymbol{\varepsilon}_{e,elas}^{n+1} = \boldsymbol{\varepsilon}_e^n + \Delta \boldsymbol{\varepsilon} \quad (1.57a)$$

$$\boldsymbol{\sigma}_{elas}^{n+1} = \boldsymbol{\sigma}^n + 2\mu \Delta \boldsymbol{\varepsilon}_e + \lambda \text{tr}(\Delta \boldsymbol{\varepsilon}_e) \mathbf{1} \quad (1.57b)$$

$$f_{vm/T,elas}(\boldsymbol{\sigma}^{n+1}) = \sigma_{eq,elas}^{n+1} - \sigma_Y \quad (1.57c)$$

$$\boldsymbol{\varepsilon}_{p,elas}^{n+1} = \boldsymbol{\varepsilon}_p^n \quad (1.57d)$$

The obtained predicted variables in the elastic prediction step may need to be corrected in the next step.

(ii) Elastoplastic correction As the variables of first step is just a prediction, its admissibility needs to be checked. By verifying the state of eq. (1.57c), one has two cases:

(ii.1) $f_{vm/T,elas}(\boldsymbol{\sigma}^{n+1}) \leq 0$ yield condition satisfied, variables at $t + \Delta t$ are updated from the ones of elastic prediction.

$$\{\boldsymbol{\sigma}^{n+1}, \boldsymbol{\varepsilon}^{n+1}, \boldsymbol{\varepsilon}_e^{n+1}, \boldsymbol{\varepsilon}_p^{n+1}, \lambda^{n+1}\} = \{\boldsymbol{\sigma}_{elas}^{n+1}, \boldsymbol{\varepsilon}_{elas}^{n+1}, \boldsymbol{\varepsilon}_{e,elas}^{n+1}, \boldsymbol{\varepsilon}_{p,elas}^{n+1}, \lambda_{elas}^{n+1}\}$$

(ii.2) $f_{vm/T,elas}(\boldsymbol{\sigma}^{n+1}) > 0$ yield condition not satisfied, the elastic prediction requires a correction (fig. 1.2). Taking the discretization eq. (1.56b) and replacing elastic strain by its additive

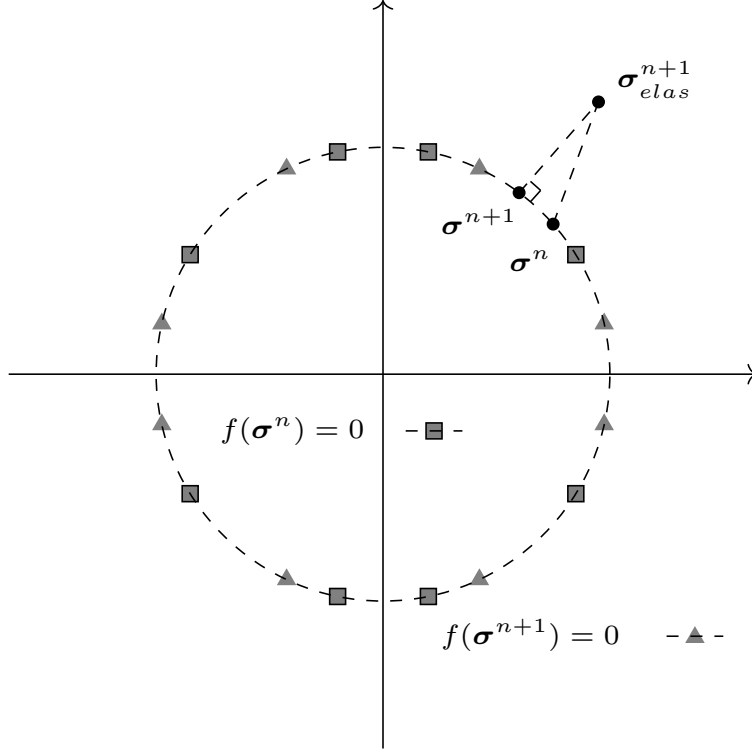


Figure 1.2: Radial return schema

decomposition, one has the elastoplastic correction:

$$\begin{aligned}
 \boldsymbol{\sigma}^{n+1} &= \boldsymbol{\sigma}_n + 2\mu(\Delta\boldsymbol{\varepsilon} - \Delta\boldsymbol{\varepsilon}_p) + \lambda\text{tr}(\Delta\boldsymbol{\varepsilon} - \Delta\boldsymbol{\varepsilon}_p)\mathbf{1} \\
 &= \boldsymbol{\sigma}_n + 2\mu\Delta\boldsymbol{\varepsilon} + \lambda\text{tr}(\Delta\boldsymbol{\varepsilon})\mathbf{1} - 2\mu\Delta\boldsymbol{\varepsilon}_p \\
 &= \boldsymbol{\sigma}_{elas}^{n+1} - 2\mu\Delta\boldsymbol{\varepsilon}_p
 \end{aligned} \tag{1.58}$$

with $2\mu\Delta\boldsymbol{\varepsilon}_p$ the elastoplastic correction. As $\text{tr}(\Delta\boldsymbol{\varepsilon}_p) = 0$, eq. (1.58) becomes:

$$\mathbf{s}^{n+1} = \mathbf{s}_{elas}^{n+1} - 2\mu\Delta\boldsymbol{\varepsilon}_p \tag{1.59}$$

For von Mises criterion, eq. (1.56d) gives:

$$\Delta\boldsymbol{\varepsilon}_p = \Delta\lambda \frac{3\mathbf{s}^{n+1}}{2\sigma_Y} \tag{1.60}$$

By combining eq. (1.59) and (1.60), one has:

$$\mathbf{s}_{elas}^{n+1} = \mathbf{s}^{n+1} \left(1 + \frac{3\mu\Delta\lambda}{\sigma_Y} \right)$$

The equivalent tensile stress can be expressed as:

$$\sigma_{eq,vm,elas}^{n+1} = \sigma_{eq,vm}^{n+1} \left(1 + \frac{3\mu\Delta\lambda}{\sigma_Y} \right) = \sigma_Y + 3\mu\Delta\lambda$$

which gives:

$$\begin{aligned} \sigma_{vm,elas}^{n+1} - \sigma_Y - 3\mu\Delta\lambda &= 0 \\ \Delta\lambda &= \frac{\sigma_{vm,elas}^{n+1} - \sigma_Y}{3\mu} \\ \Delta\varepsilon_p &= \Delta\lambda \frac{3\mathbf{s}^{n+1}}{2\sigma_Y} = \Delta\lambda \frac{3\mathbf{s}_{elas}^{n+1}}{2\sigma_Y} \end{aligned}$$

Variables at $t + \Delta t$ can be updated from the elastoplastic correction:

$$\{\boldsymbol{\sigma}^{n+1}, \boldsymbol{\varepsilon}_p^{n+1}, \lambda^{n+1}\} = \{\boldsymbol{\sigma}_{elas}^{n+1} - 2\mu\Delta\varepsilon_p, \boldsymbol{\varepsilon}_p^n + \Delta\varepsilon_p, \lambda^n + \Delta\lambda\}$$

1.3.2 LATIN method in elastoplasticity

The LARge Time INcrement method (LATIN) was introduced in (Ladevèze, 1985a,b). Comparing to the incremental method presented in the previous section, the LATIN method is not based on the consideration of small increments in the entire time interval $[0, T]$, but on a non-incremental iterative technique. With one large increment of time, the LATIN method allows to solve a complex loading history by employing some properties of the equations:

- (i) the constitutive law is non-linear but local in space,
- (ii) while the others equations such as equilibrium and boundary conditions are linear but global.

Let $s' = (\dot{\boldsymbol{\varepsilon}}, \boldsymbol{\sigma})$ be a couple of strain rate and stress defined on $[0, T] \times \Omega$. The couple s' satisfying the constitutive equations belong to a manifold Γ . The admissible couple s'' are living in an affine space A_d . The exact solution of the problem belongs to the intersection of the two manifold Γ and A_d .

The iterative strategy of the LATIN method is to find a new approximation $s_{n+1} \in A_d$ from a previous one $s_n \in A_d$, each iteration consisting in two stages in each iteration:

(i) Direction of ascent : the local, non-linear step The intermediate approximation $\hat{s}_{n+1/2} \in \Gamma$ verifying the constitutive equations anywhere in Ω and for all $t \in [0, T]$ is at the intersection of Γ and the affine space $s_n + E^+$ where the direction is E^+ is a linear space defined

locally:

$$\hat{s}_{n+1/2} - s_n \in E^+$$

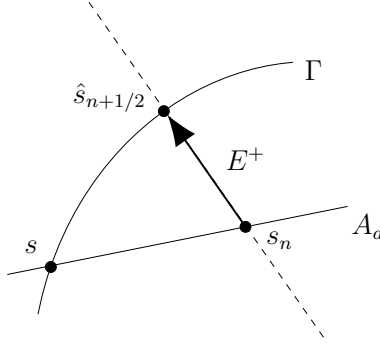


Figure 1.3: Non-linear and local step at iteration n

(ii) Direction of decent: the global, linear step The admissible point $s_{n+1} \in A_d$ is at the intersection between A_d and $\hat{s}_{n+1/2} + E^-$, the direction E^- being a linear space:

$$s_{n+1} - \hat{s}_{n+1/2} \in E^-$$

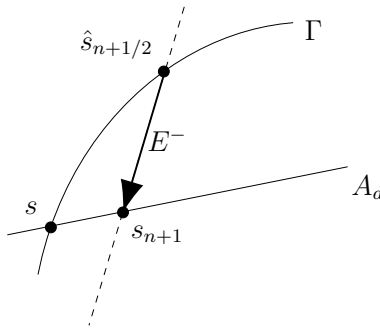


Figure 1.4: Linear and global step at iteration n

E^+ , E^- are parameters of the LATIN method. There are various algorithms to determine them, such as the Newton algorithm, the augmented Lagrangian method, etc. In the case of elastoplasticity, the tangent stiffness tensor \mathbf{C} gives:

$$\dot{\hat{\sigma}}_{n+1/2} = \mathbf{C} \dot{\hat{\varepsilon}}_{n+1/2} \quad \forall t \in [0, T]$$

With Newton algorithm, there are two stages:

1. Build of $\hat{s}_{n+1/2}$ The direction E^+ and A_d are orthogonal (fig. 1.5):

$$E^+ = \{s = (\mathbf{0}, \boldsymbol{\sigma})\}$$

The intermediate point $\hat{s}_{n+1/2} = (\hat{\boldsymbol{\epsilon}}_{n+1/2}, \hat{\boldsymbol{\sigma}}_{n+1/2})$ is defined as:

$$\hat{\boldsymbol{\epsilon}}_{n+1/2} = \hat{\boldsymbol{\epsilon}}_n \quad (1.61a)$$

$$\hat{\boldsymbol{\sigma}}_{n+1/2} = \mathbf{C} \hat{\boldsymbol{\epsilon}}_{n+1/2} \quad (1.61b)$$

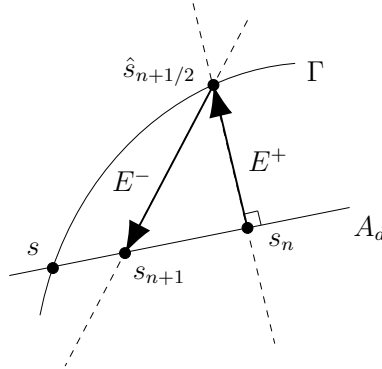


Figure 1.5: Frame the Newton algorithm

2. Build of s_{n+1} The direction E^- is given by:

$$E^- = \{s = (\dot{\boldsymbol{\epsilon}}, \boldsymbol{\sigma}) \mid \dot{\boldsymbol{\epsilon}} = \mathbf{K}^{-1} \frac{d\boldsymbol{\sigma}}{dt}\}$$

The new point $s_{n+1} = (\dot{\boldsymbol{\epsilon}}_{n+1}, \boldsymbol{\sigma}_{n+1})$ gives:

$$\dot{\boldsymbol{\epsilon}}_{n+1} \text{ kinematically admissible,} \quad (1.62a)$$

$$\boldsymbol{\sigma}_{n+1} \text{ statically admissible,} \quad (1.62b)$$

$$\dot{\boldsymbol{\epsilon}}_{n+1} - \hat{\boldsymbol{\epsilon}}_{n+1/2} = \mathbf{C}^{-1} \frac{d}{dt} (\boldsymbol{\sigma}_{n+1} - \hat{\boldsymbol{\sigma}}_{n+1/2}) \quad (1.62c)$$

Eqs. 1.62 are reformulated in a weak form:

Find a kinematically admissible \dot{u}_{n+1} minimizing:

$$\int_0^T \int_{\Omega} \text{tr} [\mathbf{C} \boldsymbol{\varepsilon}(\dot{u}_{n+1} - \dot{u}_n) \boldsymbol{\varepsilon}(\dot{u}_{n+1} - \dot{u}_n)] d\Omega dt - \int_0^T \int_{\Omega} \text{tr} \left[\frac{d}{dt} (\boldsymbol{\sigma}_n - \dot{\boldsymbol{\sigma}}_{n+1/2}) \boldsymbol{\varepsilon}(\dot{u}_{n+1} - \dot{u}_n) \right] d\Omega dt \quad (1.63)$$

Eq. (1.63) gives the new $\dot{\boldsymbol{\varepsilon}}_{n+1}$, and $\boldsymbol{\sigma}_{n+1}$ is computed from eq. (1.62c). A new point s_{n+1} is build.

A direct method for the quasi-static viscoelastoplastic problems by the Brezis-Ekeland-Nayroles principle

2.1	Formulation of the elastoplastic problems within the framework of the the Brezis-Ekeland-Nayroles principle	38
2.2	Application to the pressurized thick-walled tube	40
2.2.1	Basic equations	41
2.2.2	The mixed finite element method for thick tube problem	42
2.2.3	Discretization of the BEN functional	45
2.3	Results and discussion	48
2.3.1	Elastic response	49
2.3.2	Elastoplastic response with von Mises criterion	50
2.3.3	Elastoplastic response with Tresca criterion	53
2.3.4	Computation cost	55
2.3.5	Viscoplastic response with Norton-Odqvist law	58
2.4	Conclusion	60

This chapter is devoted to the numerical application of symplectic BEN principle for an elastic perfectly plastic and viscoplastic thick wall tube model subjected to internal pressure in statics. It turns out that the BEN variational formulation is based on a two-field functional, that leads naturally to discretize the displacement and stress fields. We present the detailing of the discretization and the numerical implementation of the minimization problem by using the mixed finite element method, which is more efficient in enforcing the yield condition. Computational accuracy and efficiency of the BEN principle are assessed by comparing the numerical results with the analytical ones and the simulations derived by the classical step-by-step finite element procedure.

2.1 Formulation of the elastoplastic problems within the framework of the the Brezis-Ekeland-Nayroles principle

Formulation of the elastoplastic problems within the framework of the the Brezis-Ekeland-Nayroles principle To illustrate the general formalism and to show how the BEN principle allows developing powerful variational principles for dissipative systems within the framework of continuum mechanics, we consider the standard plasticity and viscoplasticity in small deformations.

Consider an elastic perfectly plastic solid occupying the volume Ω with a smooth boundary $\partial\Omega$. It is loaded by given body forces \mathbf{f}^v on Ω , a prescribed displacement field \mathbf{u}^d on Γ_u and surface tractions \mathbf{t}^d exerted on the complementary part $\Gamma_t = \partial\Omega - \Gamma_u$. Recall that Γ_u and Γ_t are fixed and they satisfy $\Gamma_u \cap \Gamma_t = \emptyset$. The data set $(\mathbf{f}^v, \mathbf{t}^d, \mathbf{u}^d)$ depends on the time t in the time interval $[0, T]$ and characterizes the mechanical loading path at every point $\mathbf{x} \in \Omega$.

The strain field is decomposed into elastic and plastic strains parts:

$$\boldsymbol{\varepsilon} = \boldsymbol{\varepsilon}^e + \boldsymbol{\varepsilon}^p = \mathbf{S} \boldsymbol{\sigma} + \boldsymbol{\varepsilon}^p$$

where \mathbf{S} is the elastic compliance tensor. Let $\Omega \subset \mathbb{R}^n$ be a bounded, open set, with piecewise smooth boundary $\partial\Omega$. As usual, it is divided into disjoint parts, $\partial\Omega_0$ (called support) where the displacements are imposed and $\partial\Omega_1$ where the surface forces are imposed. U and E are suitable functional spaces of displacement and stress fields on Ω . The standard duality between stress and strain fields is:

$$\langle \boldsymbol{\sigma}, \boldsymbol{\varepsilon} \rangle = \int_{\Omega} \boldsymbol{\sigma} : \boldsymbol{\varepsilon} \, d\Omega$$

Let φ be a convex lower semicontinuous dissipation potential and φ^* be its Fenchel transform. The symmetric gradient is denoted ∇ . Applied to the quasi-static plasticity, the BEN principle

claims that the evolution curves $\boldsymbol{\sigma} : [0, T] \rightarrow E$ and $\mathbf{u} : [0, T] \rightarrow U$ minimize (Buliga and de Saxcé, 2017):

$$\bar{\Pi}(\boldsymbol{\sigma}, \dot{\mathbf{u}}) = \int_0^T \{\varphi(\boldsymbol{\sigma}) + \varphi^*(\nabla \dot{\mathbf{u}} - \mathbf{S}\dot{\boldsymbol{\sigma}}) - \langle \boldsymbol{\sigma}, \nabla \dot{\mathbf{u}} - \mathbf{S}\dot{\boldsymbol{\sigma}} \rangle\} dt \quad (2.1)$$

among all curves satisfying:

- the equilibrium equations:

$$\operatorname{div} \boldsymbol{\sigma} + \mathbf{f} = \mathbf{0} \quad \text{in } \Omega, \quad \boldsymbol{\sigma} \cdot \mathbf{n} = \bar{\mathbf{t}} \quad \text{on } \partial\Omega_1 \quad (2.2)$$

- the kinematical conditions on supports:

$$\mathbf{u} = \bar{\mathbf{u}} \quad \text{on } \partial\Omega_0 \quad (2.3)$$

- and the initial conditions:

$$\boldsymbol{\sigma}(0) = \boldsymbol{\sigma}_0, \quad \mathbf{u}(0) = \mathbf{u}_0 \quad (2.4)$$

Proof

Introducing densities ϕ and ϕ^* such that:

$$\varphi(\boldsymbol{\sigma}) = \int_{\Omega} \phi(\boldsymbol{\sigma}) d\Omega, \quad \varphi^*(\boldsymbol{\varepsilon}^p) = \int_{\Omega} \phi^*(\boldsymbol{\varepsilon}^p) d\Omega,$$

Equation (2.1) reads:

$$\bar{\Pi}(\boldsymbol{\sigma}, \dot{\mathbf{u}}) = \int_{\Omega} \int_0^T [\phi(\boldsymbol{\sigma}) + \phi^*(\nabla \dot{\mathbf{u}} - \mathbf{S}\dot{\boldsymbol{\sigma}}) - \boldsymbol{\sigma} : (\nabla \dot{\mathbf{u}} - \mathbf{S}\dot{\boldsymbol{\sigma}})] dt d\Omega \quad (2.5)$$

Because of Fenchel's inequality:

$$\forall \boldsymbol{\sigma}', \dot{\boldsymbol{\varepsilon}}'^p, \quad \phi(\boldsymbol{\sigma}') + \phi^*(\dot{\boldsymbol{\varepsilon}}'^p) \geq \boldsymbol{\sigma}' : \dot{\boldsymbol{\varepsilon}}'^p$$

we have the minimum principle:

$$\forall \boldsymbol{\sigma}', \dot{\mathbf{u}}', \quad \bar{\Pi}(\boldsymbol{\sigma}', \dot{\mathbf{u}}') \geq 0$$

The minimum is realized if almost everywhere the couple $(\boldsymbol{\sigma}, \nabla \dot{\mathbf{u}} - \mathbf{S}\dot{\boldsymbol{\sigma}})$ is extremal:

$$\phi(\boldsymbol{\sigma}) + \phi^*(\nabla \dot{\mathbf{u}} - \mathbf{S}\dot{\boldsymbol{\sigma}}) = \boldsymbol{\sigma} : (\nabla \dot{\mathbf{u}} - \mathbf{S}\dot{\boldsymbol{\sigma}})$$

or, equivalently, the differential inclusion:

$$\nabla \dot{\mathbf{u}} \in \mathbf{S} \dot{\boldsymbol{\sigma}} + \partial \phi(\boldsymbol{\sigma}) \quad (2.6)$$

that is the strain decomposition into the elastic part and the plastic one, combined with the flow rule, and:

$$\boldsymbol{\sigma} \in \partial \phi^*(\nabla \dot{\mathbf{u}} - \mathbf{S} \dot{\boldsymbol{\sigma}})$$

that is the inverse law. These differential inclusions must be satisfied together with the *a priori* admissibility conditions (2.2) to (2.4).

For the particular case of plasticity, the potential ϕ being the indicatory function of the elastic domain K , the differential inclusion (2.6) means:

$$\forall \boldsymbol{\sigma}' \in K, \quad (\nabla \dot{\mathbf{u}} - \mathbf{S} \dot{\boldsymbol{\sigma}}) : (\boldsymbol{\sigma}' - \boldsymbol{\sigma}) \leq 0$$

that is Hill's maximum principle.

2.2 Application to the pressurized thick-walled tube

Thanks to the eqs. (2.1,2.2,2.3,2.4), the structural problem can be solved as a constrained optimization problem. To start up, we choose a classical academic example, the thick-walled tube subjected to an internal pressure. The internal and external radii of the tube are a and b respectively. The material parameters are the Young modulus E , Poisson's coefficient ν and the yield stress σ_Y . We suppose that the thick tube is in plane strain and the initial fields are vanishing. If the internal pressure grows monotonically from zero to the limit load, the internal surface of the tube $r = a$ will come to yield first, next the plastic yielding will spread within the tube up to reach the external surface $r = b$.

Three nonlinear constitutive laws are considered in the sequel: (i) an elastic perfectly plastic behavior with von Mises criterion, (ii) an elastic perfectly plastic tube with Tresca model and (iii) the Norton-Odqvist viscoplastic law. The Norton-Odqvist law will be discussed separately due to its special character. In this section, we first specialize the functional (2.5) of the BEN principle to the thick tube problem, then we present the mixed FEM discretization.

2.2.1 Basic equations

As the BEN principle applies the dissipation potential and its Fenchel transform, their analytical expressions for the thick tube problem need to be deduced firstly. Taking into account the hypotheses of axisymmetry and plane strain, 1D axisymmetric element along the radius is employed. The displacement field \mathbf{u} is radial and depends only on the radial coordinate :

$$\mathbf{u} = u_r(r) \mathbf{e}_r$$

The stress and strain tensors are given in small deformations hypothesis by:

$$\boldsymbol{\sigma} = \begin{pmatrix} \sigma_r & 0 \\ 0 & \sigma_\theta \end{pmatrix}, \quad \boldsymbol{\varepsilon} = \begin{pmatrix} \frac{du_r}{dr} & 0 \\ 0 & \frac{u_r}{r} \end{pmatrix} \quad (2.7)$$

Hooke's law in plane strain is:

$$\varepsilon_r = \frac{1}{\bar{E}}(\sigma_r - \bar{\nu}\sigma_\theta) \quad , \quad \varepsilon_\theta = \frac{1}{\bar{E}}(\sigma_\theta - \bar{\nu}\sigma_r)$$

with:

$$\bar{E} = \frac{E}{1-\nu^2} \quad , \quad \bar{\nu} = \frac{\nu}{1-\nu}$$

Tresca criterion reads:

$$f_T(\boldsymbol{\sigma}) = |\sigma_\theta - \sigma_r| - \sigma_Y \leq 0 \quad (2.8)$$

Denoting the deviatoric stress by \mathbf{s} , von Mises yield condition is:

$$f_{VM}(\boldsymbol{\sigma}) = \sigma_{eq}(\mathbf{s}) - \sigma_Y = \sqrt{\frac{3}{2} \mathbf{s} : \mathbf{s}} - \sigma_Y \leq 0 \quad \text{with} \quad \mathbf{s} = \boldsymbol{\sigma} - \frac{1}{3} \text{tr} \boldsymbol{\sigma} \mathbb{1} \quad (2.9)$$

The convex elastic domain is:

$$K = \{\boldsymbol{\sigma} \quad \text{such that} \quad f(\boldsymbol{\sigma}) \leq 0\}$$

where f is f_T or f_{VM} depending on the model. The dissipation power by unit volume is given by:

$$D = \boldsymbol{\sigma} : \dot{\boldsymbol{\varepsilon}}^P$$

where $\boldsymbol{\sigma}$ and $\dot{\boldsymbol{\varepsilon}}^P$ are associated by the normality law. As we impose an internal pressure, we can suppose that $\sigma_\theta > \sigma_r$. For Tresca criterion, the normality rule gives $\dot{\varepsilon}_\theta^P = -\dot{\varepsilon}_r^P = \lambda$ ($\lambda > 0$ is the

plastic multiplier) and the dissipation power is:

$$D = \sigma_\theta \dot{\varepsilon}_\theta^p + \sigma_r \dot{\varepsilon}_r^p = (\sigma_\theta - \sigma_r) \dot{\varepsilon}_\theta^p = \sigma_Y \lambda \quad (2.10)$$

With von Mises criterion, the normality rule is $\dot{\varepsilon}^p = \lambda \frac{3\mathbf{s}}{2\sigma_{\text{eq}}}$. The dissipation power has the same expression as the one of Tresca criterion:

$$D = \lambda \frac{3\mathbf{s} : \mathbf{s}}{2\sigma_{\text{eq}}} = \lambda \frac{\sigma_{\text{eq}}^2}{\sigma_{\text{eq}}} = \lambda \sigma_{\text{eq}} = \sigma_Y \lambda \quad (2.11)$$

The dissipation potential for both criteria is:

$$\varphi(\boldsymbol{\sigma}) = \int_{\Omega} \chi_K d\Omega$$

where χ_K is the indicator function of the elastic domain K . The Fenchel transform is:

$$\varphi^*(\dot{\varepsilon}^p) = \int_{\Omega} D d\Omega$$

Applying the BEN principle, we minimize the functional (2.5) that reads:

$$\bar{\Pi}(\boldsymbol{\sigma}, \mathbf{u}) = \int_0^T \int_{\Omega} (D - \langle \boldsymbol{\sigma}, \nabla \dot{\mathbf{u}} - \mathbf{S} \dot{\boldsymbol{\sigma}} \rangle) d\Omega dt \quad (2.12)$$

among all the curves $(\boldsymbol{\sigma}, \mathbf{u}) : [0, T] \rightarrow U \times E$ such that $\boldsymbol{\sigma}(0) = \mathbf{0}$, $\mathbf{u}(0) = \mathbf{0}$, satisfying Tresca or von Mises yield condition, the normality rule and the equilibrium equations.

2.2.2 The mixed finite element method for thick tube problem

To implement the BEN principle numerically, we need to discretize the functional (2.12). As discussed in the introduction, the standard or displacement finite elements are widely used in FEM software. Although easy to implement, this kind of element exhibits a displacement field convergence faster than the one of the stress field, a weak quantity satisfying the equilibrium only in an average sense. For this reason, local stress values are deemed to be not very accurate. This is particularly harmful in plasticity because the yield criterion is expressed directly in terms of the stresses.

The BEN principle is based on a 2-field functional, that leads naturally to discretize the displacement and stress fields, which is especially welcome in plasticity to satisfy more accurately the yield criterion. For this reason, we opt for a mixed finite element. It is worth noting that the choice of the mixed formulation is not mandatory, and it is also possible to combine the BEN

principle with standard displacement elements. In fact, in the minimum principle, the stress field can be replaced by the relation $\boldsymbol{\sigma} = \mathbf{S}^{-1} : (\boldsymbol{\varepsilon} - \boldsymbol{\varepsilon}^p)$.

For the thick tube problem, there are three unknown fields: the stress tensor, the radial displacement and the plastic multiplier. These fields are not independent one of each other because the constraints of the optimization problem must be satisfied *a priori*.

1. The stress field We consider a reference axisymmetric element of thick tube with $\alpha \leq r \leq \beta$. There are two stress connectors (radial σ_r and hoop σ_θ stresses) per extremity, gathered in the elementary vector:

$$\mathbf{g}_e = \begin{bmatrix} g_1 \\ g_2 \\ g_3 \\ g_4 \end{bmatrix} = \begin{bmatrix} \sigma_r |_{r=\alpha} \\ \sigma_\theta |_{r=\alpha} \\ \sigma_r |_{r=\beta} \\ \sigma_\theta |_{r=\beta} \end{bmatrix} \quad (2.13)$$

We choose a polynomial elementary stress field $\boldsymbol{\sigma}_e$ which depends on the stress parameters \mathbf{h} of the element. The expression of the hoop stress is derived from the equilibrium equation $\sigma_\theta = \frac{d}{dr}(r\sigma_r)$, that gives in matrix form:

$$\boldsymbol{\sigma}_e(r) = \mathbf{R}_e(r) \mathbf{h} \quad (2.14)$$

$$\begin{bmatrix} \sigma_r \\ \sigma_\theta \end{bmatrix} = \begin{bmatrix} 1 & r & r^2 & r^3 \\ 1 & 2r & 3r^2 & 4r^3 \end{bmatrix} \begin{bmatrix} h_1 \\ h_2 \\ h_3 \\ h_4 \end{bmatrix} \quad (2.15)$$

Owing to (2.13,2.15), we obtain the elementary stress connectors \mathbf{g}_e in terms of the stress parameters \mathbf{h} :

$$\mathbf{g}_e = \mathbf{C}_e \mathbf{h} \quad (2.16)$$

$$\begin{bmatrix} g_1 \\ g_2 \\ g_3 \\ g_4 \end{bmatrix} = \begin{bmatrix} 1 & \alpha & \alpha^2 & \alpha^3 \\ 1 & 2\alpha & 3\alpha^2 & 4\alpha^3 \\ 1 & \beta & \beta^2 & \beta^3 \\ 1 & 2\beta & 3\beta^2 & 4\beta^3 \end{bmatrix} \begin{bmatrix} h_1 \\ h_2 \\ h_3 \\ h_4 \end{bmatrix}$$

By eliminating the stress parameters between (2.14,2.16), the elementary stress field $\boldsymbol{\sigma}_e$ is expressed in terms of stress connector \mathbf{g}_e of the element:

$$\boldsymbol{\sigma}_e(r) = \mathbf{R}_e(r)\mathbf{C}_e^{-1}\mathbf{g}_e = \mathbf{T}_e(r)\mathbf{g}_e \quad (2.17)$$

2. The displacement field For the same element occupying $\alpha \leq r \leq \beta$, there is one displacement degree of freedom \mathbf{q}_e at each extremity:

$$q_1 = u_r |_{r=\alpha} \quad q_2 = u_r |_{r=\beta}$$

In order to provide a strain field which has the same number of parameters as the one of the stress field, we add two intermediate equidistant nodes inside the element:

$$r = \gamma = \frac{2\alpha + \beta}{3} \quad r = \delta = \frac{\alpha + 2\beta}{3}$$

and two extra degrees of freedom associated to bubble modes:

$$q_3 = u_r |_{r=\gamma} \quad q_4 = u_r |_{r=\delta}$$

The four displacement degrees of freedom are gathered in the vector:

$$\mathbf{q}_e = \begin{bmatrix} q_1 \\ q_2 \\ q_3 \\ q_4 \end{bmatrix} = \begin{bmatrix} u_r |_{r=\alpha} \\ u_r |_{r=\beta} \\ u_r |_{r=\gamma} \\ u_r |_{r=\delta} \end{bmatrix} \quad (2.18)$$

For a cubic Lagrange interpolation, the displacement field u_r depends on the displacement degree of freedom \mathbf{q}_e through:

$$u_r(r) = \mathbf{N}_e(r)\mathbf{q}_e \quad (2.19)$$

with:

$$\mathbf{N}_e^T(r) = \frac{1}{16} \begin{bmatrix} -(1-\eta)(1-9\eta^2) \\ -(1+\eta)(1-9\eta^2) \\ 9(1-\eta^2)(1-3\eta) \\ 9(1-\eta^2)(1+3\eta) \end{bmatrix} \quad \eta = \frac{2r - (\beta + \alpha)}{\beta - \alpha}$$

Taking into account (2.7), the strain field reads:

$$\boldsymbol{\varepsilon}_e(r) = \mathbf{B}_e(r) \mathbf{q}_e \quad (2.20)$$

with:

$$\mathbf{B}_e^T(r) = \frac{1}{16} \begin{bmatrix} J(1 + 18\eta - 27\eta^2) & -\frac{1}{r}(1 - \eta)(1 - 9\eta^2) \\ J(-1 + 18\eta + 27\eta^2) & -\frac{1}{r}(1 + \eta)(1 - 9\eta^2) \\ J(-27 - 18\eta + 81\eta^2) & \frac{9}{r}(1 - \eta^2)(1 - 3\eta) \\ J(27 - 18\eta - 81\eta^2) & \frac{9}{r}(1 - \eta^2)(1 + 3\eta) \end{bmatrix} \quad J = \frac{d\eta}{dr} = \frac{2}{\beta - \alpha}$$

3. The plastic multiplier field The plastic criterion is enforced only at the four Gauss points g , running from 1 to 4, of position r_g (Seitz et al., 2015), that is sufficient to compute the integral of the dissipation. Introducing the local value λ_g of the plastic multipliers at the Gauss points of the elements, the flow rule reads:

$$\dot{\boldsymbol{\varepsilon}}_e^p(r_g) = \lambda_g \frac{\partial f}{\partial \boldsymbol{\sigma}} \Big|_{r=r_g} \quad (2.21)$$

The values λ_g of the plastic multipliers at the integration points are gathered in the vector $\boldsymbol{\lambda}_e$. For the thick tube problem, we have three discretized fields for one element $\alpha \leq r \leq \beta$, stress $\boldsymbol{\sigma}_e$, displacement \mathbf{u}_r and plastic strain rate $\dot{\boldsymbol{\varepsilon}}_e^p$ which depend on each degrees of freedom, stress \mathbf{g}_e , displacement \mathbf{q}_e and plastic multipliers $\boldsymbol{\lambda}_e$:

$$\boldsymbol{\sigma}_e(r) = \mathbf{T}_e(r) \mathbf{g}_e \quad \mathbf{u}_r(r) = \mathbf{N}_e(r) \mathbf{q}_e \quad \dot{\boldsymbol{\varepsilon}}_e^p(r_g) = \lambda_g \frac{\partial f}{\partial \boldsymbol{\sigma}} \Big|_{r=r_g}$$

2.2.3 Discretization of the BEN functional

As the BEN functional (2.12) is a space-time integral dependent, two kinds of discretization methods are applied.

Space integral discretization The space integral is approximated by the usual Gaussian quadrature numerical integration method on every elementary axisymmetric element:

$$\int_{\alpha}^{\beta} \mathbf{A}(r) 2\pi r dr \cong \sum_{g=1}^4 w_g \mathbf{A}(r_g) 2\pi r_g$$

Thanks to the localization matrices $\mathbf{M}_e, \mathbf{L}_e, \mathbf{P}_e$ for each unknown field, we can carry out the assembling:

$$\mathbf{g}_e = \mathbf{M}_e \mathbf{g}, \quad \mathbf{q}_e = \mathbf{L}_e \mathbf{q}, \quad \boldsymbol{\lambda}_e = \mathbf{P}_e \boldsymbol{\lambda}$$

The spatial discretized form of the functional (2.12) is:

$$\bar{\Pi}(\mathbf{g}, \mathbf{q}, \boldsymbol{\lambda}) = \int_0^T (\boldsymbol{\Lambda}^T \boldsymbol{\lambda}(t) - \dot{\mathbf{q}}^T(t) \mathbf{G} \mathbf{g}(t) + \dot{\mathbf{g}}^T(t) \mathbf{F} \mathbf{g}(t)) \, dt \quad (2.22)$$

with:

$$\begin{aligned} \boldsymbol{\Lambda} &= \sum_{e=1}^{ne} \mathbf{P}_e^T \boldsymbol{\Lambda}_e, \\ \mathbf{G} &= \sum_{e=1}^{ne} \int_{\alpha}^{\beta} \mathbf{L}_e^T \mathbf{B}_e^T(r) \mathbf{T}_e(r) \mathbf{M}_e 2\pi r \, dr \\ \mathbf{F} &= \sum_{e=1}^{ne} \int_{\alpha}^{\beta} \mathbf{M}_e^T \mathbf{T}_e^T(r) \mathbf{S} \mathbf{T}_e(r) \mathbf{M}_e 2\pi r \, dr \end{aligned}$$

and:

$$\boldsymbol{\Lambda}_e = 2\pi \sigma_Y \begin{bmatrix} w_1 r_1 \\ w_2 r_2 \\ w_3 r_3 \\ w_4 r_4 \end{bmatrix}$$

under the constraints of:

- equilibrium (on the boundary, the internal equilibrium being satisfied *a priori*):

$$g(t) |_{r=a} = -p(t), \quad g(t) |_{r=b} = 0 \quad (2.23)$$

- plastic criterion (at every Gauss point g of every element e):

$$f_e(r_g) - \sigma_Y \leq 0, \quad \lambda_g \geq 0, \quad \lambda_g \frac{\partial f}{\partial \boldsymbol{\sigma}} |_{r=r_g} = \mathbf{B}_e(r_g) \dot{\mathbf{q}}_e - \mathbf{S} \mathbf{T}_e(r_g) \dot{\mathbf{g}}_e \quad (2.24)$$

- initial conditions:

$$\mathbf{g}(0) = \mathbf{0}, \quad \mathbf{q}(0) = \mathbf{0}, \quad \boldsymbol{\lambda}(0) = \mathbf{0} \quad (2.25)$$

with ne the total element number, and $f_e(r_g)$ linear for Tresca criterion and quadratic for von Mises one. Eqs. (2.23) means that the internal surface is subjected to the pressure and the external one is free force. Eqs. (2.24) are the plasticity conditions discretized at every Gauss

point, the first one being the plastic criterion, the last one being the decomposition of the total strains rate. Eqs. (2.25) are the initial conditions.

Time integral discretization We impose t_j as the temporal points with $j = [0, \dots, m-1, m]$. There are m time steps with $m+1$ temporal points. For any physical quantity a at temporal point t_j , we note:

$$a_j = a(t_j) \quad \Delta a_j = a_j - a_{j-1} \quad \Delta t_j = t_j - t_{j-1} \quad j = 1, \dots, m$$

On each step, we approximate the time rate by:

$$\dot{a}_j = \frac{\Delta a_j}{\Delta t_j}$$

As the plasticity is independent of the time parameterization in quasi-static situation, we use fictive time for convenience sake:

$$\Delta t_j = 1 \tag{2.26}$$

The time integral is simply approximated by using the rectangular:

$$\int_0^T f(t) dt = \sum_{j=1}^m f(t_j) \Delta t_j$$

This rule can appear rather rough but the numerical experience for the problem under consideration showed that changing of this quadrature rule by another one, for instance the midpoint rule, does not provide significant improvements.

Considering m time step from t_0 to t_m and enforcing the yield condition only at the beginning and the end of the step, we have to minimize the objective function:

$$\bar{\Pi}(\mathbf{g}_0, \dots, \mathbf{g}_m, \mathbf{q}_0, \dots, \mathbf{q}_m, \boldsymbol{\lambda}_0, \dots, \boldsymbol{\lambda}_m) = \sum_{j=1}^m (\boldsymbol{\Lambda}^T \boldsymbol{\lambda}_j - \Delta \mathbf{q}_j^T \mathbf{G} \mathbf{g}_j + \Delta \mathbf{g}_j^T \mathbf{F} \mathbf{g}_j) \tag{2.27}$$

under the constraints of:

- equilibrium (on the boundary, at each end of the time step):

$$g_j |_{r=a} = -p(t_j), \quad g_j |_{r=b} = 0 \tag{2.28}$$

- plastic criterion (at every Gauss point g of every element e and at every end of the time

step):

$$f_{e,j}(r_g) - \sigma_Y \leq 0, \quad \lambda_{g,j} \geq 0 \quad \lambda_{g,j} \frac{\partial f}{\partial \boldsymbol{\sigma}} \Big|_{r=r_{g,j}} = \mathbf{B}_e(r_g) \mathbf{L}_e \Delta \mathbf{q}_j - \mathbf{S} \mathbf{T}_e(r_g) \mathbf{M}_e \Delta \mathbf{g}_j \quad (2.29)$$

- initial conditions:

$$\mathbf{g}_0 = \mathbf{0}, \quad \mathbf{q}_0 = \mathbf{0}, \quad \boldsymbol{\lambda}_0 = \mathbf{0} \quad (2.30)$$

After the discretization of spatial and temporal integrals, all constraints are verified at each Gauss point for all temporal points at once.

We have transformed an evolution problem into a constrained optimization problem as shown in eqs. (2.27,2.28,2.29,2.30). Its solution provides the values of every field at each spatially discretized point and each temporal point. Instead of solving the problem step-by-step, we simultaneously determine the mechanical quantities for all steps. On the one hand, we are no longer concerned by the choice of the time integrators, which are very sensitive to convergence and stability troubles. On the other hand, because the variational principle is on the space-time, our strategy could lead to larger size problems to a time-consuming resolution if we do not optimize the solving algorithm. For the moment, our aim is only to verify the feasibility of the numerical method based on the BEN principle, postponing to a subsequent work the optimization task.

2.3 Results and discussion

The algorithm presented in the previous sections is implemented in MATLAB code and the solver `fmincon` which provides a local minimum of a linear or quadratic constrained nonlinear multivariable function is used. The functional (2.27) is a quadrature non-linear function under linear constraints for Tresca criterion or quadratic ones for von Mises model.

The spacial integrals are computed numerically by using the Gaussian quadrature method while the time integrals are approximated by the rectangular rule. Moreover, basing upon numerical experiences, it is preferred to impose a tiny tolerance for the equality optimization constraint (2.29). The tolerance is selected such that the numerical minimum of the cost functional (2.27) is closest to zero because the theoretical minimum of the objective function is vanishing.

For all fields and at any time t , the optimization 'starting points' values are 0.1 aiming to reduce computation time as the analytical minimum of the functional is zero .

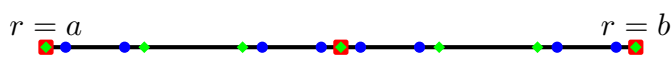
In the sequel, the following cases are studied :

- elastoplastic regime with von Mises model,

- elastoplastic response with Tresca criterion,
- viscoplastic response with Norton-Odqvist model.

The geometric parameters and the material coefficients used are $a = 100$ mm, $b = 200$ mm, $E = 210$ GPa, $\nu = 0.3$ and $\sigma_Y = 360$ MPa. For all numerical examples, starting from an initial stress free state, the internal pressure is increasing linearly with the time from 0 to desired value p .

Figure 2.1 displays the numbering system with two elements and two temporal points for the thick-walled tube problem. The total number of degrees of freedom (dof) for different numbers of temporal points (nt) and number of elements (ne) are shown in table 2.1:



first temporal point $t = 0$	1			3			5
	2			4			6
	7	9	10	8	12	13	11
	14	15	16	17 18	19	20	21
second temporal point $t = 1$	22			24			26
	23			25			27
	28	30	31	29	33	34	32
	35	36	37	38 39	40	41	42

Figure 2.1: Numbering system for the 1D axisymmetric thick-walled tube (solid black line) with two elements ($ne = 2$) and two temporal points ($nt = 2$) the stresses \mathbf{g} (red), displacement \mathbf{q} (green) and plastic multiplier λ (blue) fields.

Table 2.1: Degrees of freedom (dof) for different numbers of temporal points (nt) and elements (ne)

dof	ne = 1	ne = 2	ne = 4	ne = 6
nt = 2	24	42	78	114
nt = 3	36	63	117	171

The numerical results obtained by the BEN principle are compared to the incremental numerical predictions performed with the finite element code *Cast3M* (Cast3M, 2019) (an open-source incremental software developed by French Alternative Energies and Atomic Energy Commission (CEA)).

The loading path is plotted in figure 2.2.

2.3.1 Elastic response

Let us consider two temporal points, $t = 0$ and $t = 1$. Without loss of generality, we suppose that the initial values ($t = 0$) of all mechanical fields are vanishing and for $t = 1$, the imposed

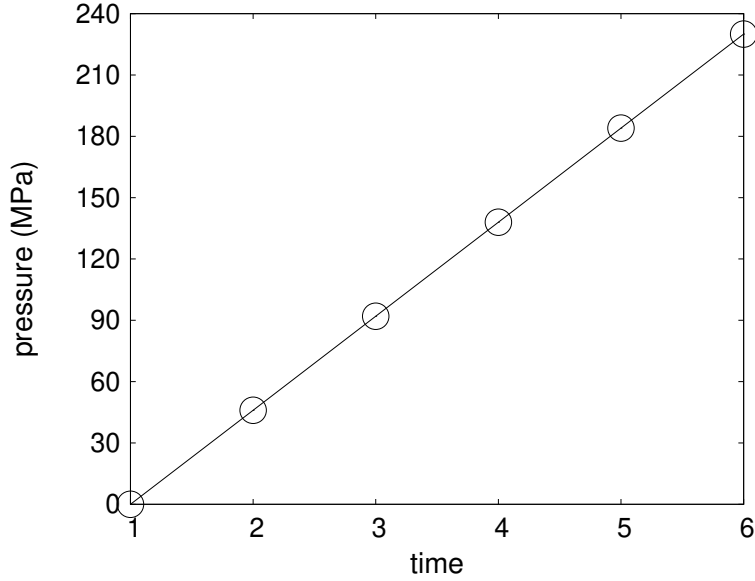


Figure 2.2: The loading path with 6 temporal points.

pressure is $p = 100$ MPa ($p > p_e$). Simulation results are shown in 2.3 and 2.4. It can be observed that with only one element ($ne = 1$), the convergence of the radial stress is better than the one of the hoop stress because the pressure is imposed on the internal surface (2.3). A good accuracy is reached in practice with 4 elements (Fig. 2.4) for the stresses and the displacement. As the plastic multipliers are equal to zero in the elastic regime, they are not displayed here. By increasing the number of element to 3, the BEN principle result already converges to the analytical solution.

To conclude for the elastic regime, as expected the BEN principle solution converges quickly to the analytical solution while refining the mesh even though this principle has been developed for dissipative media. Moreover, for one element, the convergence of the stress field is faster than the one of the displacement.

2.3.2 Elastoplastic response with von Mises criterion

It is worth to observe that in classical step-by-step methods, a prediction-corrector scheme as the radial return algorithm is required to integrate the non-linear elastoplastic constitutive law. With the BEN principle, it is not so.

The elastoplastic solution is computed by the BEN method simultaneously at the 6 temporal points while Cast3M's predictions are computed causally step-by-step. Figures 2.5 and 2.6 display the stress and displacement fields respectively as function of radius at the instant $t = 3$, that is the elastic regime under an internal pressure $p = 92$ MPa. Therefore, the BEN principle which

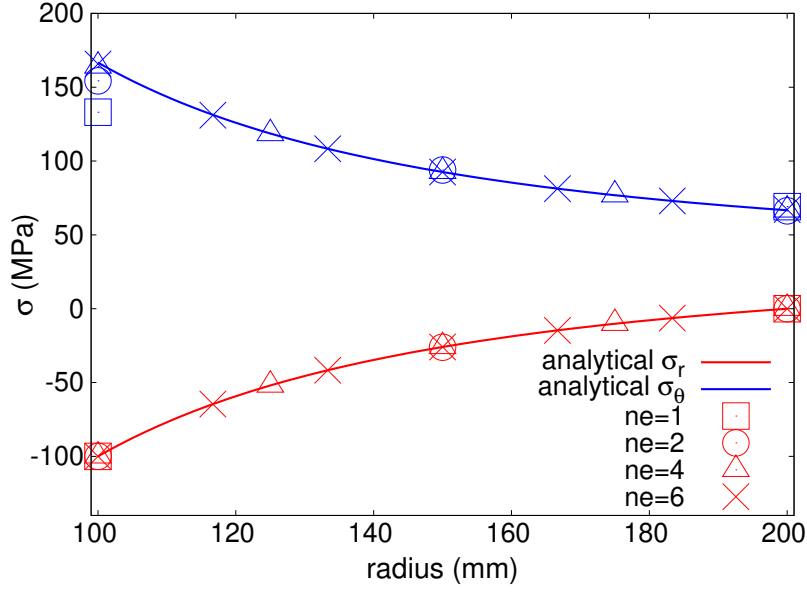


Figure 2.3: Comparison between the BEN principle solution (symbols) and analytical solution (solid line) in the elastic regime: the radial σ_r (red) and hoop σ_θ (blue) stresses with 1, 2, 4 and 6 elements (ne) for $p = 100$ MPa when $t = 1$.

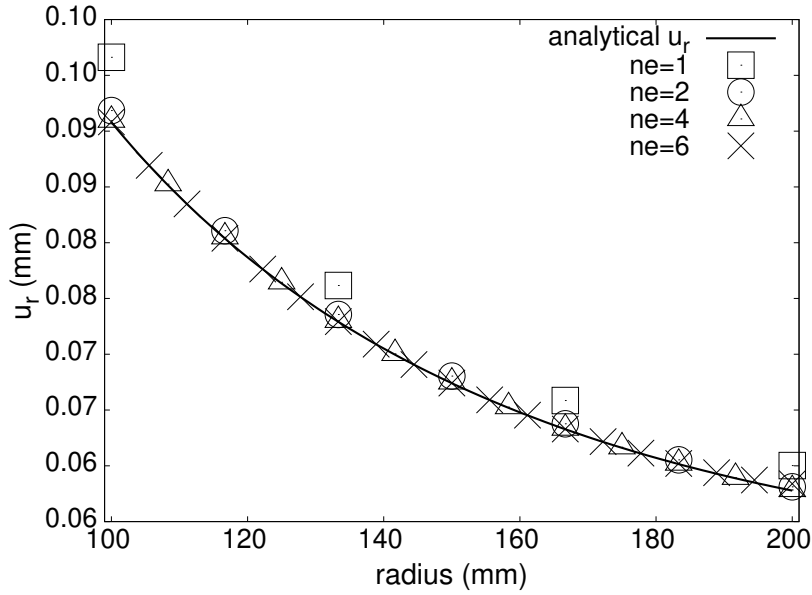


Figure 2.4: Comparison between the BEN principle solution (symbols) and analytical solution (solid line) in the elastic regime: the radial displacement u_r with 1, 2, 4 and 6 elements (ne) for $p = 100$ MPa when $t = 1$.

is devoted to dissipative systems works also for elasticity. Here, the elastic case has been tested to verify that the method allows also to detect and to solve the elastic problem in the event that the yield limit is not reached everywhere. Of course, if we know a priori that the problem is elastic, it is more efficient to use a solver of linear problems.

For the temporal points $t = 5$ and $t = 6$, the applied internal pressure is greater than p_e and the thick-walled tube experiences elastoplastic behavior such that irreversible plastic deformation

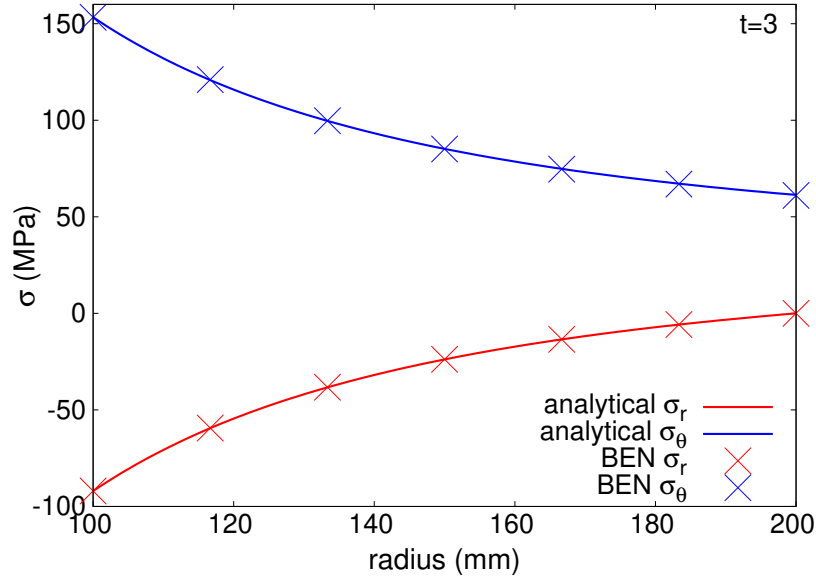


Figure 2.5: Comparison between the BEN principle solution (symbols) and analytical reference solution (solid line) in the elastic regime: the radial σ_r (red) and hoop σ_θ (blue) stresses for $t = 3$ and with 6 elements under an internal pressure $p = 92$ MPa.

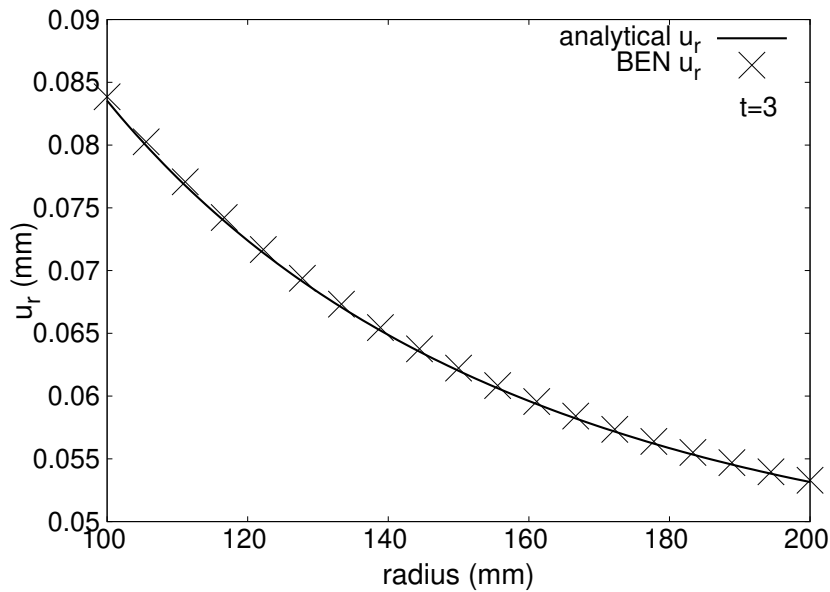


Figure 2.6: Comparison between the BEN principle solution (symbols) and analytical solution (solid line) in the elastic regime: the radial displacement u_r for $t = 3$ and with 6 elements under an internal pressure $p = 92$ MPa.

develops on a part of the tube. Figures 2.7 and 2.8 illustrate the comparison between the radial and hoop stress components obtained by the BEN method and the step-by-step numerical results provided by Cast3M. In figure 2.9 the radial displacement component computed by both procedures is plotted. Figure 2.10 depicts the field of plastic multiplier computed by BEN's Method and by Cast3M. The numerical results prove the good accuracy of the non-incremental BEN method.

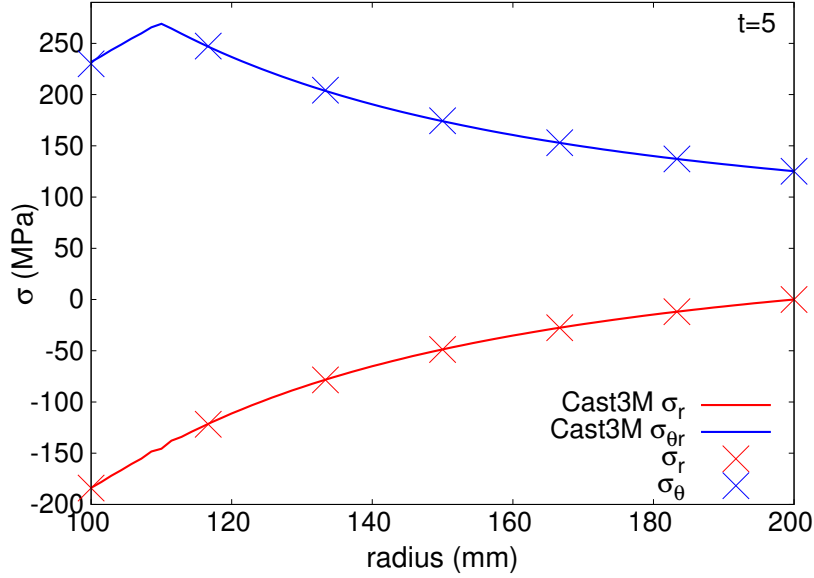


Figure 2.7: Comparison between the non-incremental BEN principle results (symbols) and step-by-step numerical predictions (solid line) in the elastoplastic regime with **von Mises criterion**: the radial σ_r (red) and hoop σ_θ (blue) stresses for $t = 5$ and with 6 elements under an internal pressure $p = 184$ MPa.

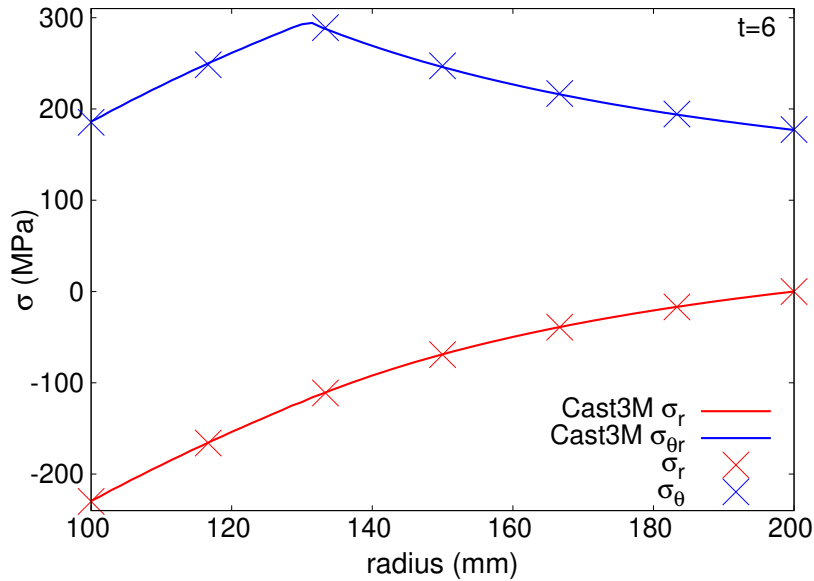


Figure 2.8: Comparison between the non-incremental BEN principle results (symbols) and numerical reference solution (solid line) in the elastoplastic regime with **von Mises criterion**: the radial σ_r (red) and hoop σ_θ (blue) stresses for $t = 6$ and with 6 elements under an internal pressure $p = 230$ MPa.

2.3.3 Elastoplastic response with Tresca criterion

The only difference between Tresca and von Mises criterion is the optimization constraint (2.29) involving to the plastic criterion. Numerical computations are conducted with 2 temporal times, and in order to shorten the paper, we present only elastoplastic results for the final temporal point correspondent to the applied pressure $p = 200$ MPa.

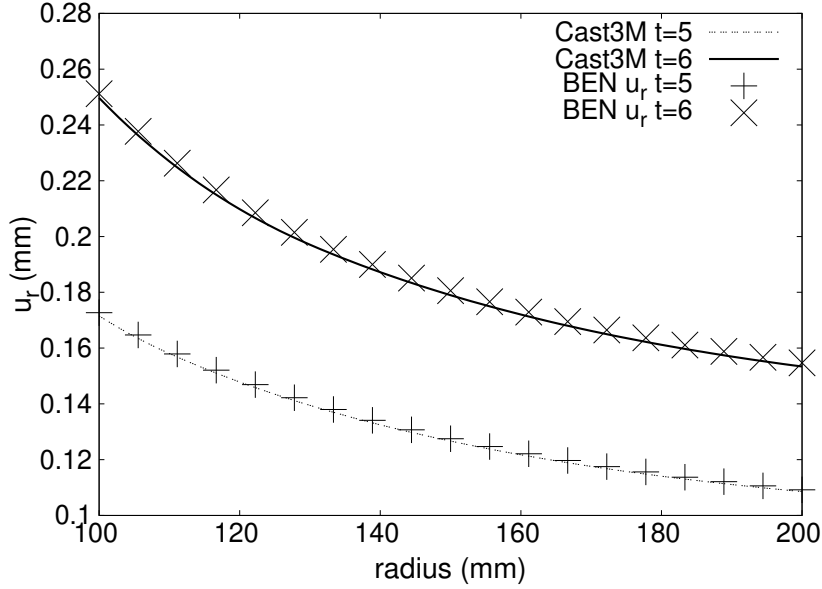


Figure 2.9: Comparison between the BEN principle solution (symbols) and numerical reference solution (solid line) in the elastoplastic regime with *von Mises criterion*: the radial displacement u_r for temporal times $t = 5$ and $t = 6$ with 6 elements.

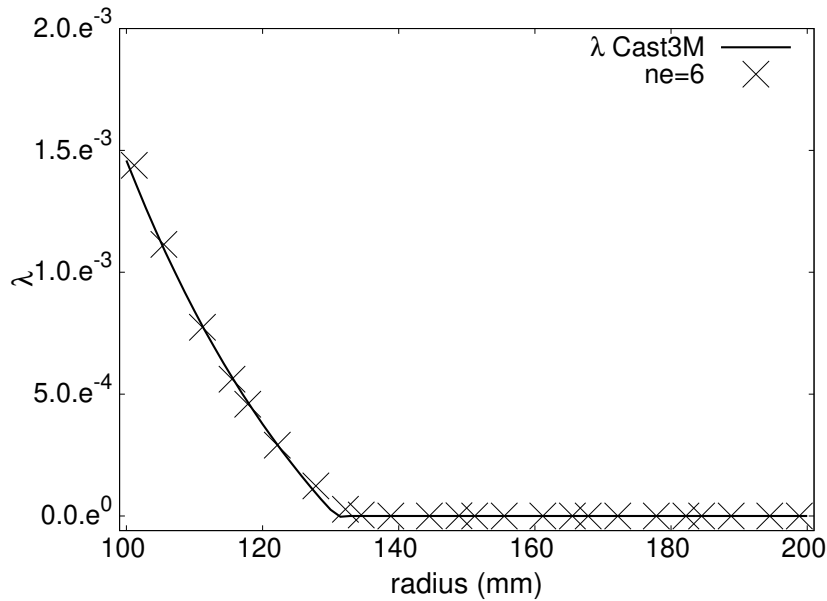


Figure 2.10: The plastic multiplier λ computed by the BEN principle method (symbols) and by incremental procedure (solid line) in the elastoplastic regime with *von Mises criterion* for the temporal point $t = 6$ and with 6 elements.

In figure 2.11 the stress components computed by the BEN variational principle are plotted together with the analytical solution provided in (Prager and Hodge, 1968; Save et al., 1997) and incremental numerical predictions performed by *Cast3M*. Figures 2.12 and 2.13 depict respectively the comparison between the radial displacement and the estimations of the plastic multipliers obtained by the BEN method and by *Cast3M*. An excellent agreement is observed and, as expected, convergence of the BEN method is better with the increase of elements number.

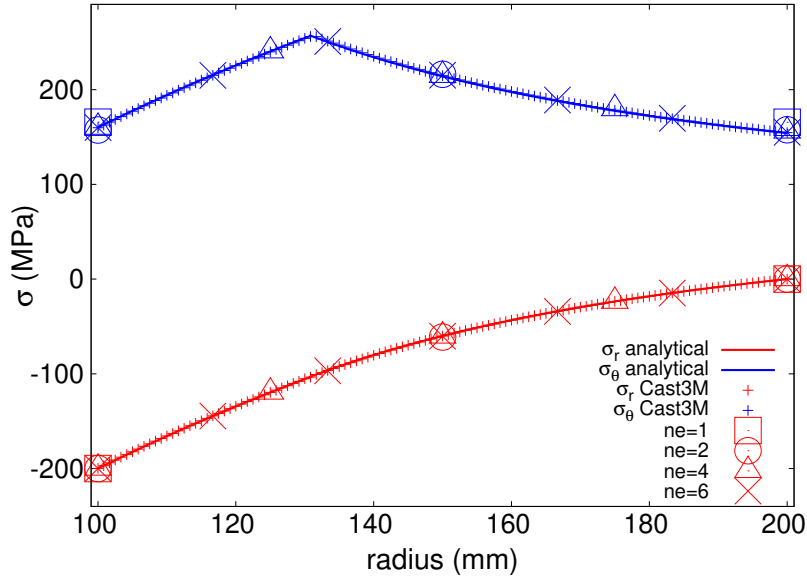


Figure 2.11: Comparison between the BEN principle solution (symbols) and numerical reference solution (solid line) in the elastoplastic regime with **Tresca criterion**: the radial σ_r (red) and hoop σ_θ (blue) stresses with 1, 2, 4 and 6 elements (ne) for $p = 200$ MPa.

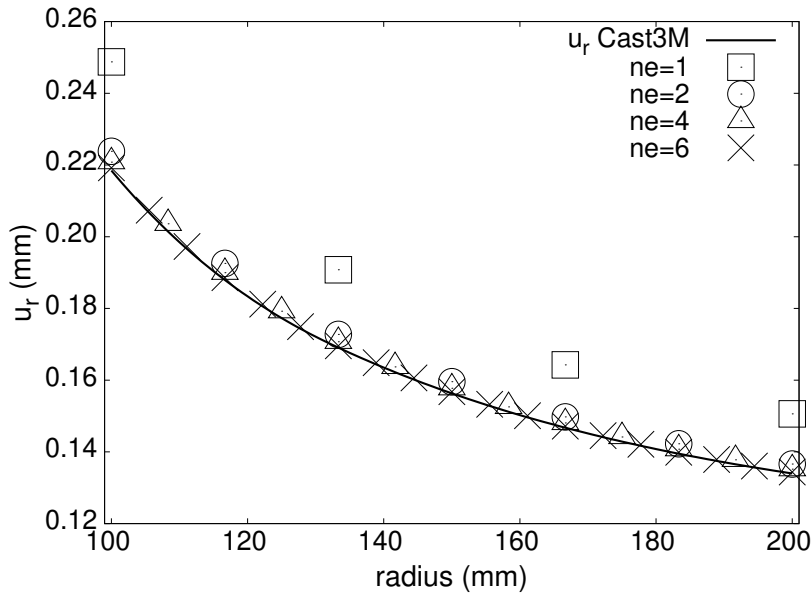


Figure 2.12: Comparison between the BEN principle solution (symbols) and numerical reference solution (solid line) in the elastoplastic regime with **Tresca criterion**: the radial displacement u_r with 1, 2, 4 and 6 elements (ne) for $p = 200$ MPa.

2.3.4 Computation cost

Matlab does not require implementation of the gradient of the functional (2.27) to perform the minimization process under constraints (2.28, 2.29, 2.30). However, its implementation should accelerate the computation process. Therefore computations by providing the functional gradient are also conducted and the corresponding results are referred "with gradient". Results obtained

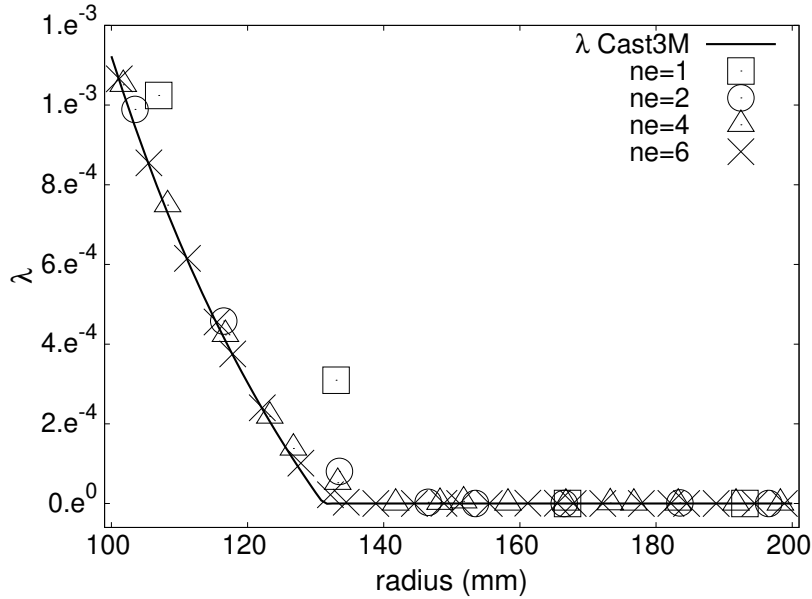


Figure 2.13: Comparison between the BEN principle solution (symbols) and the step-by-step numerical results (solid line) in the elastoplastic regime with **Tresca criterion**: the plastic multiplier λ with 1, 2, 4 and 6 elements (ne) for $p = 200$ MPa.

by the Matlab's blackbox solver *fmincon* are noted "without gradient".

The numerical simulations were performed on an Intel Core i7-6820HQ (Quad Core 2.70GHz, 3.60GHz Turbo) processor with a memory of 16Go 2400MHz DDR4 (2x8Go). The computation costs as well as the equality tolerances for the case of the elastoplastic response with von Mises criterion are presented in tables 2.2 and 2.3.

Table 2.2: Computation costs for different implementations **without** implementation of gradients ($nt = 2$), starting points are 0.01

ne	1	2	4	6	8	10	12
dof	24	42	78	114	150	186	222
optimization iterations	1096	292	120	105	282	102	132
dof×iter.	26304	13986	9360	11970	42300	18972	28638
tolerances	3.0e-5	1.1e-5	2.8e-6	6.6e-7	2.9e-7	1.6e-7	5.9e-8
functional values	-35.49	-10.54	-24.62	-0.32	-0.68	-0.79	-0.10
CPU time, s	26.39	10.75	7.11	10.73	37.91	19.96	32.93

Analyzing and comparing these two tables, the following remarks can be drawn:

- the imposed equality tolerances decreases while refining the mesh,
- the local minimums of the functional converge to zero,
- the computation cost is related both with number of dof and iterations,
- a significant reduction of the computing time is observed by providing and implementing the gradient of the cost functional.

Table 2.3: Computation costs for different implementations **with** implementation of gradient ($nt = 2$), starting points are 0.01

ne	1	2	4	6	8	10	12
dof	24	42	78	114	150	186	222
optimization iterations	125	221	555	189	462	361	565
dof \times iter.	3000	9282	43290	21546	69300	67146	125430
tolerances	2.99e-5	1.10e-5	2.60e-6	6.60e-7	2.90e-7	1.54e-7	1.24e-7
functional values	-29.59	-10.96	-4.06	-0.32	-0.68	-0.11	-7.24
CPU time, s	2.80	4.61	18.00	7.24	15.76	14.85	24.36

From the numeral point of view, the BEN principle transforms a nonlinear mechanical problem into a minimization problem for all time steps instead of the incremental method. The computing time not only depends on the total dof as the one of step-by-step, but also on the number of optimization iterations. Each optimization iteration takes more time with a refined mesh, i.e. more dof or optimization variables.

Figure 2.14 displays the relation of computation time in function of the product of the numbers of dof and iterations in bilogarithmic scale. It can be observed that there is a linear relation for the case without furnishing the gradient of the objective functional.

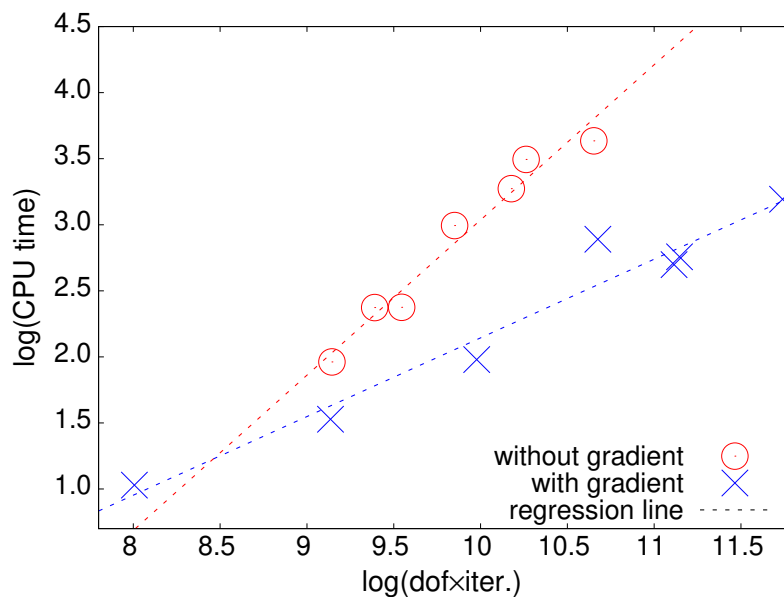


Figure 2.14: Log-log plot of the computation time in function of the product of numbers of dof and iterations.

2.3.5 Viscoplastic response with Norton-Odqvist law

Unlike the elastoplastic behavior, the Norton-Odqvist law is a rate-dependent constitutive law for which the dissipation potential density ϕ writes:

$$\phi(\boldsymbol{\sigma}) = \frac{K}{n+1} \left(\frac{\langle\langle \sigma_{eq}(\boldsymbol{\sigma}) - \sigma_Y \rangle\rangle}{K} \right)^{n+1} \quad (2.31)$$

where K , n are two material parameters and $\langle\langle x \rangle\rangle$ is the positive part of x defined by:

$$\langle\langle x \rangle\rangle = \begin{cases} x & \text{if } x > 0 \\ 0 & \text{if } x \leq 0 \end{cases}$$

The viscoplastic strain rate is given by:

$$\dot{\boldsymbol{\varepsilon}}^{vp} = \left(\frac{\langle\langle \sigma_{eq}(\boldsymbol{\sigma}) - \sigma_Y \rangle\rangle}{K} \right)^n \frac{\partial \sigma_{eq}}{\partial \boldsymbol{\sigma}}(\boldsymbol{\sigma}) = \left(\frac{\langle\langle \sigma_{eq}(\boldsymbol{\sigma}) - \sigma_Y \rangle\rangle}{K} \right)^n \frac{3}{2} \frac{\mathbf{s}}{\sigma_{eq}} \quad (2.32)$$

From the relation (2.32), it is obvious that the viscous strain depends only on the stress field. Therefore, there is no need to consider the plastic multiplier field and there are only two unknown fields in the numerical procedure, the stress \mathbf{g} and the displacement \mathbf{q} fields.

The Fenchel transform of ϕ is given by:

$$\phi^*(\dot{\boldsymbol{\varepsilon}}^{vp}) = \sup_{\boldsymbol{\sigma}} [\boldsymbol{\sigma} : \dot{\boldsymbol{\varepsilon}}^{vp} - \phi(\boldsymbol{\sigma})] = \sigma_Y \dot{\varepsilon}_{eq} + \frac{nK}{n+1} (\varepsilon_{eq}(\dot{\boldsymbol{\varepsilon}}^{vp}))^{\frac{n+1}{n}} \quad (2.33)$$

where $\varepsilon_{eq}(\dot{\boldsymbol{\varepsilon}}^{vp}) = \sqrt{\frac{2}{3} \dot{\boldsymbol{\varepsilon}}^{vp} : \dot{\boldsymbol{\varepsilon}}^{vp}}$ is the comparison strain rate. Hence the BEN functional to minimize reads:

$$\begin{aligned} \bar{\Pi}(\boldsymbol{\sigma}, \mathbf{u}) = \int_0^T \left\{ \int_{\Omega} \frac{K}{n+1} \left(\frac{\langle\langle \sigma_{eq}(\boldsymbol{\sigma}) \rangle\rangle - \sigma_Y}{K} \right)^{n+1} \right. \\ \left. + \sigma_Y \dot{\varepsilon}_{eq} + \frac{nK}{n+1} (\varepsilon_{eq}(\nabla \dot{\mathbf{u}} - \mathbf{S} \dot{\boldsymbol{\sigma}}))^{\frac{n+1}{n}} - \langle \boldsymbol{\sigma}, \nabla \dot{\mathbf{u}} - \mathbf{S} \dot{\boldsymbol{\sigma}} \rangle d\Omega \right\} dt \end{aligned} \quad (2.34)$$

In order to compare BEN's numerical predictions with analytic solutions, we start by studying the simple model of perfect viscoplastic constitutive law with a vanishing elastic yield. Numerically, this can be achieved by imposing a very large value of Young's modulus.

In this case, the dissipation potential density (2.31) reduces to:

$$\phi(\boldsymbol{\sigma}) = \frac{K}{n+1} \left(\frac{\sigma_{eq}(\boldsymbol{\sigma})}{K} \right)^{n+1} \quad (2.35)$$

and the correspondent functional to minimize is given by:

$$\bar{\Pi}(\boldsymbol{\sigma}, \mathbf{u}) = \int_0^T \left\{ \int_{\Omega} \frac{K}{n+1} \left(\frac{\sigma_{eq}(\boldsymbol{\sigma})}{K} \right)^{n+1} + \frac{nK}{n+1} (\varepsilon_{eq}(\nabla \dot{\mathbf{u}} - \mathbf{S}\dot{\boldsymbol{\sigma}}))^{\frac{n+1}{n}} - \langle \boldsymbol{\sigma}, \nabla \dot{\mathbf{u}} - \mathbf{S}\dot{\boldsymbol{\sigma}} \rangle d\Omega \right\} dt \quad (2.36)$$

Neglecting the elastic strains, the analytical solution of the pressurized thick tube with the Norton-Odqvist law is available and the stress distribution reads:

$$\sigma_r(r) = -p \frac{\left(\frac{b}{r}\right)^{\frac{2}{n}} - 1}{\left(\frac{b}{a}\right)^{\frac{2}{n}} - 1}, \quad \sigma_{\theta}(r) = p \frac{\left(\frac{2}{n} - 1\right) \left(\frac{b}{r}\right)^{\frac{2}{n}} + 1}{\left(\frac{b}{a}\right)^{\frac{2}{n}} - 1} \quad (2.37)$$

The material parameters are $n = 4.39$ and $K = 253.55$ MPa with Young's modulus $E = 1000$ GPa and Poisson's ratio equals $\nu = 0.3$ so that the elastic strain is negligible compared to the viscoplastic one.

Two computational examples are carried out. The first one considers 10 time-increments and the second one with 2 temporal points, the beginning and the end points of the loading history. The applied pressure increases linearly with respect to time from 0 to 100 MPa as shown in figure 2.15.

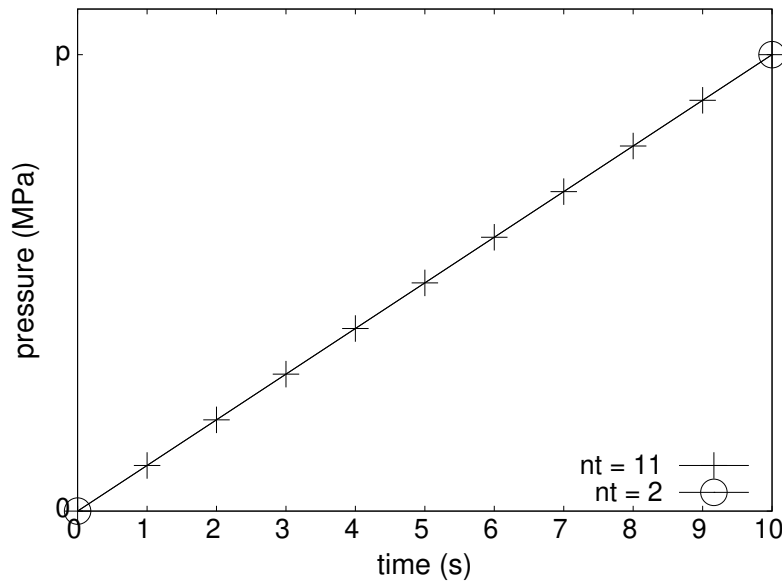


Figure 2.15: Loading history with 11 or 2 temporal points.

Figure 2.16 plots the comparison between the exact stress solution and the numerical results (σ_r and σ_{θ}) at the last temporal point ($t = 10$ s). A good agreement is observed even with one element and with the simplest temporal discretization method (rectangular rule).

Let us come back to the nonlinear creep of the thick-walled tube with Norton-Odqvist law

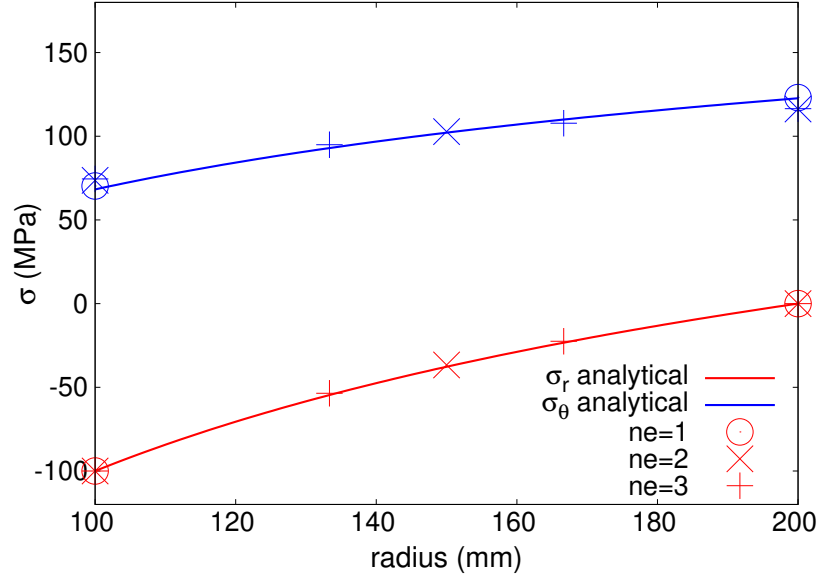


Figure 2.16: Comparison between the BEN principle solution (symbols) and analytical solution (solid line) for radial σ_r (red) and hoop σ_θ (blue) stresses with 1 & 2 & 3 elements (ne) for perfect viscoplastic law with $p = 100$ MPa when $t = 10$ s, $nt = 11$.

with an elastic domain defined by (2.31) and (2.32). We use the set of parameters $n = 4.39$, $K = 253.55$ MPa and $\sigma_Y = 360$ MPa and the internal pressure increases linearly with respect to time from 0 to 20 MPa. Computations are carried out by considering 2 and 11 temporal points and one spatial finite element.

Figures 2.17 and 2.18 show the comparison between BEN's numerical predictions and the simulations derived out by Cast3M for the radial and hoop stress respectively. Again a good agreement is observed.

2.4 Conclusion

This chapter aims to investigate the feasibility of the BEN principle for the numerical analysis of dissipative media. This principle has been efficiently applied to the numerical simulations of the nonlinear responses of an elastoplastic and a viscoplastic thick-walled tube under internal pressure. A good agreement is observed when the BEN's numerical results are compared with the analytical ones and computations obtained by the classical incremental process. The main advantage of the BEN formulation is its ability to work simultaneously on all time steps contrary to the step-by-step procedure. Moreover, it has been found that the BEN principle has a fast convergence to the reference solution, especially for the stress field, which is crucial for ensuring the plastic yielding condition. Regarding numerical implementation, considering sophisticated and complex nonlinear constitutive laws does not involve additional numerical efforts contrary

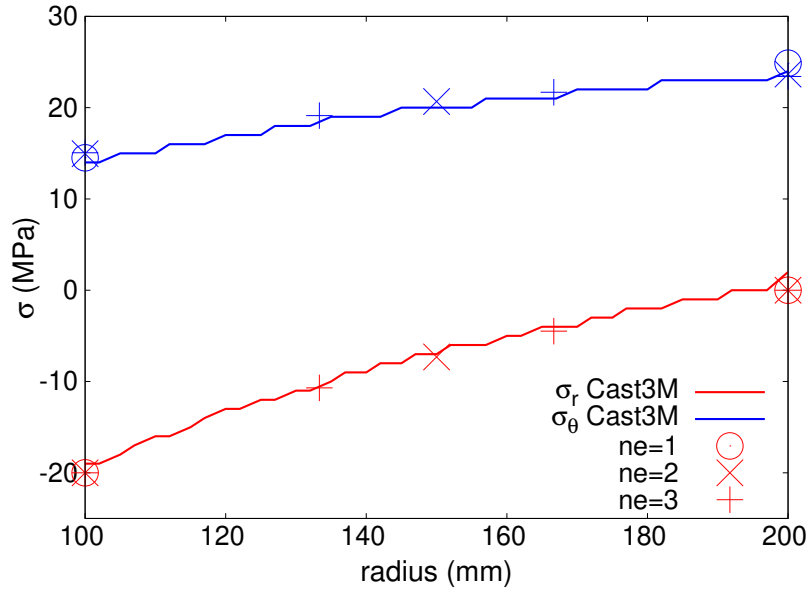


Figure 2.17: Comparison between the BEN solution (symbols) and the numerical solution (solid line) for radial σ_r (red) and hoop σ_θ (blue) stresses (viscoelastoplastic Norton-Odqvist law) with $p = 20$ MPa and $t = 10$ s with $nt = 11$ and $nt = 2$

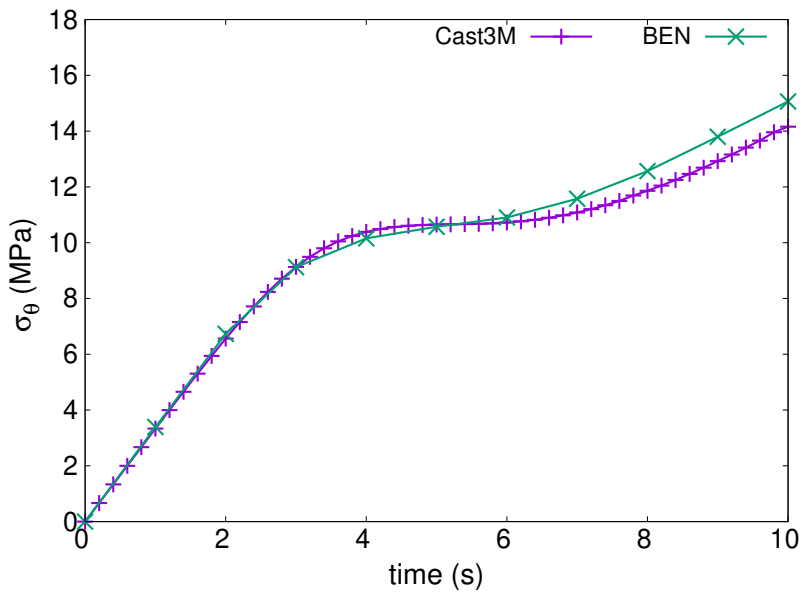


Figure 2.18: Comparison between the BEN principle solution and Cast3M result for the hoop stress σ_θ evolution of the internal wall with $p = 20$ MPa (viscoelastoplastic Norton-Odqvist law).

to the nonlinear incremental procedure. Remarkably, we do not need with BEN to use numerical integration as radial return scheme in elastoplasticity or similar ones. This issue is irrelevant.

Numerical simulation of quasi-static
elastoplastic circular plates by the
Brezis-Ekeland-Nayroles principle

3.1	The problem statement	64
3.1.1	Love-Kirchhoff plate model	65
3.1.2	The Reissner-Mindlin plate model	68
3.2	Numerical implementation	70
3.2.1	Numerical implementation for the circular Love-Kirchhoff plate	70
3.2.2	Numerical implementation for the circular Reissner-Mindlin plates	76
3.3	Results and discussion	80
3.3.1	The Love-Kirchhoff plates	81
3.3.2	The Reissner-Mindlin plates	83
3.4	Conclusion	86

The present work is a part of the international cooperation project *Dissipative Dynamical Systems by Geometrical and Variational Methods and Application to Viscoplastic Structures Subjected to Shock Waves* (DDGV). Subsequently, this chapter is devoted to the numerical study of the Love-Kirchhoff and Reissner-Mindlin circular plates undergoing uniform pressure by using the non-incremental BEN principle. The numerical results are compared to analytical solutions provided in the literature and simulations computed by the standard step-by-step procedure.

3.1 The problem statement

Let us consider an elastoplastic circular plate occupying the domain

$$\Omega = \{M(r, \theta, z) \text{ such that } 0 \leq r \leq R, 0 \leq \theta \leq 2\pi, -H/2 \leq z \leq H/2\}$$

where (r, θ, z) are the coordinates of the material point in the cylindrical frame. R and H are called the radius and the thickness of the plate respectively. The middle plane is defined by $z = 0$.

In this work, the BEN principle is applied to solve numerically the bending of the solid Ω undergoing a uniformly distributed $p\mathbf{e}_z$ as shown in Fig.3.1. Moreover, the plate edge is clamped and body forces are neglected.

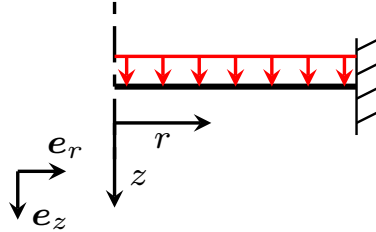


Figure 3.1: The clamped circular plate under a uniform pressure.

Under the plane stress hypothesis, the normal stress component σ_{zz} through the thickness is zero. Moreover, the shear stresses $\sigma_{r\theta}$ and $\sigma_{\theta z}$ are cancelled because of the axisymmetric symmetry. Therefore, the stress $\boldsymbol{\sigma}(r, z)$ and strain $\boldsymbol{\varepsilon}(r, z)$ tensors are given by:

$$\boldsymbol{\sigma} = \begin{pmatrix} \sigma_{rr} & 0 & \sigma_{rz} \\ 0 & \sigma_{\theta\theta} & 0 \\ \sigma_{rz} & 0 & 0 \end{pmatrix} \quad \boldsymbol{\varepsilon} = \begin{pmatrix} \varepsilon_{rr} & 0 & \varepsilon_{rz} \\ 0 & \varepsilon_{\theta\theta} & 0 \\ \varepsilon_{rz} & 0 & \varepsilon_{zz} \end{pmatrix}$$

According to the general theory of plates, the expansions of the stress and strain fields are given in the following power series of the coordinate z :

$$\sigma(r, z) = \bar{\sigma}(r) + z\tilde{\sigma}(r) + z^2\hat{\sigma}(r) + \dots \quad (3.1)$$

$$\varepsilon(r, z) = \bar{\varepsilon}(r) + z\tilde{\varepsilon}(r) + \dots \quad (3.2)$$

where $\bar{\sigma}(r)$, $\bar{\varepsilon}(r)$ are the membrane stress and strain, $z\tilde{\sigma}(r)$, $z\tilde{\varepsilon}(r)$ denote the linear parts with respect to z , $z^2\hat{\sigma}(r)$ and $z^2\hat{\varepsilon}(r)$ are the quadratic terms, etc. Under small deformation hypothesis, membrane stress and strain are neglected. Finally, we have the simplified expressions:

$$\sigma(r, z) = z\tilde{\sigma}(r) + z^2\hat{\sigma}(r) + \dots \quad (3.3)$$

$$\varepsilon(r, z) = z\tilde{\varepsilon}(r) + \dots \quad (3.4)$$

Furthermore, in the sequel, we assume that within the elastic and elastoplastic ranges, the strain field is linear with respect to z and writes:

$$\varepsilon(r, z) = z\tilde{\varepsilon}(r)$$

3.1.1 Love-Kirchhoff plate model

Love-Kirchhoff plate theory (Love, 1887) was firstly developed by Love in 1888 by extending the Euler-Bernoulli beam theory to flat and thin solids. The Love-Kirchhoff plate theory assumes that:

- straight and orthogonal lines to the undeformed middle plane remain straight and normal to the deformed neutral plane, that is shear deformations are neglected,
- the variation of the thickness of the plate during deformation is neglected.

Basing upon these assumptions, it is easy to show that the displacement field of any material point of the plate is given by (Oñate, 2013):

$$\mathbf{u}(r, z) = \begin{bmatrix} U(r, z) \\ 0 \\ W(r) \end{bmatrix} = \begin{bmatrix} -z \frac{dw}{dr} \\ 0 \\ w(r) \end{bmatrix} \quad (3.5)$$

It entails that the strain and stress tensors are given by:

$$\boldsymbol{\sigma} = \begin{pmatrix} \sigma_{rr} & 0 \\ 0 & \sigma_{\theta\theta} \end{pmatrix}, \quad \boldsymbol{\varepsilon} = \begin{pmatrix} \frac{\partial U}{dr} & 0 \\ 0 & \frac{U}{r} \end{pmatrix} \quad (3.6)$$

Moreover, the normal stresses σ_{rr} and $\sigma_{\theta\theta}$ are linear with respect to the coordinate z :

$$\sigma_{rr}(r, z) \approx z\tilde{\sigma}_{rr}(r)$$

$$\sigma_{\theta\theta}(r, z) \approx z\tilde{\sigma}_{\theta\theta}(r)$$

In elasticity theory, Hooke's law in plane stress writes:

$$\begin{bmatrix} \varepsilon_{rr} \\ \varepsilon_{\theta\theta} \end{bmatrix} = \begin{bmatrix} \frac{1}{E} & -\frac{\nu}{E} \\ -\frac{\nu}{E} & \frac{1}{E} \end{bmatrix} \begin{bmatrix} \sigma_{rr} \\ \sigma_{\theta\theta} \end{bmatrix}$$

In the plate theory, expressions of generalized stress and moments are given as:

$$F_{rr} = \int_{-H/2}^{H/2} \sigma_{rr} dz \quad F_{\theta\theta} = \int_{-H/2}^{H/2} \sigma_{\theta\theta} dz \quad F_{rz} = \int_{-H/2}^{H/2} \sigma_{rz} dz \quad (3.7)$$

$$M_{rr} = \int_{-H/2}^{H/2} z \sigma_{rr} dz \quad M_{\theta\theta} = \int_{-H/2}^{H/2} z \sigma_{\theta\theta} dz \quad (3.8)$$

By using the Love-Kirchhoff hypothesis, we have :

$$F_{rr} = \int_{-H/2}^{H/2} z\tilde{\sigma}_{rr} dz = 0 \quad F_{\theta\theta} = \int_{-H/2}^{H/2} z\tilde{\sigma}_{\theta\theta} dz = 0 \quad (3.9)$$

$$F_{rz} = \int_{-H/2}^{H/2} \bar{\sigma}_{rz} + z\tilde{\sigma}_{rz} dz = H\bar{\sigma} \quad (3.10)$$

$$M_{rr} = \int_{-H/2}^{H/2} z^2 \tilde{\sigma}_{rr} dz = \frac{H^3}{12} \tilde{\sigma}_{rr} \quad M_{\theta\theta} = \int_{-H/2}^{H/2} z^2 \tilde{\sigma}_{\theta\theta} dz = \frac{H^3}{12} \tilde{\sigma}_{\theta\theta} \quad (3.11)$$

The plate equilibrium equations in the cylinder coordinates frame read:

$$\sum F_{rr} = 0 : \frac{F_r - F_\theta}{r} + \frac{dF_r}{dr} = 0 \quad (3.12)$$

$$\sum F_{zz} = 0 : \frac{\partial F_{rz}}{\partial r} + \frac{F_{rz}}{r} + p = 0 \quad (3.13)$$

$$\sum M_{\theta\theta} = 0 : \frac{\partial M_{rr}}{\partial r} + \frac{M_{rr} - M_{\theta\theta}}{r} = F_{rz} \quad (3.14)$$

$$\sum M_{zz} = 0 : F_{r\theta} - F_{r\theta} = 0 \quad (3.15)$$

Eq. (3.12) is satisfied by means of small deflection hypothesis. Furthermore, eliminating F_{rz} from equations (3.14) and (3.13) yields:

$$\frac{\partial^2 M_{rr}}{\partial r^2} + \frac{2}{r} \frac{\partial M_{rr}}{\partial r} - \frac{1}{r} \frac{\partial M_{\theta\theta}}{\partial r} + p = 0 \quad (3.16)$$

By injecting the expressions of the moments given in (3.11) into the equation (3.16), one obtains:

$$\left(\frac{d^2 \tilde{\sigma}_{rr}}{dr^2} + \frac{2}{r} \frac{d\tilde{\sigma}_{rr}}{dr} - \frac{1}{r} \frac{d\tilde{\sigma}_{\theta\theta}}{dr} \right) + \frac{12}{H^3} p = 0 \quad (3.17)$$

Let us eliminate the hoop stress $\tilde{\sigma}_{\theta\theta}$ from (3.17). To this end, the solution of this differential equation (3.17) is obtained as the sum of the homogeneous solution and a particular one. Simple computations allow one to get the homogeneous solution as follows:

$$\sigma_{\theta\theta,h} = \frac{d(r\sigma_{rr})}{dr}$$

In order to built a particular solution, we choose to consider $\sigma_{rr} = 0$ in eq. (3.17). Therefore, a corresponding particular solution is given by:

$$\sigma_{\theta\theta,p} = \frac{12}{H^3} \frac{pr^2}{2}$$

Thus one of the general solution of eq. (3.17) is:

$$\tilde{\sigma}_{\theta\theta} = \sigma_{\theta\theta,h} + \sigma_{\theta\theta,p} = \frac{d(r\tilde{\sigma}_{rr})}{dr} + \frac{12}{H^3} \frac{pr^2}{2} \quad (3.18)$$

It is important to notice that the equilibrium equation (3.18) is independent of z . Thus the radius-thickness 2D axisymmetric circular plate model is simplified into a 1D problem along the radius.

3.1.2 The Reissner-Mindlin plate model

The Love-Kirchhoff plate theory presented in the previous subsection applies to thin plates. Moreover, the C^1 continuity requirement for Kirchhoff elements poses some difficulties for deriving a conforming deflection field (Oñate, 2013). For the study of thick plates, the Reissner-Mindlin plate theory (Mindlin, 1951) has been proposed. This model relies on the following hypotheses:

- Straight lines normal to the undeformed middle plane remains straight but no longer perpendicular to the neutral plane. This assumption is similar to the one adopted for rotation of the cross section in Timoshenko beams.
- The shear strain (ε_{rz}) through the thickness is no more negligible.
- The thickness of the plate does not change during the deformation.

Objective in this subsection is to implement the BEN principle for Mindlin plate theory in elastic and elastoplastic cases. The same plate model in fig. (3.1) is exterminated with a thicker thickness.

As a normal line remains not necessarily perpendicular to the middle surface in the Mindlin theory, the rotation angle ζ is not linked derivative of the transverse displacement as in the Love-Kirchhoff plate model. Thus, the rotation angle field ζ is appended and the expression of the displacement of a material point of the plate writes:

$$\mathbf{u}(r, z) = \begin{bmatrix} U(r, z) \\ 0 \\ W(r) \end{bmatrix} = \begin{bmatrix} u(r) + z \zeta(r) \\ 0 \\ w(r) \end{bmatrix} \approx \begin{bmatrix} z \zeta(r) \\ 0 \\ w(r) \end{bmatrix} \quad (3.19)$$

By using Kelvin's notation, the strain tensor reads in the cylindrical coordinates frame :

$$\boldsymbol{\varepsilon}(r, z) = \begin{bmatrix} \varepsilon_{rr} \\ \varepsilon_{\theta\theta} \\ \sqrt{2} \varepsilon_{rz} \end{bmatrix} = \begin{bmatrix} \frac{\partial U}{\partial r} \\ \frac{U}{r} \\ \frac{\sqrt{2}}{2} \left(\frac{\partial U}{\partial z} + \frac{\partial W}{\partial r} \right) \end{bmatrix} \quad (3.20)$$

Moreover, the Reissner-Mindlin plate theory assumes that normal stresses (σ_{rr} , $\sigma_{\theta\theta}$) are linear with respect to z while the shear stress (σ_{rz}) is quadratic. Under plane stress hypothesis, the

expression of stress field with the Voigt notation is given by :

$$\boldsymbol{\sigma}(r, z) = \begin{bmatrix} \sigma_{rr} \\ \sigma_{\theta\theta} \\ \sqrt{2} \sigma_{rz} \end{bmatrix} = \begin{bmatrix} 0 \\ 0 \\ \sqrt{2} \bar{\sigma}_{rz}(r) \end{bmatrix} + z \begin{bmatrix} \tilde{\sigma}_{rr}(r) \\ \tilde{\sigma}_{\theta\theta}(r) \\ 0 \end{bmatrix} + z^2 \begin{bmatrix} 0 \\ 0 \\ \sqrt{2} \hat{\sigma}_{rz}(r) \end{bmatrix}$$

In elasticity theory, Hooke's law in plane stress writes :

$$\begin{bmatrix} \varepsilon_{rr} \\ \varepsilon_{\theta\theta} \\ \sqrt{2} \varepsilon_{rz} \end{bmatrix} = \begin{bmatrix} \frac{1}{E} & -\frac{\nu}{E} & 0 \\ -\frac{\nu}{E} & \frac{1}{E} & 0 \\ 0 & 0 & \frac{(1+\nu)}{E} \end{bmatrix} \begin{bmatrix} \sigma_{rr} \\ \sigma_{\theta\theta} \\ \sqrt{2} \sigma_{rz} \end{bmatrix}$$

Within the framework of Reissner-Mindlin plate theory, the following expressions of forces and moments can be obtained :

$$F_{rr} = 0 \qquad F_{\theta\theta} = 0 \qquad F_{rz} = H\bar{\sigma}_{rz} + \frac{H^3}{12} \hat{\sigma}_{rz} \quad (3.21)$$

$$M_{rr} = \frac{H^3}{12} \tilde{\sigma}_{rr} \qquad M_{\theta\theta} = \frac{H^3}{12} \tilde{\sigma}_{\theta\theta} \quad (3.22)$$

Simple computations similar to the ones conducted for the Love-Kirchhoff plates permits one to derive the two following equilibrium equations:

$$H \left[\frac{d\bar{\sigma}_{rz}}{dr} + \frac{\bar{\sigma}_{rz}}{r} \right] + \frac{H^3}{12} \left[\frac{d\hat{\sigma}_{rz}}{dr} + \frac{\hat{\sigma}_{rz}}{r} \right] + p = 0 \quad (3.23)$$

$$\frac{H^3}{12} \left[\frac{d\tilde{\sigma}_{rr}}{dr} + \frac{\tilde{\sigma}_{rr} - \tilde{\sigma}_{\theta\theta}}{r} \right] = H\bar{\sigma}_{rz}(r) + \frac{H^3}{12} \hat{\sigma}_{rz}(r) \quad (3.24)$$

Similar computations to the those carried out for the Love-Kirchhoff plates permits one to obtain the homogeneous solution of eq. (3.23) as follows:

$$H\bar{\sigma}_{rz} + \frac{H^3}{12} \hat{\sigma}_{rz} = 0$$

Then, by considering $\bar{\sigma}_{rz} = 0$ in eq. (3.23), a particular solution can be built:

$$\hat{\sigma}_{rz} = \frac{12}{H^3} \frac{pr}{2}$$

Consequently, eq.(3.23) is reduced to:

$$\frac{d(r\tilde{\sigma}_{rr})}{dr} - \tilde{\sigma}_{\theta\theta} + \frac{12}{H^3} \frac{pr^2}{2} = 0$$

Finally, for the Mindlin theory plate, there are two equilibrium equations to be satisfied:

$$H\bar{\sigma}_{rz} + \frac{H^3}{12}\hat{\sigma}_{rz} + \frac{pr}{2} = 0 \quad (3.25)$$

$$\frac{d(r\tilde{\sigma}_{rr})}{dr} - \tilde{\sigma}_{\theta\theta} + \frac{12}{H^3} \frac{pr^2}{2} = 0 \quad (3.26)$$

3.2 Numerical implementation

The mixed finite element method (FEM) is applied to implement the BEN principle. It is important to underline that mixed finite element method is not mandatory and the standard displacement method can be combined with the BEN principle. However, we recall that in the displacement-based FEM, the stress field is deduced from the displacement one and thus is not statically admissible which may be less accurate for plasticity.

3.2.1 Numerical implementation for the circular Love-Kirchhoff plate

For the Love-Kirchhoff plates, there three unknown fields, namely the radial and hoop stresses, the transverse displacement and plastic multiplier.

The displacement field

Thanks to the axisymmetry of the considered problem, we consider a 1D element ($\alpha \leq r \leq \beta$, z^*) with $-H/2 \leq z^* \leq H/2$. Expression of the displacement field $\mathbf{u}(r, z^*)$ of any material point of the plate is provided in relation (3.5).

We use 4 degrees of freedom for $w(r)$:

$$q_1 = w|_{r=\alpha, z=z^*} \quad q_2 = w|_{r=\beta, z=z^*} \quad q_3 = w|_{r=\gamma, z=z^*} \quad q_4 = w|_{r=\delta, z=z^*}$$

with γ and δ two intermediary points:

$$\gamma = \frac{2\alpha + \beta}{3} \quad \delta = \frac{\alpha + 2\beta}{3}$$

that defines a Lagrange interpolation. By gathering the four displacement degrees of freedom in

a vector \mathbf{q}_e , we obtain :

$$w(r) = \mathbf{N}_e(r) \mathbf{q}_e \quad (3.27)$$

with:

$$\mathbf{q}_e = \begin{bmatrix} q_1 \\ q_2 \\ q_3 \\ q_4 \end{bmatrix} = \begin{bmatrix} w |_{r=\alpha, z=z^*} \\ w |_{r=\beta, z=z^*} \\ w |_{r=\gamma, z=z^*} \\ w |_{r=\delta, z=z^*} \end{bmatrix} \quad (3.28)$$

$$\mathbf{N}_e^T(r) = \frac{1}{16} \begin{bmatrix} -(1-\rho)(1-9\rho^2) \\ -(1+\rho)(1-9\rho^2) \\ +9(1-\rho^2)(1-3\rho) \\ +9(1-\rho^2)(1+3\rho) \end{bmatrix}$$

where:

$$\rho = \frac{2r - (\beta + \alpha)}{\beta - \alpha}$$

Therefore, the displacement can be written as follows:

$$\mathbf{u}(r, z^*) = \begin{bmatrix} -z^* N_{e,r}(r) \\ 0 \\ \mathbf{N}_e(r) \end{bmatrix} \mathbf{q}_e \quad (3.29)$$

Taking into consideration eqs.(3.6) and (3.27), expression of strain is given by :

$$\boldsymbol{\varepsilon}(r, z^*) = \begin{bmatrix} \varepsilon_{rr} \\ \varepsilon_{\theta\theta} \end{bmatrix} = z^* \begin{bmatrix} -\mathbf{N}_{e,rr} \\ -\frac{1}{r} \mathbf{N}_{e,r} \end{bmatrix} \mathbf{q}_e = z^* \mathbf{B}(r) \mathbf{q}_e$$

where:

$$\mathbf{N}_{e,r}^T = \frac{1}{16} \begin{bmatrix} J(1 + 18\rho - 27\rho^2) \\ J(-1 + 18\rho + 27\rho^2) \\ J(-27 - 18\rho + 81\rho^2) \\ J(27 - 18\rho - 81\rho^2) \end{bmatrix}$$

$$\mathbf{N}_{e,rr}^T = \frac{1}{16} \begin{bmatrix} J^2(18 - 54\rho) \\ J^2(18 + 54\rho) \\ J^2(-18 + 162\rho) \\ J^2(-18 - 162\rho) \end{bmatrix}$$

with:

$$J = \frac{d\rho}{dr} = \frac{2}{\beta - \alpha}$$

The stress field

With the same finite element, we consider 8 degrees of freedom \mathbf{g}_e for linear terms along z of the radial $\tilde{\sigma}_{rr}$ and hoop $\tilde{\sigma}_{\theta\theta}$ stresses :

$$\begin{aligned} g_1 &= \tilde{\sigma}_{rr} |_{r=\alpha, z=z^*} & g_2 &= \tilde{\sigma}_{rr} |_{r=\beta, z=z^*} & g_3 &= \tilde{\sigma}_{rr} |_{r=\gamma, z=z^*} & g_4 &= \tilde{\sigma}_{rr} |_{r=\delta, z=z^*} \\ g_5 &= \tilde{\sigma}_{\theta\theta} |_{r=\alpha, z=z^*} & g_6 &= \tilde{\sigma}_{\theta\theta} |_{r=\beta, z=z^*} & g_7 &= \tilde{\sigma}_{\theta\theta} |_{r=\gamma, z=z^*} & g_8 &= \tilde{\sigma}_{\theta\theta} |_{r=\delta, z=z^*} \end{aligned}$$

with:

$$\begin{aligned} \mathbf{g}_e^T &= \left[\tilde{\sigma}_{rr} |_{r=\alpha, z=z^*} \quad \tilde{\sigma}_{rr} |_{r=\beta, z=z^*} \quad \tilde{\sigma}_{rr} |_{r=\gamma, z=z^*} \quad \tilde{\sigma}_{rr} |_{r=\delta, z=z^*} \right. \\ &\quad \left. \tilde{\sigma}_{\theta\theta} |_{r=\alpha, z=z^*} \quad \tilde{\sigma}_{\theta\theta} |_{r=\beta, z=z^*} \quad \tilde{\sigma}_{\theta\theta} |_{r=\gamma, z=z^*} \quad \tilde{\sigma}_{\theta\theta} |_{r=\delta, z=z^*} \right] \end{aligned} \quad (3.30)$$

Similarly the displacement field, a cubic Lagrange interpolation is considered :

$$\boldsymbol{\sigma}(r, z^*) = \begin{bmatrix} \sigma_{rr} \\ \sigma_{\theta\theta} \end{bmatrix} = z^* \mathbf{R}_e(r) \mathbf{g}_e = z^* \begin{bmatrix} \mathbf{N}_e(r) & \mathbf{0} \\ \mathbf{0} & \mathbf{N}_e(r) \end{bmatrix} \mathbf{g}_e$$

The plastic multiplier rate field

Introducing the plastic multiplier rate $\boldsymbol{\lambda}$ which is located in four Gauss point for each element ($\alpha \leq r \leq \beta$, z^*) at $r_g |_{g=1,2,3,4}$, the flow rule reads:

$$\dot{\boldsymbol{\epsilon}}_e^p(r, z^*) = \lambda_e(r, z^*) \frac{\partial \mathbf{f}}{\partial \boldsymbol{\sigma}}(r, z^*) \quad (3.31)$$

and the dissipation power becomes:

$$D = \sigma_Y \lambda$$

In particular, the total dissipation power in the element reads:

$$\int_{\alpha}^{\beta} D(r) 2 \pi r dr = \Lambda_e^T \lambda_e$$

where:

$$\mathbf{\Lambda}_e = \sigma_Y \begin{bmatrix} w_1 2 \pi r_1 \\ \dots \\ w_{n_e} 2 \pi r_{n_e} \end{bmatrix}, \quad \boldsymbol{\lambda}_e = \begin{bmatrix} \lambda_1 \\ \dots \\ \lambda_{n_e} \end{bmatrix}$$

For the circular Love-Kirchhoff plate problem, there are three types degrees of freedom, stress \mathbf{g}_e , displacement \mathbf{q}_e and plastic multiplier rate $\boldsymbol{\lambda}_e$:

$$\begin{aligned} \mathbf{u}(r, z^*) &= \begin{bmatrix} -z^* N_{e,r}(r) \\ 0 \\ N_e(r) \end{bmatrix} \mathbf{q}_e \\ \boldsymbol{\sigma}(r, z^*) &= \begin{bmatrix} \sigma_{rr} \\ \sigma_{\theta\theta} \end{bmatrix} = z^* \mathbf{R}_e(r) \mathbf{g}_e = z^* \begin{bmatrix} N_e(r) & \mathbf{0} \\ \mathbf{0} & N_e(r) \end{bmatrix} \mathbf{g}_e \\ \dot{\boldsymbol{\epsilon}}_e^p(r, z^*) &= \lambda_e(r, z^*) \frac{\partial f}{\partial \boldsymbol{\sigma}}(r, z^*) \end{aligned} \quad (3.32)$$

Discretization of the BEN principle

The BEN functional involves time and space integrations. The classical Gaussian quadrature method for the spatial integration and the simple rectangular rule for the temporal one are adopted. It is worth noting that the rectangular rule may be rather rough but numerical experiences showed that it yields to sufficient accurate results. Of course, employing more sophisticated integration rule should improve the numerical predictions.

Spatial discretization

The spatial integration over the plate finite element ($\alpha \leq r \leq \beta$, z^*) is carried out as follows:

$$\begin{aligned} \int_{-H/2}^{H/2} \int_{\alpha}^{\beta} \mathbf{A}(r) 2 \pi r dr dz &\cong H \sum_{g=1}^4 w_g \mathbf{A}(r_g) 2 \pi r_g \\ \int_{-H/2}^{H/2} \int_{\alpha}^{\beta} z^2 \mathbf{A}(r) 2 \pi r dr dz &\cong \frac{H^3}{12} \sum_{g=1}^4 w_g \mathbf{A}(r_g) 2 \pi r_g \end{aligned}$$

Performing the assembling thanks to the localization matrices $\mathbf{L}_e, \mathbf{M}_e, \mathbf{P}_e$ such that:

$$\mathbf{g}_e = \mathbf{M}_e \mathbf{g}, \quad \mathbf{q}_e = \mathbf{L}_e \mathbf{q}, \quad \boldsymbol{\lambda}_e = \mathbf{P}_e \boldsymbol{\lambda}$$

yields to the following discretized form of the BEN functional :

$$\bar{\Pi}(\mathbf{g}, \mathbf{q}, \boldsymbol{\lambda}) = \int_{t_0}^{t_1} (\boldsymbol{\Lambda}^T \boldsymbol{\lambda}(t) - \dot{\mathbf{q}}^T(t) \mathbf{G} \mathbf{g}(t) + \dot{\mathbf{g}}^T(t) \mathbf{F} \mathbf{g}(t)) dt \quad (3.33)$$

with:

$$\begin{aligned} \boldsymbol{\Lambda} &= \int_{-H/2}^{H/2} \sum_{e=1}^n \mathbf{P}_e^T \boldsymbol{\Lambda}_e dz, \\ \mathbf{G} &= \sum_{e=1}^n \int_{-H/2}^{H/2} \int_{\alpha}^{\beta} \mathbf{L}_e^T z \mathbf{B}_e^T(r) z \mathbf{R}_e(r) \mathbf{M}_e 2\pi r dr dz \\ \mathbf{F} &= \sum_{e=1}^n \int_{-H/2}^{H/2} \int_{\alpha}^{\beta} \mathbf{M}_e^T z \mathbf{R}_e^T(r) \mathbf{S} z \mathbf{R}_e(r) \mathbf{M}_e 2\pi r dr dz \end{aligned}$$

The Brezis-Ekeland-Nayroles variational principle claims that the solution minimizes the functional (3.33) under the some constraints which will be listed hereafter.

Temporal discretization

We impose t_j as the temporal points with $j = [0, \dots, m-1, m]$. There are m time steps with $m+1$ temporal points. For any physical quantity a at temporal point t_j , we note:

$$a_j = a(t_j) \quad \Delta a_j = a_j - a_{j-1} \quad \Delta t_j = t_j - t_{j-1} \quad j = 1, \dots, m$$

On each step, we approximate the time rate by:

$$\dot{a}_j = \frac{\Delta a_j}{\Delta t_j}$$

As the plasticity is independent of the time parameterization in quasi-static situation, we use fictive time for convenience sake:

$$\Delta t_j = 1$$

Moreover, the rectangular rule is applied for the temporal integration.

$$\int_0^T f(t) dt = \sum_{j=1}^m f(t_j) \Delta t_j$$

Subsequently, the final expression of the discretized BEN functional reads:

$$\bar{\Pi}(\mathbf{g}, \mathbf{q}, \boldsymbol{\lambda}) = \sum_{j=1}^m (\boldsymbol{\Lambda}^T \boldsymbol{\lambda}_j - \Delta \mathbf{q}_j^T \mathbf{G} \mathbf{g}_j + \Delta \mathbf{g}_j^T \mathbf{F} \mathbf{g}_j) \quad (3.34)$$

under the following constrains :

- The boundary and symmetry conditions :

$$w(r = R, t_j) = 0$$

$$\frac{dw}{dr}(r = 0, t_j) = 0 \quad \frac{dw}{dr}(r = R, t_j) = 0$$

$$-\sigma_Y \leq z^* \tilde{\sigma}_{rr}(r = 0, t_j) = z^* \tilde{\sigma}_{\theta\theta}(r = 0, t_j) \leq \sigma_Y (\text{symmetry})$$

- The C^0 continuity of the rotation angle on the boundary of two adjacent finite elements e_{i-1} and e_i at each time step :

$$\left. \frac{dw}{dr}(r = \alpha, t_j) \right|_{e_{i-1}} = \left. \frac{dw}{dr}(r = \alpha, t_j) \right|_{e_i} \quad \left. \frac{dw}{dr}(r = \beta, t_j) \right|_{e_i} = \left. \frac{dw}{dr}(r = \beta, t_j) \right|_{e_{i+1}} \quad (3.35)$$

- The equilibrium equation at every integration points (r_g) of each finite element at each time step :

$$\frac{d(r_g \tilde{\sigma}_{rr})}{dr}(r_g, t_j) - \tilde{\sigma}_{\theta\theta}(r_g, t_j) + \frac{12}{H^3} \frac{pr_g^2}{2} = 0$$

- Enforcing plasticity (at every integration point g of every element e , at each time step):

$$f_j(\mathbf{g}(r_g, z_g)) - \sigma_Y \leq 0, \quad \lambda_{g,j} \geq 0$$

$$\lambda_{g,j} \frac{\partial f_j(r_g, z_g^*)}{\partial \boldsymbol{\sigma}} = z^* \mathbf{B}_e(r_g) \Delta \mathbf{q}_j - \mathbf{S} z^* \mathbf{R}_e(r_g) \Delta \mathbf{g}_j$$

- The initial conditions:

$$\mathbf{g}(0) = \mathbf{0}, \quad \mathbf{q}(0) = \mathbf{0}, \quad \boldsymbol{\lambda}(0) = \mathbf{0}$$

At this stage, it is worth to notice that in almost FEM codes, the Hermite interpolation is applied in order to ensure the C^1 continuity of displacement field. In the present work, the rotation angle is the derivative of displacement and Lagrange interpolation is applied for displacement field. The C^0 continuity of the rotation angle is enforced as an optimization constraint in (3.35).

Figure (3.2) displays the numbering system for the axisymmetric Love-Kirchhoff plate element for two elements along radius ($ne = 2$) and two fictive temporal points ($nt = 2$) in statics $t = 0, 1$.

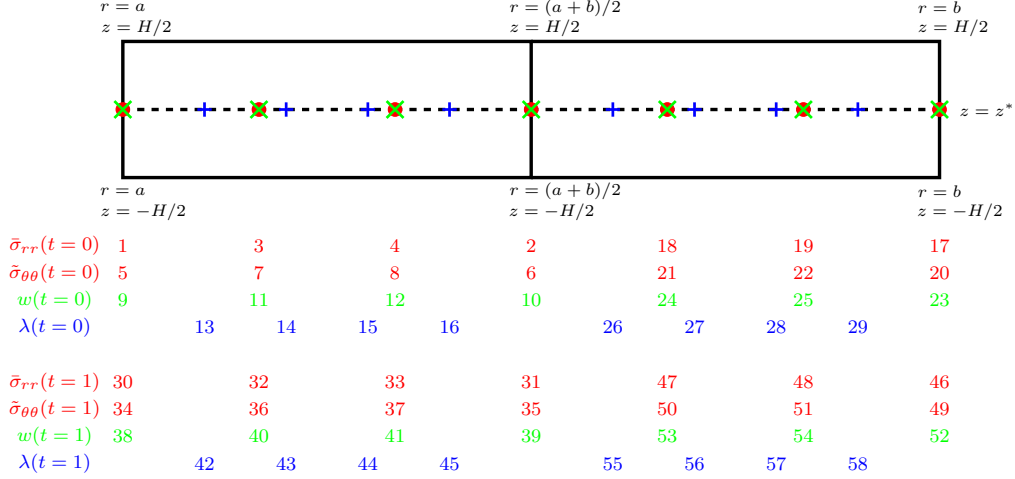


Figure 3.2: Numbering system of Love-Kirchhoff plate model for the axisymmetric plate element with 2 elements along radius

3.2.2 Numerical implementation for the circular Reissner-Mindlin plates

The mixed finite element method is applied to implement the BEN principle for the Reissner-Mindlin plate model as done in the previous subsection. For this plate model, there are four unknown fields, namely the radial and hoop stresses, the transverse displacement, the rotation angle and the plastic multiplier.

The displacement and rotation angle fields

Consider an axisymmetric 1D element ($\alpha \leq r \leq \beta$, z^*) with $-\frac{H}{2} \leq z \leq \frac{H}{2}$. The 4 degrees of freedom for w and ζ are :

$$\tilde{q}_1 = w|_{r=\alpha} \quad \tilde{q}_2 = w|_{r=\beta} \quad \tilde{q}_3 = w|_{r=\gamma} \quad \tilde{q}_4 = w|_{r=\delta}$$

$$\hat{q}_1 = \zeta|_{r=\alpha} \quad \hat{q}_2 = \zeta|_{r=\beta} \quad \hat{q}_3 = \zeta|_{r=\gamma} \quad \hat{q}_4 = \zeta|_{r=\delta}$$

By assembling the four degrees of freedom of displacement and rotation angle as a vector $\tilde{\mathbf{q}}_e$ and $\hat{\mathbf{q}}_e$ respectively we can write :

$$w(r) = \mathbf{N}_e(r) \tilde{\mathbf{q}}_e \quad \zeta(r) = \mathbf{N}_e(r) \hat{\mathbf{q}}_e$$

with:

$$\tilde{\mathbf{q}}_e = \begin{bmatrix} \tilde{q}_1 \\ \tilde{q}_2 \\ \tilde{q}_3 \\ \tilde{q}_4 \end{bmatrix} = \begin{bmatrix} w |_{r=\alpha, z=z^*} \\ w |_{r=\beta, z=z^*} \\ w |_{r=\gamma, z=z^*} \\ w |_{r=\delta, z=z^*} \end{bmatrix} \quad \hat{\mathbf{q}}_e = \begin{bmatrix} \hat{q}_1 \\ \hat{q}_2 \\ \hat{q}_3 \\ \hat{q}_4 \end{bmatrix} = \begin{bmatrix} \zeta |_{r=\alpha, z=z^*} \\ \zeta |_{r=\beta, z=z^*} \\ \zeta |_{r=\gamma, z=z^*} \\ \zeta |_{r=\delta, z=z^*} \end{bmatrix} \quad (3.36)$$

The displacement field can be written as follows :

$$\mathbf{u}(r, z^*) = \begin{bmatrix} z^* \mathbf{N}_e(r) \tilde{\mathbf{q}}_e \\ 0 \\ \mathbf{N}_e(r) \hat{\mathbf{q}}_e \end{bmatrix} \quad (3.37)$$

But using Kelvin's notation, the strain field can be written under the form :

$$\boldsymbol{\varepsilon}(r, z^*) = \begin{bmatrix} \varepsilon_{rr} \\ \varepsilon_{\theta\theta} \\ \sqrt{2} \varepsilon_{rz} \end{bmatrix} = \begin{bmatrix} \mathbf{0} \\ \mathbf{0} \\ \frac{\sqrt{2}}{2} \mathbf{N}_{e,r} \end{bmatrix} \tilde{\mathbf{q}}_e + \begin{bmatrix} z^* \mathbf{N}_{e,r} \\ \frac{z^*}{r} \mathbf{N}_e \\ \frac{\sqrt{2}}{2} \mathbf{N}_e \end{bmatrix} \hat{\mathbf{q}}_e = \mathbf{B}_1(r) \tilde{\mathbf{q}}_e + \mathbf{B}_2(r, z^*) \hat{\mathbf{q}}_e$$

By gathering the two vectors $\tilde{\mathbf{q}}_e$ and $\hat{\mathbf{q}}_e$ together, one has :

$$\boldsymbol{\varepsilon}(r, z) = \mathbf{B}(r, z) \mathbf{q}_e = \begin{bmatrix} \mathbf{B}_1 & \mathbf{B}_2 \end{bmatrix} \begin{bmatrix} \tilde{\mathbf{q}}_e \\ \hat{\mathbf{q}}_e \end{bmatrix}$$

The stress field

Similarly to the displacement interpolation, we consider 4 degrees of freedom for each field $\bar{\sigma}_{rz}$, $\tilde{\sigma}_{rr}$, $\tilde{\sigma}_{\theta\theta}$ and $\hat{\sigma}_{rz}$:

$$\begin{aligned} \bar{g}_1 &= \bar{\sigma}_{rz} |_{r=\alpha, z=z^*} & \bar{g}_2 &= \bar{\sigma}_{rz} |_{r=\beta, z=z^*} & \bar{g}_3 &= \bar{\sigma}_{rz} |_{r=\gamma, z=z^*} & \bar{g}_4 &= \bar{\sigma}_{rz} |_{r=\delta, z=z^*} \\ \tilde{g}_1 &= \tilde{\sigma}_{rr} |_{r=\alpha, z=z^*} & \tilde{g}_2 &= \tilde{\sigma}_{rr} |_{r=\beta, z=z^*} & \tilde{g}_3 &= \tilde{\sigma}_{rr} |_{r=\gamma, z=z^*} & \tilde{g}_4 &= \tilde{\sigma}_{rr} |_{r=\delta, z=z^*} \\ \tilde{g}_5 &= \tilde{\sigma}_{\theta\theta} |_{r=\alpha, z=z^*} & \tilde{g}_6 &= \tilde{\sigma}_{\theta\theta} |_{r=\beta, z=z^*} & \tilde{g}_7 &= \tilde{\sigma}_{\theta\theta} |_{r=\gamma, z=z^*} & \tilde{g}_8 &= \tilde{\sigma}_{\theta\theta} |_{r=\delta, z=z^*} \\ \hat{g}_1 &= \hat{\sigma}_{rz} |_{r=\alpha, z=z^*} & \hat{g}_2 &= \hat{\sigma}_{rz} |_{r=\beta, z=z^*} & \hat{g}_3 &= \hat{\sigma}_{rz} |_{r=\gamma, z=z^*} & \hat{g}_4 &= \hat{\sigma}_{rz} |_{r=\delta, z=z^*} \end{aligned}$$

A cubic Lagrange interpolation is addressed for each field:

$$\bar{\boldsymbol{\sigma}} = \begin{bmatrix} 0 \\ 0 \\ \sqrt{2} \bar{\sigma}_{rz} \end{bmatrix} = \bar{\mathbf{R}}_e(r) \bar{\mathbf{g}}_e = \begin{bmatrix} \mathbf{0} \\ \mathbf{0} \\ \sqrt{2} N_e \end{bmatrix} \bar{\mathbf{g}}_{rz} \quad (3.38)$$

$$\tilde{\boldsymbol{\sigma}} = \begin{bmatrix} \tilde{\sigma}_{rr} \\ \tilde{\sigma}_{\theta\theta} \\ 0 \end{bmatrix} = \tilde{\mathbf{R}}_e(r) \tilde{\mathbf{g}}_e = \begin{bmatrix} N_e & \mathbf{0} \\ \mathbf{0} & N_e \\ \mathbf{0} & \mathbf{0} \end{bmatrix} \begin{bmatrix} \tilde{\mathbf{g}}_{rr} \\ \tilde{\mathbf{g}}_{\theta\theta} \end{bmatrix} \quad (3.39)$$

$$\hat{\boldsymbol{\sigma}} = \begin{bmatrix} 0 \\ 0 \\ \sqrt{2} \hat{\sigma}_{rz} \end{bmatrix} = \hat{\mathbf{R}}_e(r) \hat{\mathbf{g}}_e = \begin{bmatrix} \mathbf{0} \\ \mathbf{0} \\ \sqrt{2} N_e \end{bmatrix} \hat{\mathbf{g}}_{rz} \quad (3.40)$$

By gathering these four fields together, the stress tensor is expressed as follows :

$$\boldsymbol{\sigma}(r, z^*) = \begin{bmatrix} \sigma_{rr} \\ \sigma_{\theta\theta} \\ \sqrt{2} \sigma_{rz} \end{bmatrix} = \mathbf{R}_e(r, z^*) \mathbf{g}_e = \begin{bmatrix} \bar{\mathbf{R}}_e(r) & z^* \tilde{\mathbf{R}}_e(r) & z^{*2} \hat{\mathbf{R}}_e(r) \end{bmatrix} \begin{bmatrix} \bar{\mathbf{g}}_e \\ \tilde{\mathbf{g}}_e \\ \hat{\mathbf{g}}_e \end{bmatrix}$$

with:

$$\mathbf{R}_e(r, z^*) \mathbf{g}_e = \begin{bmatrix} \mathbf{0} & z^* N_e & \mathbf{0} & \mathbf{0} \\ \mathbf{0} & \mathbf{0} & z^* N_e & \mathbf{0} \\ \sqrt{2} N_e & \mathbf{0} & \mathbf{0} & \sqrt{2} z^{*2} N_e \end{bmatrix} \begin{bmatrix} \bar{\mathbf{g}}_{rz} \\ \tilde{\mathbf{g}}_{rr} \\ \tilde{\mathbf{g}}_{\theta\theta} \\ \hat{\mathbf{g}}_{rz} \end{bmatrix}$$

The plastic multiplier field

With an axisymmetric 2D element, $\alpha \leq r \leq \beta$, $m \leq z \leq n$, 16 Gauss points are considered where the plastic multiplier rate is calculated. The flow rule is:

$$\dot{\boldsymbol{\epsilon}}_e^p(r, z) = \lambda_e(r, z) \frac{\partial f}{\partial \boldsymbol{\sigma}}(r, z) \quad (3.41)$$

and the expression of the dissipation power is identical the one of Love-Kirchhoff plates.

Discretization of the BEN functional

In order to minimize the BEN functional, the two integrals in eq. (2.5) need to be numerically computed.

Similarly to the Love-Kirchhoff plates, the spatial and time discretization are carried out basing upon the Gauss quadrature and the rectangular rule respectively.

Same as the temporal discretization in Love-Kirchhoff plate theory, we have the temporal discretized BEN functional in statics for Mindlin plate:

The discretized BEN principle for the clamped circular Reissner-Mindlin plate writes:

$$\bar{\Pi}(\mathbf{g}, \mathbf{q}, \boldsymbol{\lambda}) = \sum_{j=1}^m (\boldsymbol{\Lambda}^T \boldsymbol{\lambda} - \Delta \mathbf{q}^T \mathbf{G} \mathbf{g} + \Delta \mathbf{g}^T \mathbf{F} \mathbf{g}) \quad (3.42)$$

where

$$\begin{aligned} \boldsymbol{\Lambda} &= \sum_{e=1}^n \mathbf{P}_e^T \boldsymbol{\Lambda}_e, \\ \mathbf{G} &= \sum_{e=1}^n \int_m^n \int_\alpha^\beta \mathbf{L}_e^T \mathbf{B}_e^T(r) \mathbf{R}_e(r) \mathbf{M}_e 2\pi r dr dz \\ \mathbf{F} &= \sum_{e=1}^n \int_m^n \int_\alpha^\beta \mathbf{M}_e^T \mathbf{R}_e^T(r) \mathbf{S}^T \mathbf{R}_e(r) \mathbf{M}_e 2\pi r dr dz \end{aligned}$$

and $\mathbf{L}_e, \mathbf{M}_e, \mathbf{P}_e$ are the localization matrices.

The BEN principle consists in minimizing the functional (3.42) under the following constraints:

- The boundary and symmetry conditions :

$$\zeta(r=0, t_j) = 0 \quad \zeta(r=R, t_j) = 0 \quad w(r=R, t_j) = 0$$

$$-\sigma_Y \leq z^* \tilde{\sigma}_{rr}(r=0, t_j) = z^* \tilde{\sigma}_{\theta\theta}(r=0, t_j) \leq \sigma_Y$$

$$\sigma_{rz}(r, z = \pm \frac{H}{2}, t_j) = 0$$

- The equilibrium equations :

$$H \bar{\sigma}_{rz}(r_g, t_j) + \frac{H^3}{12} \hat{\sigma}_{rz}(r_g, t_j) + \frac{pr_g}{2} = 0 \quad (3.43)$$

$$\frac{d(r_g \tilde{\sigma}_{rr})}{dr}(r_g, t_j) - \tilde{\sigma}_{\theta\theta}(r_g, t_j) + \frac{12}{H^3} \frac{pr_g^2}{2} = 0 \quad (3.44)$$

- Enforcing the plastic criterion :

$$f_j(\mathbf{g}(r_g, z_g)) - \sigma_Y \leq 0, \quad \lambda_{g,j} \geq 0$$

$$\lambda_{g,j} \frac{\partial f_j(r_g, z_g)}{\partial \boldsymbol{\sigma}} = \mathbf{B}_e(r_g) \Delta \mathbf{q}_e - \mathbf{S} \mathbf{T}_e(r_g) \Delta \mathbf{g}_e$$

- the initial conditions:

$$\mathbf{g}(0) = \mathbf{0}, \quad \mathbf{q}(0) = \mathbf{0}, \quad \boldsymbol{\lambda}(0) = \mathbf{0}$$

The numbering system of the circular Reissner-Mindlin plate element principle is displayed in fig.(3.3) with two elements and two temporal points. The displacement, the rotation angle and the stress fields are located in a 1D axisymmetric element on the straight and lines at $z = z^*$. The plastic multiplier rate fields are calculated in Gauss points in a 2D axisymmetric element.

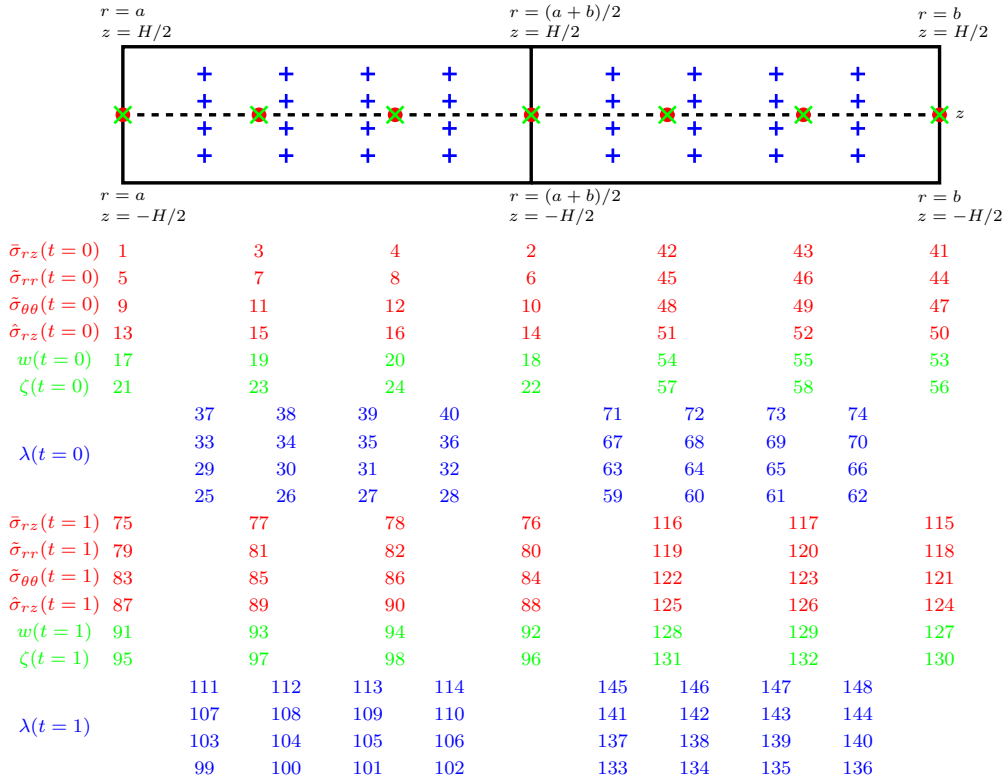


Figure 3.3: Numbering system of Mindlin plate model for the 2D axisymmetric element with 2 elements along radius

3.3 Results and discussion

In this section, we present the numerical results delivered by the BEN variational principle and we compare them to the analytical solution within the elastic regime and the elastoplastic predictions obtained by the step-by-step procedure by using the software Abaqus. von Mises plasticity criterion is employed in the implements.

The algorithm presented in the previous sections is implemented with *Python* language and the *scipy.optimize.minimize* numerical tool is applied so as to find the minimum of the discretized BEN functional. The loading history is displayed in fig. (3.4).

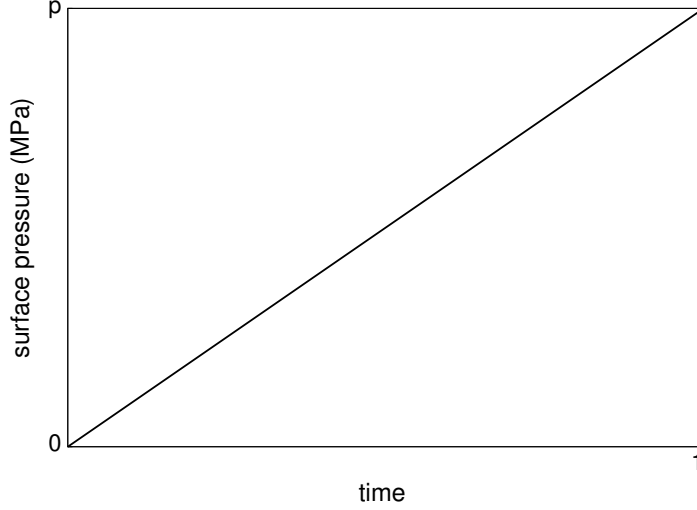


Figure 3.4: The loading path

3.3.1 The Love-Kirchhoff plates

The numerical simulations are carried out with the following data set: the radius $R = 100$ mm, the thickness $H = 4$ mm, Young's modulus $E = 210$ GPa, Poisson's coefficient $\nu = 0.3$ and the plastic yield stress $\sigma_Y = 360$ MPa.

The analytical solution of the studied plate problem in elastic regime exists in the literature (Donnell, 1976). The closed form expression of the transverse displacement w reads:

$$w(r) = -\frac{PR^4}{64D} \left[1 - \left(\frac{r^2}{R^2} \right) \right]^2 \quad (3.45)$$

where

$$D = \frac{E H^3}{12(1 - \nu^2)}$$

The radial moment is given by :

$$M_r(r) = \frac{p}{16} [(1 + \nu)R^2 - (3 + \nu)r^2]$$

Moreover, the radial stress expression at $z = H/2$ is equal to :

$$\sigma_r|_{z=H/2} = \frac{12M_r z}{H^3} = \frac{12H}{2H^3} \frac{p}{16} [(1 + \nu)R^2 - (3 + \nu)r^2]$$

From the equilibrium equation, we get expression of hoop stress in $z = H/2$:

$$\sigma_{\theta}|_{z=H/2} = \frac{12M_r z}{H^3} = \frac{12H}{2H^3} \frac{p}{16} [(1 + \nu)R^2 - 3(3 + \nu)r^2] + \frac{12H}{2H^3} \frac{pr^2}{2}$$

Figure (3.5) displays the transverse displacement along radius in elastic regime with $p = 0.4$ MPa when $t = 1$. Simulation results of radial and hoop stresses are shown in fig. (3.6 and 3.7). From these figures, a good agreement between the BEN predictions and the analytical solution is observed with 2 finite elements.

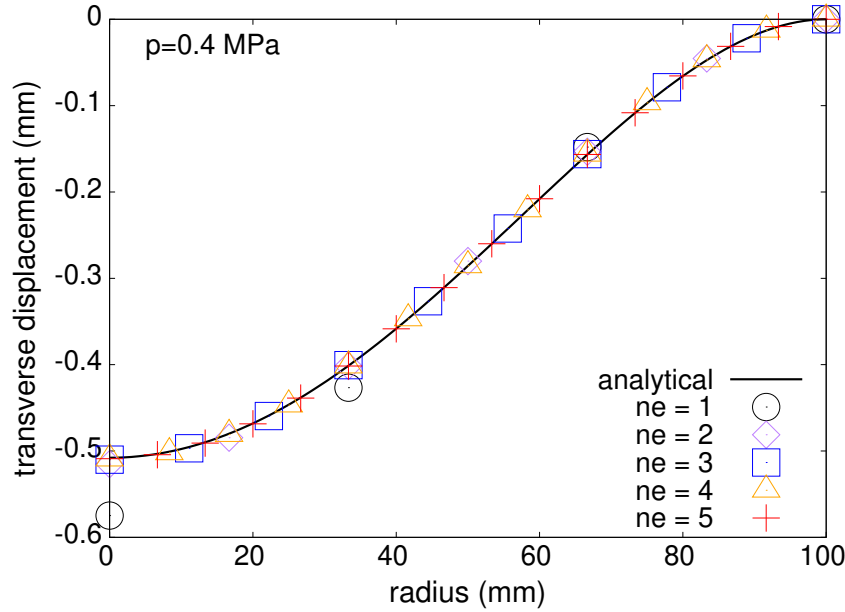


Figure 3.5: Elastic regime / Love-Kirchhoff plate / Comparison of transverse displacement along the radius between the analytical solution (solid black line) and the BEN principle predictions (colored symbols) with different number of elements (ne) under the pressure $p = 0.4$ MPa.

For the elastoplastic response of the plate, analytical solutions are not available. Hence, the BEN principle predictions are compared to the incremental results obtained by the finite element software *Abaqus*. It is important to notice that there are various types of finite elements for plate models in *Abaqus*. We chose *S4R5* element which is a 4-node doubly curved thin shell, reduced integration, hourglass control, using five degrees of freedom per node. The *S4R5* element is suitable to thin plate under Love-Kirchhoff theory.

Figure (3.8) displays the transverse displacement along radius when the plate comes to yield. A good agreement between the BEN solution and the reference *Abaqus* one is observed. The comparisons of radial and hoop stresses plotted in fig.(3.9 and 3.10). An small difference between the BEN simulations and the *Abaqus* predictions is observed. However, it can be seen that BEN's numerical results converge to the same solution with increasing the number of elements.

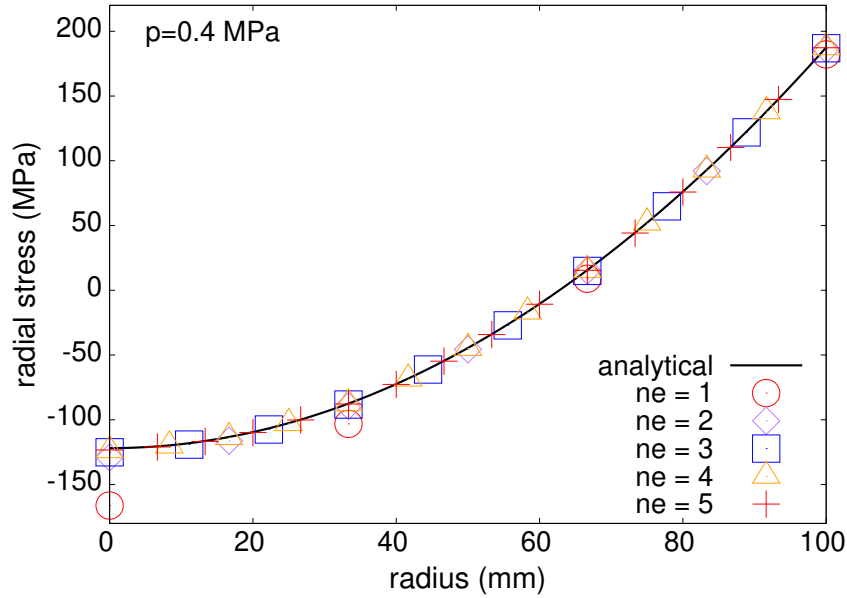


Figure 3.6: Elastic regime / Love-Kirchhoff plate / Comparison of radial stress along the radius between the analytical solution (solid black line) and the BEN principle solution (colored symbols) with different number of elements (ne) under the pressure $p = 0.4$ MPa.

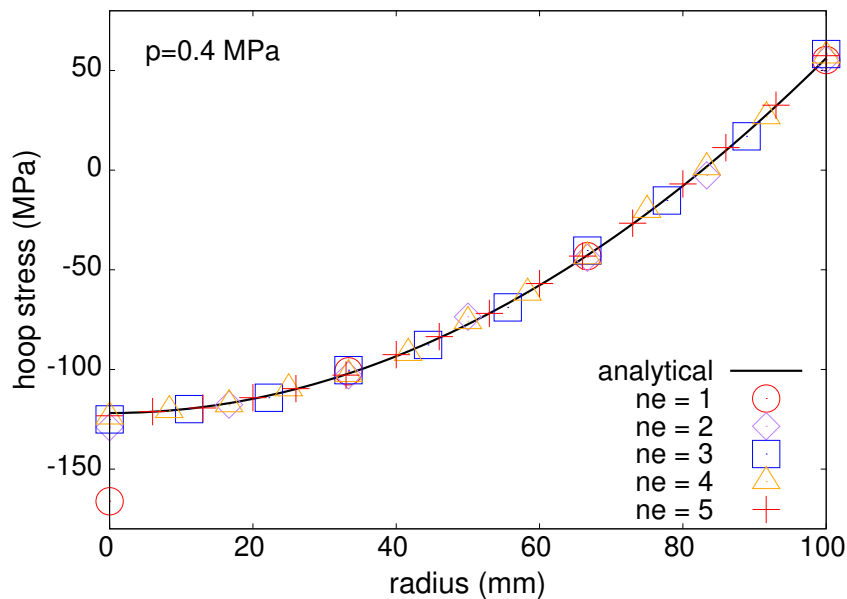


Figure 3.7: Elastic regime / Love-Kirchhoff plate / Comparison of hoop stress along the radius between the analytical solution (solid black line) and the BEN principle solution (colored symbols) with different number of elements (ne) under the pressure $p = 0.4$ MPa.

3.3.2 The Reissner-Mindlin plates

We use the same numerical values as the Love-Kirchhoff plate unless the thickness which is now taken to be $H = 16$ mm.

For Mindlin plate, We chose $S4R$ element which is a 4-node doubly curved thin or thick shell, reduced integration, hourglass control, finite membrane strains. The $S4R5$ element is suitable

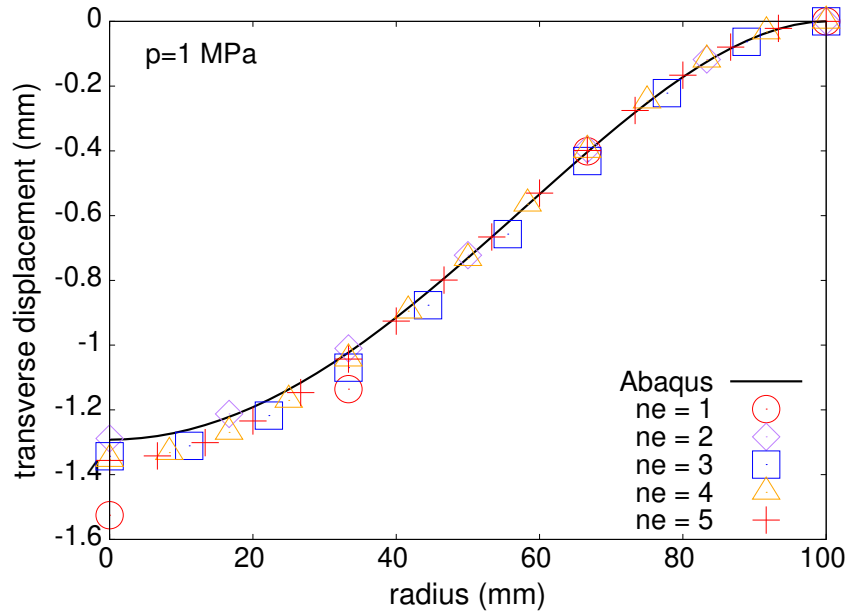


Figure 3.8: Elastoplastic regime / Love-Kirchhoff plate / Comparison of transverse displacement along the radius between the Abaqus solution (solid black line) and the BEN principle solution (colored symbols) with different number of elements (ne) under the pressure $p = 1$ MPa.

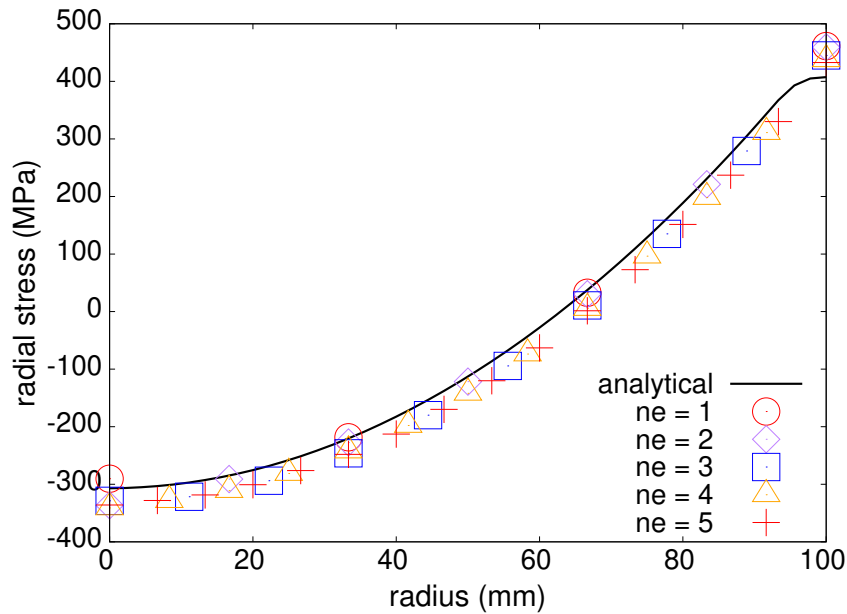


Figure 3.9: Elastoplastic regime / Love-Kirchhoff plate / Comparison of radial stress along the radius between the analytical solution (solid black line) and the BEN principle solution (colored symbols) with different number of elements (ne) under the pressure $p = 1$ MPa.

to thin and thick plate under Mindlin theory.

Under the applied pressure $p = 10$ MPa, the Reissner-Mindlin is in an elastic state. The transverse displacement in elastic regime is displayed in fig. (3.11). Comparisons of radial and hoop stresses obtained by the BEN principle with the Abaqus results solution are displayed in figs.(3.12, 3.12). A good agreement is observed.

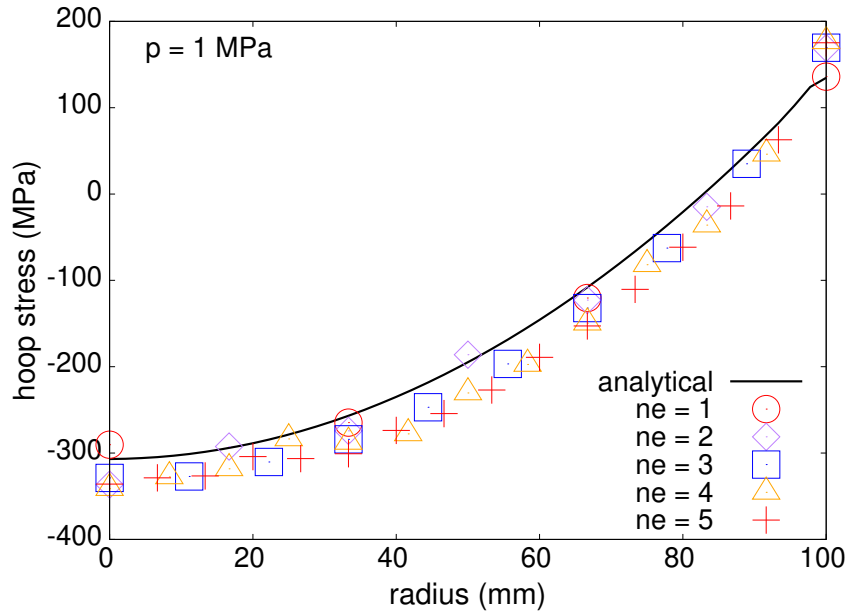


Figure 3.10: Elastoplastic regime / Love-Kirchhoff plate / Comparison of hoop stress along the radius between the analytical solution (solid black line) and the BEN principle solution (colored symbols) with different number of elements (ne) under the pressure $p = 1$ MPa.

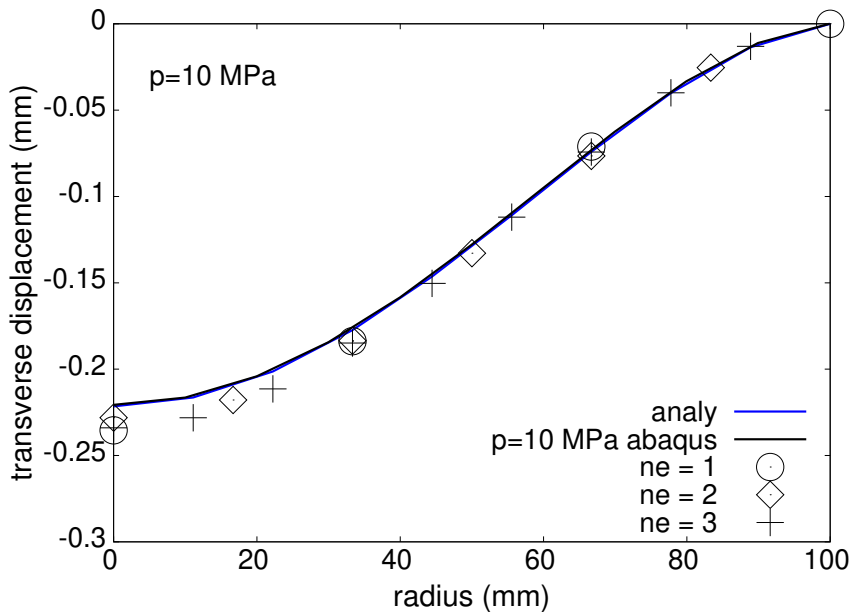


Figure 3.11: Elastic regime / Reissner-Mindlin plate / The comparison between the analytical solution and the numerical results along the radius under the pressure $p = 10$ MPa.

When the exerted uniform pressure increases, the plate comes to yield. For instance, under the pressure $p = 16$ MPa, Fig.(3.14, 3.15 and 3.16) compare the transverse displacement, the radial and the hoop stress along radius obtained by the BEN principle and Abaqus incremental results. Again a good agreement between the predictions is observed.

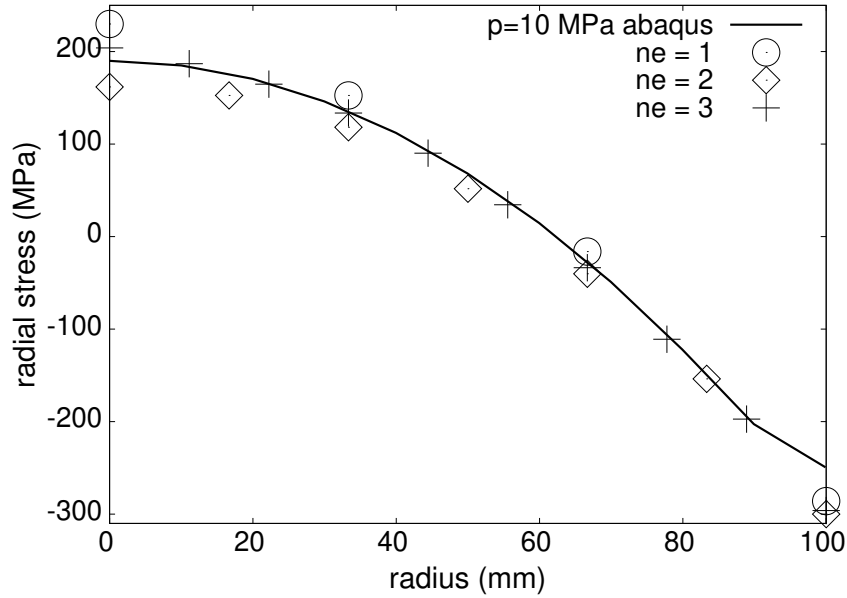


Figure 3.12: Elastic regime / Reissner-Mindlin plate / Comparison of the analytical solution for the radial stress and numerical predictions along the radius under the pressure $p = 10$ MPa.

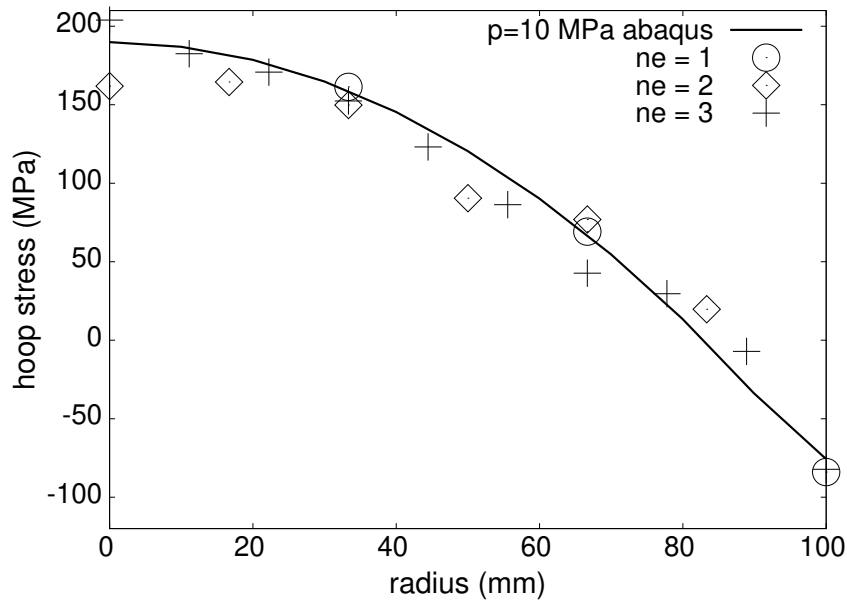


Figure 3.13: Elastic regime / Reissner-Mindlin plate / comparison of the analytical solution giving the hoop stress and the numerical predictions along the radius under the pressure $p = 10$ MPa.

3.4 Conclusion

In this chapter, numerical implementation of the BEN method in two types of plate models is achieved. An axisymmetric circular thin or thick plate under a surface pressure is examined. The BEN principle has transformed a circular plate mechanical problem into a constrained optimization mathematical one. Comparing to the last chapter, the BEN principle is now implemented

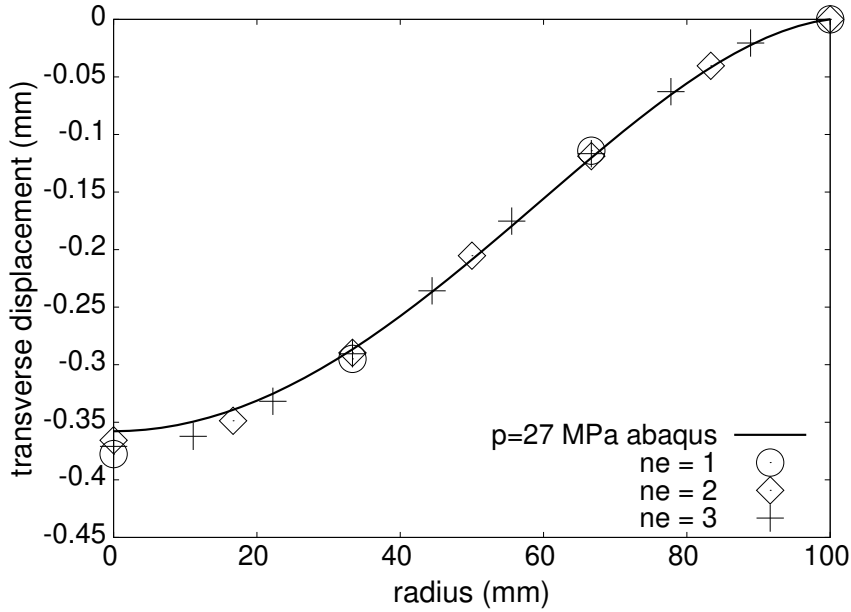


Figure 3.14: Elastoplastic response / Reissner-Mindlin plate / Comparison of the BEN results and Abaqus predictions for the displacement field along the radius under the pressure $p = 16$ MPa.

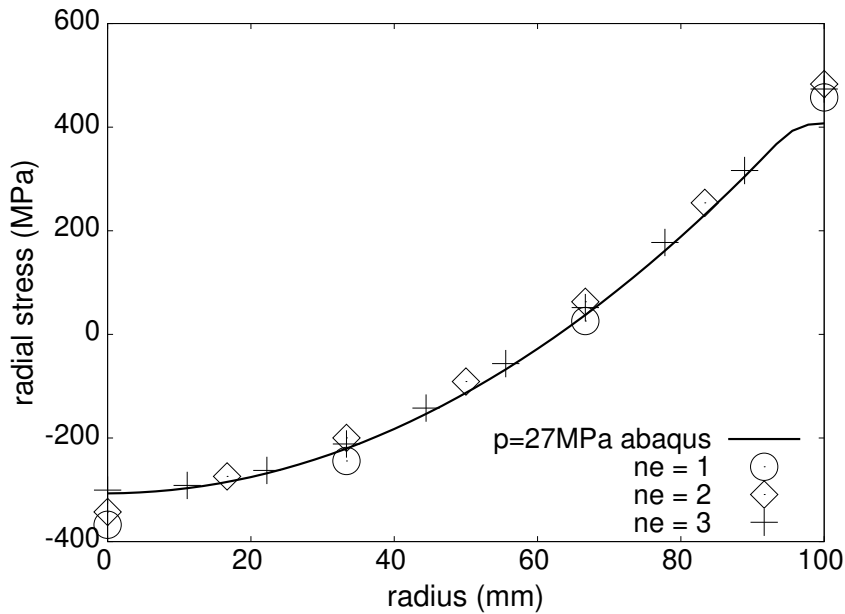


Figure 3.15: Elastoplastic response / Reissner-Mindlin plate / Comparison of the BEN results and Abaqus predictions for the radial stress along the radius under the pressure $p = 16$ MPa.

in *Python* language which is more and more applied in programming.

The classical step-by-step incremental method is able to provide good simulation results. The peculiarity of BEN method for solving all time steps simultaneously is not necessary in statics, our object is to test the feasibility of BEN method in a numerical point of view for solving a plate problem. For Love-Kirchhoff plate, interpolation of displacement is managed by Lagrange polynomial. Its continuity C^1 is ensured in optimization constraint in place of Hermite

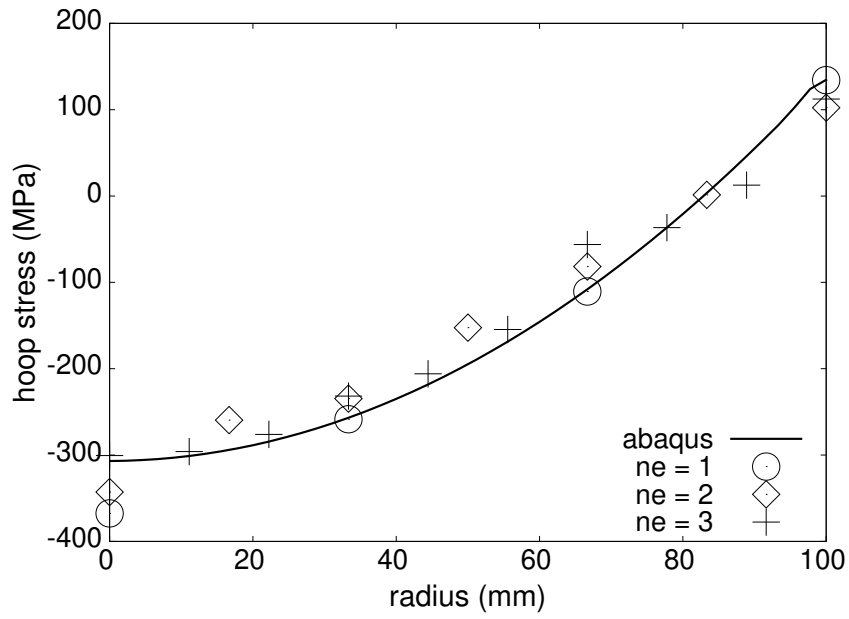


Figure 3.16: Elastoplastic response / Reissner-Mindlin plate / Comparison of the BEN results and Abaqus predictions for the hoop stress along the radius under the pressure $p = 16$ MPa.

interpolation used in incremental code. The BEN method provides an excellent result compared to the analytical or step-by-step software solution.

Chapter **4**

A non-incremental numerical method for
dynamic elastoplastic problems by the
symplectic Brezis-Ekeland-Nayroles principle

4.1	Application to dynamic plasticity	90
4.2	Computational procedure for the pressurized tube	92
4.2.1	Problem statement	92
4.2.2	Discretization of the problem	93
4.2.3	Discretization of the SBEN principle	98
4.3	Results and discussion	102
4.3.1	The thin tube	104
4.3.2	The thick-walled tube	108
4.3.3	Comparison between the methods A and B	112
4.4	Conclusion and outlook	114

This chapter is devoted to the numerical application of symplectic BEN principle for an elastic perfectly plastic and viscoplastic thick and thin wall tube model subjected to internal pressure in dynamics. The mixed finite element method is applied to the discretization and the numerical implementation of the minimization problem as previously. Two methods to satisfy the equilibrium equation are presented in detail. Good accuracy is observed compared to the analytical solution and step-by-step numerical one.

4.1 Application to dynamic plasticity

Consider an elastic perfectly plastic solid occupying the volume Ω with a smooth boundary $\partial\Omega$. It is loaded by given body forces \mathbf{f}^v on Ω , a prescribed displacement field \mathbf{u}^d on Γ_u and surface tractions \mathbf{t}^d exerted on the complementary part $\Gamma_t = \partial\Omega - \Gamma_u$. Recall that Γ_u and Γ_t are fixed and they satisfy $\Gamma_u \cap \Gamma_t = \emptyset$. The data set $(\mathbf{f}^v, \mathbf{t}^d, \mathbf{u}^d)$ depends on the time t in the time interval $[0, T]$ and characterizes the mechanical loading path at every point $\mathbf{x} \in \Omega$.

Let $(\boldsymbol{\sigma}, \boldsymbol{\varepsilon}, \mathbf{u})$ denote the dynamic elastic-plastic response to the given loading path. Within the framework of the infinitesimal transformation, the strain field is additively split into its elastic and plastic parts:

$$\boldsymbol{\varepsilon} = \boldsymbol{\varepsilon}^e + \boldsymbol{\varepsilon}^p \quad (4.1)$$

The elastic strains are related to the stresses through Hooke's law:

$$\boldsymbol{\varepsilon}^e = \mathbf{S} : \boldsymbol{\sigma} \quad (4.2)$$

where \mathbf{S} is the fourth order elastic compliance tensor with the classical major and minor symmetry properties.

Moreover, for generalized standard materials (Halphen and Nguyen, 1975), the associated flow rule ensures that plastic strain rate obeys to the normality law:

$$\dot{\boldsymbol{\varepsilon}}^p = \lambda \frac{\partial f}{\partial \boldsymbol{\sigma}}(\boldsymbol{\sigma}), \quad f(\boldsymbol{\sigma}) \leq 0, \quad \lambda \geq 0, \quad \lambda f(\boldsymbol{\sigma}) = 0 \quad (4.3)$$

where f stands for the yield criterion and λ denotes the plastic multiplier.

Within the Buliga and de Saxcé formalism, the space X is composed of the vectors $x = (\mathbf{u}, \boldsymbol{\varepsilon}^p)$ while the element of the space Y are $y = (\mathbf{p}, \boldsymbol{\pi})$ where \mathbf{p} is the linear momentum and $\dot{\boldsymbol{\pi}} = \boldsymbol{\sigma}$ (Buliga and de Saxcé, 2017). The element z of the phase space is defined by $z = (x, y)$ and the

duality between the spaces X and Y writes:

$$\langle x, y \rangle = \int_{\Omega} (\mathbf{u} \cdot \mathbf{p} + \boldsymbol{\varepsilon}^p : \boldsymbol{\pi}) \quad (4.4)$$

To recover the standard plasticity, we suppose ϕ depends explicitly only on $\dot{\boldsymbol{\pi}} = \boldsymbol{\sigma}$:

$$\phi(z) = \int_{\Omega} \varphi(\dot{\boldsymbol{\pi}}) = \int_{\Omega} \varphi(\boldsymbol{\sigma}) \quad (4.5)$$

According to Buliga and de Saxcé, the SBEN principle for dynamic plasticity writes:

Proposition 4.1.1. The SBEN principle claims that the evolution curves $\boldsymbol{\sigma}$ and \mathbf{u} minimizes the functional

$$\Phi(\boldsymbol{\sigma}, \dot{\mathbf{u}}) = \int_{\Omega} \int_0^T \{ \phi(\boldsymbol{\sigma}) + \phi^*(\nabla_s \dot{\mathbf{u}} - \mathbf{S} : \dot{\boldsymbol{\sigma}}) - \boldsymbol{\sigma} : (\nabla_s \dot{\mathbf{u}} - \mathbf{S} : \dot{\boldsymbol{\sigma}}) \} \quad (4.6)$$

among all curves satisfying:

- the balance of linear momentum:

$$\nabla \cdot \boldsymbol{\sigma} + \mathbf{f}^v = \rho \ddot{\mathbf{u}} \quad \text{on } \Omega \quad (4.7)$$

- the compatibility of the displacement

$$\boldsymbol{\varepsilon} = \nabla_s \mathbf{u} \quad (4.8)$$

- the boundary conditions

$$\mathbf{u} = \mathbf{u}^d \text{ on } \Gamma_u, \quad \text{and} \quad \boldsymbol{\sigma} \cdot \mathbf{n} = \mathbf{t}^d \text{ on } \Gamma_t \quad (4.9)$$

- the initial conditions

$$\mathbf{u}(\mathbf{x}, 0) = \mathbf{u}_0(\mathbf{x}), \quad \dot{\mathbf{u}}(\mathbf{x}, 0) = \mathbf{v}_0(\mathbf{x}) \quad \text{and} \quad \boldsymbol{\sigma}(\mathbf{x}, 0) = \boldsymbol{\sigma}_0(\mathbf{x}) \quad (4.10)$$

For the proof, the reader is referred to (Buliga and de Saxcé, 2017).

4.2 Computational procedure for the pressurized tube

4.2.1 Problem statement

In order to show the ability of the SBEN to compute at once the dynamical response of elastic-perfectly plastic solids, we consider an infinitely long tube subjected to an internal pressure under plane strain conditions. Tresca yield criterion with the associated flow rule is used. The fundamental difference with the quasi-static problems worked out in (Cao et al., 2020b) is that now the inertial effects are involved which makes the problem much more complex.

The displacement field depends on the time and, due to the symmetry of the structure, it is axisymmetric:

$$\mathbf{u}(r, t) = u_r(r, t)\mathbf{e}_r \quad (4.11)$$

Subsequently, the strain field $\boldsymbol{\varepsilon}$ writes:

$$\boldsymbol{\varepsilon}(r, t) = \begin{pmatrix} \frac{du_r}{dr} & 0 \\ 0 & \frac{u_r}{r} \end{pmatrix} \quad (4.12)$$

Moreover the stress tensor is given by

$$\boldsymbol{\sigma}(r, t) = \begin{pmatrix} \sigma_r & 0 \\ 0 & \sigma_\theta \end{pmatrix} \quad (4.13)$$

Application of Hooke's law in plane strains elasticity yields following relations:

$$\varepsilon_r = \frac{1}{\bar{E}}(\sigma_r - \bar{\nu}\sigma_\theta) \quad , \quad \varepsilon_\theta = \frac{1}{\bar{E}}(\sigma_\theta - \bar{\nu}\sigma_r)$$

where

$$\bar{E} = \frac{E}{1 - \nu^2} \quad , \quad \bar{\nu} = \frac{\nu}{1 - \nu}$$

Under the applied internal pressure, the hollow cylinder experiences elastic behavior as long as the stress states are strictly inside the elastic domain K defined by the convex yield function f :

$$K = \{\boldsymbol{\sigma}; f(\boldsymbol{\sigma}) \leq 0\} \quad (4.14)$$

The equation $f(\boldsymbol{\sigma}) = 0$ is the yielding condition for which irreversible plastic deformations develop. The Tresca criterion is expressed by the principle stresses in the form:

$$f(\boldsymbol{\sigma}) = \text{Sup}_{i \neq j}(|\sigma_i - \sigma_j|) - \sigma_Y = |\sigma_\theta - \sigma_r| - \sigma_Y \leq 0 \quad (4.15)$$

where σ_Y is the traction yield stress.

The dissipation potential of the solid is the indicator function of the elastic set k :

$$\varphi(\boldsymbol{\sigma}) = \chi_K(\boldsymbol{\sigma}) = \begin{cases} 0 & \text{if } f(\boldsymbol{\sigma}) < 0, \\ \infty & \text{otherwise} \end{cases} \quad (4.16)$$

Its Fenchel transformation, called the support function of K , is given by

$$\varphi^*(\boldsymbol{\varepsilon}^p) = \sup_{\boldsymbol{\sigma} \in K} (\boldsymbol{\sigma} : \boldsymbol{\varepsilon}^p) \quad (4.17)$$

4.2.2 Discretization of the problem

Due to the axisymmetric property and the plane strain conditions, the tube is discretized using 1D axisymmetric elements along the radius. Moreover, the objective function of the SBEN formulation is a 2-fields functional, depending on both the stress and displacement fields, that leads naturally to use the mixed finite element method which is more suitable for enforcing the yield condition in elastoplastic computations. However, it is important to underline that mixed finite element method is not mandatory and the standard displacement method can be combined with the SBEN principle because the stress field can be expressed in term of the displacement gradient through $\boldsymbol{\sigma} = \mathbf{S}^{-1} : (\nabla_s \mathbf{u} - \boldsymbol{\varepsilon}^p)$.

Approximation of the displacement field

Let us consider the 1D axisymmetric reference element with $\alpha \leq r \leq \beta$. The displacement field is approximated using the following polynomial interpolation:

$$u_r = v_1 + v_2 r + v_3 r^2 + v_4 r^3 \quad (4.18)$$

leading to the following approximation of the strain components:

$$\varepsilon_r = \frac{du_r}{dr} = v_2 + 2v_3 r + 3v_4 r^2, \quad \varepsilon_\theta = \frac{u_r}{r} = \frac{v_1}{r} + v_2 + v_3 r + v_4 r^2 \quad (4.19)$$

Notice that there are two connectors:

$$q_1 = u_r |_{r=\alpha}, \quad q_2 = u_r |_{r=\beta}, \quad (4.20)$$

Considering two intermediate equidistant nodes of position:

$$\gamma = \frac{2\alpha + \beta}{3}, \quad \delta = \frac{\alpha + 2\beta}{3}$$

we introduce two extra degrees of freedom internal to the element (not connected with the other ones):

$$q_3 = u_r |_{r=\gamma}, \quad q_4 = u_r |_{r=\delta}$$

that defines a cubic Lagrange interpolation:

$$u_r(r) = \frac{1}{16} [- (1 - \bar{r})(1 - 9\bar{r}^2), - (1 + \bar{r})(1 - 9\bar{r}^2), 9(1 - \bar{r}^2)(1 - 3\bar{r}), 9(1 - \bar{r}^2)(1 + 3\bar{r})] \begin{bmatrix} q_1 \\ q_2 \\ q_3 \\ q_4 \end{bmatrix} \quad (4.21)$$

where:

$$\bar{r} = \frac{2r - (\beta + \alpha)}{\beta - \alpha}$$

In terms of shape function matrix \mathbf{N}_e , we have:

$$u_r(r) = \mathbf{N}_e(r) \mathbf{q}_e \quad (4.22)$$

The corresponding strain field is expressed in terms of the nodal displacements as follows:

$$\boldsymbol{\varepsilon}(r) = \begin{bmatrix} \varepsilon_r \\ \varepsilon_\theta \end{bmatrix} = \begin{bmatrix} \frac{d\mathbf{N}_e}{d\bar{r}} \frac{d\bar{r}}{dr} \\ \frac{\mathbf{N}_e}{r} \end{bmatrix} \mathbf{q}_e = \mathbf{B}_e(r) \mathbf{q}_e$$

where \mathbf{B}_e is the strain or gradient matrix. Straightforward calculations lead to:

$$\mathbf{B}_e(r) = \frac{1}{16} \begin{bmatrix} J(1 + 18\bar{r} - 27\bar{r}^2) & J(-1 + 18\bar{r} + 27\bar{r}^2) & J(-27 - 18\bar{r} + 81\bar{r}^2) & J(27 - 18\bar{r} - 81\bar{r}^2) \\ -\frac{1}{r}(1 - \bar{r})(1 - 9\bar{r}^2) & -\frac{1}{r}(1 + \bar{r})(1 - 9\bar{r}^2) & \frac{9}{r}(1 - \bar{r}^2)(1 - 3\bar{r}) & \frac{9}{r}(1 - \bar{r}^2)(1 + 3\bar{r}) \end{bmatrix}$$

with:

$$J = \frac{d\bar{r}}{dr} = \frac{2}{\beta - \alpha}$$

Approximation of the stress field

In the present work, two different methods are considered for handling the stress field:

1. Method A which considers the balance of momentum equation as a constraint in the optimization procedure. It is satisfied only at Gauss points.
2. Method B which enforces the balance of momentum equation exactly.

Method A: *the balance of momentum is satisfied only at Gauss points*

The radial and hoop stress components are approximated within the finite element by the following stress fields:

$$\sigma_r = h_1 + h_2 r + h_3 r^2 + h_4 r^3 \quad (4.23)$$

$$\sigma_\theta = h_5 + h_6 r + h_7 r^2 + h_8 r^3 \quad (4.24)$$

depending on eight stress parameters h_1, \dots, h_8 that are expressed in terms of nodal values:

$$g_1 = \sigma_r |_{r=\alpha}, \quad g_2 = \sigma_r |_{r=\beta}, \quad g_3 = \sigma_r |_{r=\gamma}, \quad g_4 = \sigma_r |_{r=\delta} \quad (4.25)$$

$$s_1 = \sigma_\theta |_{r=\alpha}, \quad s_2 = \sigma_\theta |_{r=\beta}, \quad s_3 = \sigma_\theta |_{r=\gamma}, \quad s_4 = \sigma_\theta |_{r=\delta} \quad (4.26)$$

by means of shape function matrices:

$$\sigma_r(r) = \mathbf{N}_e(r) \mathbf{g}_e \quad \sigma_\theta(r) = \mathbf{N}_e(r) \mathbf{s}_e$$

or in compact form:

$$\boldsymbol{\sigma}_e(r) = \begin{bmatrix} \sigma_r \\ \sigma_\theta \end{bmatrix} = \begin{bmatrix} \mathbf{N}_e(r) & \mathbf{0} \\ \mathbf{0} & \mathbf{N}_e(r) \end{bmatrix} \begin{bmatrix} \mathbf{g}_e \\ \mathbf{s}_e \end{bmatrix} = \mathbf{T}_e(r) \mathbf{t}_e$$

Method B

With the 1D axisymmetric element occupying the segment $\alpha \leq r \leq \beta$, we consider four stress connectors:

$$g_1 = \sigma_r |_{r=\alpha}, \quad g_2 = \sigma_\theta |_{r=\alpha}, \quad g_3 = \sigma_r |_{r=\beta}, \quad g_4 = \sigma_\theta |_{r=\beta} \quad (4.27)$$

The choice of the polynomial stress field is guided by the aim to satisfy exactly the local dynamic equation. To this end, the general solution of the balance of momentum equation:

$$\nabla \cdot \boldsymbol{\sigma} = \dot{\mathbf{p}} = \rho \ddot{\mathbf{u}} \quad (4.28)$$

is the sum of the general solution $\boldsymbol{\sigma}_h$ of the homogeneous equation and a particular solution $\boldsymbol{\sigma}_d$ of the non homogeneous equation. Following Schaefer ((Schaefer, 1953), (Gurtin, 1972)), the homogeneous solution is sought under the form:

$$\boldsymbol{\sigma}_h = 2 \nabla_s \mathbf{w} - (\nabla \cdot \mathbf{w}) \mathbf{I} \quad (4.29)$$

where the vector potential \mathbf{w} is solution of

$$\nabla^2 \mathbf{w} = \dot{\mathbf{p}} \quad (4.30)$$

For the displacement field, we seek a radial vector potential. The previous equation reduces to:

$$\frac{d^2 w_r}{dr^2} + \frac{1}{r} \frac{dw_r}{dr} - \frac{w_r}{r^2} = \rho (\dot{v}_1 + \dot{v}_2 r + \dot{v}_3 r^2 + \dot{v}_4 r^3)$$

Clearly, a solution is given by a homogeneous polynomial in r of degree five. Introducing it in the previous equation, we obtain by identification:

$$w_r = \rho \left(\frac{\dot{v}_1}{3} r^2 + \frac{\dot{v}_2}{8} r^3 + \frac{\dot{v}_3}{15} r^4 + \frac{\dot{v}_4}{24} r^5 \right)$$

The relation (4.29) reads in polar coordinates:

$$\sigma_r = 2 \frac{dw_r}{dr} - \frac{1}{r} \frac{d}{dr}(r w_r), \quad \sigma_\theta = 2 \frac{w_r}{r} - \frac{1}{r} \frac{d}{dr}(r w_r)$$

and leads to the expression of the solution $\boldsymbol{\sigma}_d$ of the non homogeneous equation:

$$\sigma_r = -\sigma_\theta = \rho \left(\frac{\dot{v}_1}{3} r + \frac{\dot{v}_2}{4} r^2 + \frac{\dot{v}_3}{5} r^3 + \frac{\dot{v}_4}{6} r^4 \right)$$

Besides, the stress field being defined by four connectors, we choose for the solution $\boldsymbol{\sigma}_h$ of the homogeneous equation:

$$\sigma_r = h_1 + h_2 r + h_3 r^2 + h_4 r^3$$

Using the internal equilibrium equation, the hoop stress is:

$$\sigma_\theta = h_1 + 2h_2r + 3h_3r^2 + 4h_4r^3$$

In matrix form, the total stress field in terms of stress and displacement parameters reads:

$$\begin{bmatrix} \sigma_r \\ \sigma_\theta \end{bmatrix} = \boldsymbol{\sigma}_e(r) = \mathbf{R}_e(r) \mathbf{h}_e + \mathbf{S}_e(r) \dot{\mathbf{v}}_e$$

$$= \begin{bmatrix} 1 & r & r^2 & r^3 \\ 1 & 2r & 3r^2 & 4r^3 \end{bmatrix} \begin{bmatrix} h_1 \\ h_2 \\ h_3 \\ h_4 \end{bmatrix} + \rho \begin{bmatrix} \frac{r}{3} & \frac{r^2}{4} & \frac{r^3}{5} & \frac{r^4}{6} \\ -\frac{r}{3} & -\frac{r^2}{4} & -\frac{r^3}{5} & -\frac{r^4}{6} \end{bmatrix} \begin{bmatrix} \dot{v}_1 \\ \dot{v}_2 \\ \dot{v}_3 \\ \dot{v}_4 \end{bmatrix}$$

The stress connectors (4.27) are linearly depending on the stress and displacement parameters:

$$\mathbf{g}_e = \mathbf{C}_e \mathbf{h}_e + \mathbf{D}_e \dot{\mathbf{v}}_e$$

with the connection matrix:

$$\mathbf{C}_e = \begin{bmatrix} 1 & \alpha & \alpha^2 & \alpha^3 \\ 1 & 2\alpha & 3\alpha^2 & 4\alpha^3 \\ 1 & \beta & \beta^2 & \beta^3 \\ 1 & 2\beta & 3\beta^2 & 4\beta^3 \end{bmatrix} \quad \mathbf{D}_e = \rho \begin{bmatrix} \frac{\alpha}{3} & \frac{\alpha^2}{4} & \frac{\alpha^3}{5} & \frac{\alpha^4}{6} \\ -\frac{\alpha}{3} & -\frac{\alpha^2}{4} & -\frac{\alpha^3}{5} & -\frac{\alpha^4}{6} \\ \frac{\beta}{3} & \frac{\beta^2}{4} & \frac{\beta^3}{5} & \frac{\beta^4}{6} \\ -\frac{\beta}{3} & -\frac{\beta^2}{4} & -\frac{\beta^3}{5} & -\frac{\beta^4}{6} \end{bmatrix}$$

Hence, one has: $\mathbf{h}_e = \mathbf{C}_e^{-1}(\mathbf{g}_e - \mathbf{D}_e \dot{\mathbf{v}}_e)$.

By identification of (4.18) with (4.21), we obtain the relation between displacement parameters and connectors:

$$\mathbf{v}_e = \mathbf{A}_e \dot{\mathbf{q}}_e$$

$$\mathbf{A}_e^T =$$

$$\begin{bmatrix} \frac{1}{16} \left(9\left[\frac{\hat{\alpha}}{\hat{\beta}}\right]^3 + 9\left[\frac{\hat{\alpha}}{\hat{\beta}}\right]^2 - \frac{\hat{\alpha}}{\hat{\beta}} - 1 \right) & \frac{1}{8} \left(-27\frac{\hat{\alpha}^2}{\hat{\beta}^3} - 18\frac{\hat{\alpha}}{\hat{\beta}^2} + \frac{1}{\hat{\beta}} \right) & \frac{1}{4} \left(27\frac{\hat{\alpha}}{\hat{\beta}^3} + 9\frac{1}{\hat{\beta}^2} \right) & \frac{-9}{2\hat{\beta}^3} \\ \frac{1}{16} \left(-9\left[\frac{\hat{\alpha}}{\hat{\beta}}\right]^3 + 9\left[\frac{\hat{\alpha}}{\hat{\beta}}\right]^2 + \frac{\hat{\alpha}}{\hat{\beta}} - 1 \right) & \frac{1}{8} \left(27\frac{\hat{\alpha}^2}{\hat{\beta}^3} - 18\frac{\hat{\alpha}}{\hat{\beta}^2} - \frac{1}{\hat{\beta}} \right) & \frac{1}{4} \left(-27\frac{\hat{\alpha}}{\hat{\beta}^3} + 9\frac{1}{\hat{\beta}^2} \right) & \frac{9}{2\hat{\beta}^3} \\ \frac{1}{16} \left(-27\left[\frac{\hat{\alpha}}{\hat{\beta}}\right]^3 - 9\left[\frac{\hat{\alpha}}{\hat{\beta}}\right]^2 + 27\frac{\hat{\alpha}}{\hat{\beta}} + 9 \right) & \frac{1}{8} \left(81\frac{\hat{\alpha}^2}{\hat{\beta}^3} + 18\frac{\hat{\alpha}}{\hat{\beta}^2} - \frac{27}{\hat{\beta}} \right) & \frac{1}{4} \left(-81\frac{\hat{\alpha}}{\hat{\beta}^3} - 9\frac{1}{\hat{\beta}^2} \right) & \frac{27}{2\hat{\beta}^3} \\ \frac{1}{16} \left(27\left[\frac{\hat{\alpha}}{\hat{\beta}}\right]^3 - 9\left[\frac{\hat{\alpha}}{\hat{\beta}}\right]^2 - 27\frac{\hat{\alpha}}{\hat{\beta}} + 9 \right) & \frac{1}{8} \left(-81\frac{\hat{\alpha}^2}{\hat{\beta}^3} + 18\frac{\hat{\alpha}}{\hat{\beta}^2} + \frac{27}{\hat{\beta}} \right) & \frac{1}{4} \left(81\frac{\hat{\alpha}}{\hat{\beta}^3} - 9\frac{1}{\hat{\beta}^2} \right) & \frac{-27}{2\hat{\beta}^3} \end{bmatrix}$$

where: $\hat{\alpha} = \alpha + \beta$, $\hat{\beta} = \beta - \alpha$. Eliminating the stress parameters provides the stress field in terms of stress and displacement connectors:

$$\boldsymbol{\sigma}_e(r) = \mathbf{T}_e(r)\mathbf{g}_e + \mathbf{U}_e(r)\ddot{\mathbf{q}}_e$$

where:

$$\mathbf{T}_e(r) = \mathbf{R}_e(r)\mathbf{C}_e^{-1}, \quad \mathbf{U}_e(r) = (\mathbf{S}_e(r) - \mathbf{R}_e(r)\mathbf{C}_e^{-1}\mathbf{D}_e)\mathbf{A}_e$$

The plastic multiplier field

The yield condition $f(\boldsymbol{\sigma}) \leq 0$ is performed at each of the four Gauss points of position r_g within the reference element. Let the value of the plastic multiplier at the Gauss point be λ_g . Subsequently, if at each Gauss point $f(\boldsymbol{\sigma}) < 0$ then the behavior is elastic ($\lambda_g = 0$) otherwise ($f(\boldsymbol{\sigma}) = 0$) the plastic yielding may occur. For the later case, the normal flow rule writes:

$$\dot{\boldsymbol{\epsilon}}_e^p(r_g) = \lambda_g \left. \frac{\partial f}{\partial \boldsymbol{\sigma}} \right|_{r=r_g} \quad (4.31)$$

The values λ_g of the plastic multipliers at the Gauss points are gathered in the elementary vector $\boldsymbol{\lambda}_e$.

4.2.3 Discretization of the SBEN principle

The SBEN variational formulation (4.6) involves space and time integration which would be carried out numerically. The Gaussian quadrature method which replaces the integral of a function by a bounded sum of its values at integration points multiplied by corresponding weight coefficients, is the most used method in space integrations for computing elementary matrices and vectors. For 1D axisymmetric element we have:

$$\int_{\alpha}^{\beta} \mathbf{A}(r) 2\pi r dr \cong \sum_{g=1}^{n_e} w_g \mathbf{A}(r_g) 2\pi r_g$$

In particular, the total dissipation power in the element reads:

$$\int_{\alpha}^{\beta} D(r) 2\pi r dr = \boldsymbol{\Lambda}_e^T \boldsymbol{\lambda}_e$$

where:

$$\mathbf{\Lambda}_e = \sigma_Y \begin{bmatrix} w_1 2\pi r_1 \\ \dots \\ w_{n_e} 2\pi r_{n_e} \end{bmatrix}, \quad \boldsymbol{\lambda}_e = \begin{bmatrix} \dot{\lambda}_1 \\ \dots \\ \dot{\lambda}_{n_e} \end{bmatrix}$$

On the other hand, the time integral is simply approximated by using the rectangular rule:

$$\int_0^T f(t) dt = \sum_{j=1}^m f(t_j) \Delta t_j$$

This approximation can appear rather rough but numerical experiences for the problem under consideration showed that changing of this quadrature rule by another one, for instance the midpoint rule, does not provide significant improvements.

We describe now the two variants of the optimization procedure proposed before:

Method A The assembly of elementary matrices and vectors is carried out by means of the localization matrices $\mathbf{L}_e, \mathbf{M}_e, \mathbf{P}_e$:

$$\mathbf{t}_e = \mathbf{M}_e \mathbf{t}, \quad \mathbf{q}_e = \mathbf{L}_e \mathbf{q}, \quad \boldsymbol{\lambda}_e = \mathbf{P}_e \boldsymbol{\lambda}$$

It follows that the discretized form of the functional (4.6) writes:

$$\bar{\Pi}(\mathbf{t}, \mathbf{q}, \boldsymbol{\lambda}) = \int_{t_0}^{t_1} (\boldsymbol{\Lambda}^T \boldsymbol{\lambda}(t) - \dot{\mathbf{q}}^T(t) \mathbf{G} \mathbf{t}(t) + \dot{\mathbf{t}}^T(t) \mathbf{F} \mathbf{t}(t)) dt \quad (4.32)$$

with:

$$\boldsymbol{\Lambda} = \sum_{e=1}^n \mathbf{P}_e^T \boldsymbol{\Lambda}_e,$$

$$\mathbf{G} = \sum_{e=1}^n \int_{\alpha}^{\beta} \mathbf{L}_e^T \mathbf{B}_e^T(r) \mathbf{T}_e(r) \mathbf{M}_e 2\pi r dr \quad \mathbf{F} = \sum_{e=1}^n \int_{\alpha}^{\beta} \mathbf{M}_e^T \mathbf{T}_e^T(r) \mathbf{S} \mathbf{T}_e(r) \mathbf{M}_e 2\pi r dr$$

The SBEN claims that the minimum of (4.32) is sought under the following constrains:

- balance of momentum at each Gauss point g of every element e :

$$\frac{d}{dr} \sigma_r(r_g) + \frac{1}{r_g} [\sigma_r(r_g) - \sigma_\theta(r_g)] = \rho \ddot{u}_r(r_g)$$

- boundary conditions:

$$t_{r=a}(t) = -p(t), \quad t_{r=b}(t) = 0$$

- plastic flow rule at every integration point g of every element e :

$$f_g(\mathbf{t}) - \sigma_Y \leq 0, \quad \lambda_g \geq 0, \quad N_Y \lambda_g = \mathbf{B}_e(r_g) \dot{\mathbf{q}}_e - \mathbf{S} \mathbf{T}_e(r_g) \dot{\mathbf{t}}_e$$

- initial conditions:

$$\mathbf{t}(t_0) = \mathbf{0}, \quad \mathbf{q}(t_0) = \mathbf{0}, \quad \boldsymbol{\lambda}(t_0) = \mathbf{0}, \quad \dot{\mathbf{t}}(t_0) = \mathbf{0}, \quad \dot{\mathbf{q}}(t_0) = \mathbf{0}, \quad \ddot{\mathbf{q}}(t_0) = \mathbf{0}$$

Concerning the time discretization, we consider m time step from t_0 to t_m . Enforcing the yield condition only at the beginning and the end of the step, we minimize the objective function:

$$\bar{\Pi}(\mathbf{t}_0, \dots, \mathbf{t}_m, \mathbf{q}_0, \dots, \mathbf{q}_m, \boldsymbol{\lambda}_0, \dots, \boldsymbol{\lambda}_m) = \sum_{j=1}^{j=m} (\boldsymbol{\Lambda}^T \boldsymbol{\lambda}_j - \dot{\mathbf{q}}_j^T \mathbf{G} \mathbf{t}_j + \dot{\mathbf{t}}_j^T \mathbf{F} \mathbf{t}_j) \quad (4.33)$$

under the following constrains:

- balance of momentum equation at every integration point g of every element e and at every time step:

$$t_{r=a,j} = -p(t_j), \quad t_{r=b,j} = 0, \quad \frac{d}{dr} \sigma_r(r_{g,j}) + \frac{1}{r_{g,j}} [\sigma_r(r_{g,j}) - \sigma_\theta(r_{g,j})] = \rho \ddot{u}_r(r_{g,j})$$

- plastic flow rule (at every integration point g of every element e and at every time step):

$$f_{g,j}(\mathbf{t}) - \sigma_Y \leq 0, \quad \lambda_{g,j} \geq 0, \quad N_Y(r_g) \lambda_{g,j} = \mathbf{B}_e(r_g) \mathbf{L}_e \dot{\mathbf{q}}_j - \mathbf{S} \mathbf{T}_e(r_g) \mathbf{M}_e \dot{\mathbf{t}}_j$$

- initial conditions:

$$\mathbf{t}_0 = \mathbf{0}, \quad \mathbf{q}_0 = \mathbf{0}, \quad \boldsymbol{\lambda}_0 = \mathbf{0}, \quad \dot{\mathbf{t}}_0 = \mathbf{0}, \quad \dot{\mathbf{q}}_0 = \mathbf{0}, \quad \ddot{\mathbf{q}}_0 = \mathbf{0}$$

Method B Performing the assembling thanks to the localization matrices $\mathbf{L}_e, \mathbf{M}_e, \mathbf{P}_e$ such that:

$$\mathbf{g}_e = \mathbf{M}_e \mathbf{g}, \quad \mathbf{q}_e = \mathbf{L}_e \mathbf{q}, \quad \boldsymbol{\lambda}_e = \mathbf{P}_e \boldsymbol{\lambda}$$

the discretized form of the functional is:

$$\begin{aligned} \bar{\Pi}(\mathbf{g}, \mathbf{q}, \boldsymbol{\lambda}) = \int_0^T & \left[\boldsymbol{\Lambda}^T \boldsymbol{\lambda}(t) - \dot{\mathbf{q}}^T(t) (\mathbf{G} \mathbf{g}(t) + \tilde{\mathbf{G}} \ddot{\mathbf{q}}(t)) \right. \\ & \left. + \mathbf{g}^T(t) \mathbf{F}_1 \dot{\mathbf{g}}(t) + \dot{\mathbf{q}}^T(t) \mathbf{F}_2 \dot{\mathbf{g}}(t) + \mathbf{g}^T(t) \mathbf{F}_3 \ddot{\mathbf{q}}(t) + \dot{\mathbf{q}}^T(t) \mathbf{F}_4 \ddot{\mathbf{q}}(t) \right] dt \end{aligned} \quad (4.34)$$

with:

$$\Lambda = \sum_{e=1}^n \mathbf{P}_e^T \Lambda_e,$$

$$\mathbf{G} = \sum_{e=1}^n \int_{\alpha}^{\beta} \mathbf{L}_e^T \mathbf{B}_e^T(r) \mathbf{T}_e(r) \mathbf{M}_e 2\pi r dr, \quad \tilde{\mathbf{G}} = \sum_{e=1}^n \int_{\alpha}^{\beta} \mathbf{L}_e^T \mathbf{B}_e^T(r) \mathbf{U}_e(r) \mathbf{L}_e 2\pi r dr,$$

$$\mathbf{F}_1 = \sum_{e=1}^n \int_{\alpha}^{\beta} \mathbf{M}_e^T \mathbf{T}_e^T(r) \mathbf{S} \mathbf{T}_e(r) \mathbf{M}_e 2\pi r dr \quad \mathbf{F}_2 = \sum_{e=1}^n \int_{\alpha}^{\beta} \mathbf{L}_e^T \mathbf{U}_e^T(r) \mathbf{S} \mathbf{T}_e(r) \mathbf{M}_e 2\pi r dr$$

$$\mathbf{F}_3 = \sum_{e=1}^n \int_{\alpha}^{\beta} \mathbf{M}_e^T \mathbf{T}_e^T(r) \mathbf{S} \mathbf{U}_e(r) \mathbf{L}_e 2\pi r dr \quad \mathbf{F}_4 = \sum_{e=1}^n \int_{\alpha}^{\beta} \mathbf{L}_e^T \mathbf{U}_e^T(r) \mathbf{S} \mathbf{U}_e(r) \mathbf{L}_e 2\pi r dr$$

The SBEN principle claims that we have to find the minimum of (4.34) with respect to the path $t \mapsto (\mathbf{g}(t), \mathbf{q}(t), \boldsymbol{\lambda}(t))$ under the constrains of:

- equilibrium (on the boundary, the balance of momentum within the body being satisfies *a priori*):

$$g_{r=a}(t) = -p(t), \quad g_{r=b}(t) = 0$$

- plastic flow rule (at every integration point g of every element e):

$$f_g(\mathbf{g}, \ddot{\mathbf{q}}) - \sigma_Y \leq 0, \quad \lambda_g \geq 0$$

$$\mathbf{N}_Y \lambda_g = \mathbf{B}_e(r_g) \dot{\mathbf{q}}_e - \mathbf{S}(\mathbf{T}_e(r_g) \dot{\mathbf{g}}_e + \mathbf{U}_e(r) \ddot{\mathbf{q}}_e)$$

- initial conditions:

$$\mathbf{g}(t_0) = \mathbf{0}, \quad \mathbf{q}(t_0) = \mathbf{0}, \quad \boldsymbol{\lambda}(t_0) = \mathbf{0}$$

$$\dot{\mathbf{g}}(t_0) = \mathbf{0}, \quad \dot{\mathbf{q}}(t_0) = \mathbf{0}, \quad \dot{\boldsymbol{\lambda}}(t_0) = \mathbf{0}, \quad \ddot{\mathbf{q}}(t_0) = \mathbf{0}$$

Concerning time-discretization, the interval of interest $[0, T]$ divided into time-steps $0 < t_1 < t_2 < \dots < t_j < \dots < T$. For any physical quantity a , we define

$$a_j = a(t_j), \quad \dot{a}_j = \dot{a}(t_j), \quad \dots$$

and on each step, we approximate the time rates at $t = t_j$ by:

$$\dot{a}_j = \frac{a_j - a_{j-1}}{t_j - t_{j-1}}, \quad \ddot{a}_j = \frac{\dot{a}_j - \dot{a}_{j-1}}{t_j - t_{j-1}}, \quad \ddot{\ddot{a}}_j = \frac{\ddot{a}_j - \ddot{a}_{j-1}}{t_j - t_{j-1}}$$

Considering m time step from 0 to T and enforcing the yield condition only at the beginning and the end of the step, we have to minimize the objective function:

$$\begin{aligned} \bar{\Pi}(\mathbf{g}_0, \dots, \mathbf{g}_m, \mathbf{q}_0, \dots, \mathbf{q}_m, \lambda_0, \dots, \lambda_m) = & \sum_{j=1}^{j=m} \left[\boldsymbol{\Lambda}^T \boldsymbol{\lambda}_j - \dot{\mathbf{q}}_j^T \left(\mathbf{G} \mathbf{g}_j + \tilde{\mathbf{G}} \ddot{\mathbf{q}}_j \right) + \mathbf{g}_j^T(t) \mathbf{F}_1 \dot{\mathbf{g}}_j(t) \right. \\ & \left. + \ddot{\mathbf{q}}_j^T(t) \mathbf{F}_2 \dot{\mathbf{g}}_j(t) + \mathbf{g}_j^T(t) \mathbf{F}_3 \ddot{\mathbf{q}}_j(t) + \ddot{\mathbf{q}}_j^T(t) \mathbf{F}_4 \ddot{\mathbf{q}}_j(t) \right] (t_j - t_{j-1}) \end{aligned} \quad (4.35)$$

under the constrains:

- equilibrium (on the boundary, at each time step):

$$g_{r=a,j}(t_j) = -p(t), \quad g_{r=b,j}(t_j) = 0$$

- plastic flow rule (at every integration point g of every element e and at every time step):

$$f_{g,j}(\mathbf{g}, \ddot{\mathbf{q}}) - \sigma_Y \leq 0, \quad \lambda_{g,j} \geq 0,$$

$$\mathbf{N}_Y \lambda_{g,j} = \mathbf{B}_e(r_g) \mathbf{L}_e \dot{\mathbf{q}}_j^T - \mathbf{S} [\mathbf{T}_e(r_g) \mathbf{M}_e \dot{\mathbf{g}}_j + \mathbf{U}_e(r_g) \mathbf{L}_e \ddot{\mathbf{q}}_j]$$

- initial conditions:

$$\mathbf{g}_0 = \mathbf{0}, \quad \mathbf{q}_0 = \mathbf{0}, \quad \boldsymbol{\lambda}_0 = \mathbf{0}, \quad \dot{\mathbf{g}}_0 = \mathbf{0}, \quad \dot{\mathbf{q}}_0 = \mathbf{0}, \quad \ddot{\mathbf{q}}_0 = \mathbf{0}, \quad \ddot{\mathbf{q}}_0 = \mathbf{0}$$

It worthy noting that, in this method, a non classical term $\ddot{\mathbf{q}}$, called the jerk, appears in the time discretization.

The numbering system of both methods A and B are displayed in figs.4.1 and 4.2 respectively. For two elements and eleven temporal points, method A and B provide 319 and 231 degrees of freedom. It means that in the minimization process, there are 319 multivariables for method A in the functional (4.33).

4.3 Results and discussion

The numerical procedure described in the previous section is applied to address the pressurized elastoplastic thin and thick hollow cylinders including inertia effects. The material obeys to Tresca criterion with Young modulus $E = 210$ GPa, Poisson's ratio $\nu = 0.3$, yield stress $\sigma_Y = 360$

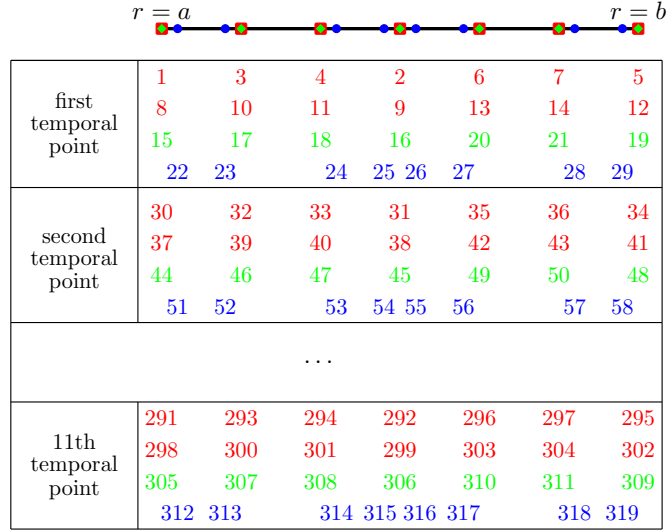


Figure 4.1: Numbering system of method A for the 1D axisymmetric tube (solid black line) with two elements ($ne = 2$) and 11 temporal points ($nt = 11$) the stresses g (red), displacement q (green) and plastic multiplier λ (blue) fields. (Color figure online)

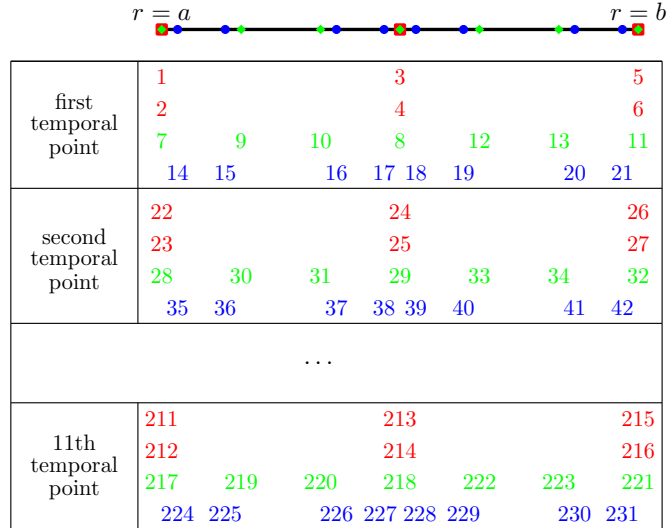


Figure 4.2: Numbering system of method B for the 1D axisymmetric tube (solid black line) with two elements ($ne = 2$) and 11 temporal points ($nt = 11$) the stresses g (red), displacement q (green) and plastic multiplier λ (blue) fields. (Color figure online)

MPa and density $\rho = 7800 \text{ kg/m}^3$. The internal pressure evolution is defined by :

$$p(t) = \begin{cases} p_0 \frac{t}{t_0} & \text{if } 0 \leq t \leq t_0 \\ p_0 & \text{if } t_0 \leq t \end{cases} \quad (4.36)$$

where p_0 and t_0 are given pressure and time respectively as shown in Fig.4.3.

The algorithm is implemented in *Matlab* and the minimization solver *fmincon* is used to find the local minimum of the constrained minimization problem (4.33, 4.35). Basing upon numerical experiences, it is preferred to impose a tiny tolerance for the equality optimization constraints.

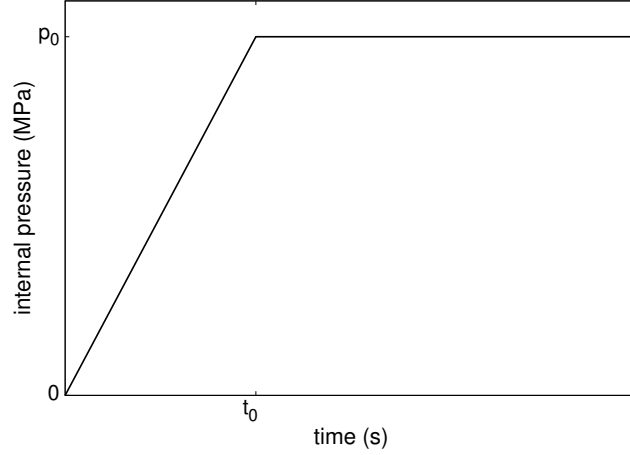


Figure 4.3: The internal applied pressure

It is selected so that the numerical minimum of the cost function is closest to zero, that is the theoretical value.

It is important to underline that the Schaefer superposition technique (method B) for which the balance of momentum equation is exactly satisfied has been privileged in this work. Of course, comparison with the method A is also provided hereafter. The results obtained by the BEN principle are compared with the incremental predictions performed with the finite element code *Cast3M* (Cast3M, 2019).

4.3.1 The thin tube

Let a thin tube of mean radius r , thickness h , in plane strain state, subjected to internal pressure (4.36). The closed form expression of the elastoplastic response can be derived within the framework of the thin cylindrical shell theory (Cao et al., 2020a) for which the hoop stress is constant through the tube thickness and the radial stress is neglected as usual. In the sequel, this Thin Cylindrical Shell solution will be referred as the TCS analytical solution.

The balance of momentum writes:

$$\rho h \ddot{u} + \frac{N}{r} = p(t) \quad (4.37)$$

where $N = h \sigma_{\theta\theta}$ is the circumferential force (by unit length). Introducing the plane strain modulus:

$$E_* = \frac{E}{1 - \nu^2}$$

the force is given in elasticity by:

$$N = E_* h \varepsilon_{\theta\theta} = E_* h \frac{u}{r} \quad (4.38)$$

and for the plastic regime, it writes $N = N_Y = h \sigma_Y$.

The elastoplastic law writes:

$$\begin{aligned} \mathbf{if} \quad N < N_Y \mathbf{ or } (N = N_Y \mathbf{ and } \dot{N} < 0) \mathbf{ then} \\ \dot{\varepsilon}_{\theta\theta}^p &= 0 && \text{! elastic loading/unloading} \\ \mathbf{else} \quad (N = N_Y \mathbf{ and } \dot{N} = 0) \\ \dot{\varepsilon}_{\theta\theta}^p &\geq 0 && \text{! plastic yielding} \end{aligned}$$

Taking into account the pressure loading (4.36), the tube responds elastically until the plastic yield limit is reached. The closed form expression of the elastic displacement reads:

$$\begin{aligned} u(t) = \frac{a_0 p_0}{t_0 \omega^3} & \left[H(t - t_0) \left(\omega(t_0 - t H(t)) + H(t) \sin(\omega(t - t_0)) \right) \right. \\ & \left. + \omega t_0 (H(t) - 1) \cos(\omega(t - t_0)) \right) \\ & \left. + H(t) (\omega t - \sin(\omega t)) \right] \end{aligned} \quad (4.39)$$

where $a_0 = \frac{1}{\rho h}$, $\omega = \frac{1}{r} \sqrt{\frac{E_*}{\rho}}$ is the pulsation and H is the Heaviside step defined by:

$$H(x - x_0) = \begin{cases} 0 & \text{if } x < x_0 \\ 1 & \text{if } x \geq x_0 \end{cases} \quad (4.40)$$

The hoop strain and stress are easily deduced by the Hooke law :

$$\varepsilon_{\theta\theta}(t) = \frac{u(t)}{r} \quad \text{and} \quad \sigma_{\theta\theta} = E_* \frac{u(t)}{r}$$

First, we are interested to the elastic response of the thin tube. Figure 4.4 compares time-evolution of the radial displacement and hoop stress of the internal wall computed by the SBEN principle with the TCS analytical results and numerical predictions carried out by the step-by-step procedure at $r = a$. The data are $r = 100$ mm, $h = 1$ mm, $p_0 = 1$ MPa, $t_0 = 10^{-4}$ s. An excellent agreement is observed: although SBEN principle is devoted to dynamical dissipative systems, it works also for the elastodynamics. It is worthy to notice that elastic regime has been

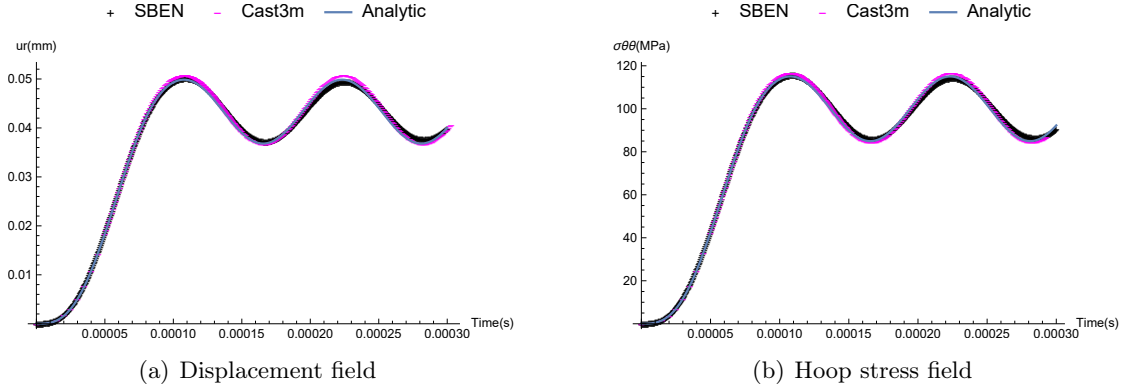


Figure 4.4: Thin tube / Elastic solution - Comparison between TCS analytical and numerical results under the internal pressure $p_0 = 1$ MPa with $ne = 1$, $nt = 600$

tested to verify that the method allows also to detect and to solve the elastic problem in the event that the yield limit is not reached. Of course, if we know *a priori* that the problem is elastic, it is more efficient to use a solver of linear problems.

If the displacement reaches a maximum without plastic yielding and then decreases, the tube is said to rebound and the response becomes purely elastic. Otherwise, beyond the time of incipient plastic yielding t_Y , plastic deformations develops. For $t > t_u$, the tube cannot be plastified any more. After a transient period ($t_Y \leq t \leq t_u$) of plastic yielding, its response becomes again elastic and the plastic dissipation is bounded. Such a behavior is similar to the so-called shakedown of elastoplastic structures under cyclic loads, initially designed for static loadings (Melan, 1938; Koiter, 1960; Hasbroucq et al., 2010, 2012). Our simulation shows that shakedown may occur also in dynamics as predicted by Polizzotto et al. (Polizzotto, 1984b,a) and Comi et al. (Comi and Corigliano, 1991).

The displacement response for the plastic state is given by:

$$\begin{aligned}
 u(t) = & -\frac{1}{2}a_y(t - t_Y)^2 + v_Y(t - t_Y) + u_Y \\
 & + \frac{a_0 p_0}{6t_0} [(3t^2 t_0 - 3t(t_0^2 + t_Y^2) + t_0^3 + 2t_Y^3) H(t - t_0) - (t - t_Y)^2(t + 2t_Y)(H(t - t_0) - 1)H(t - t_Y)]
 \end{aligned}
 \tag{4.41}$$

where u_Y and v_Y are the displacement and the velocity at the time of incipient plastic yielding t_Y .

When the ductility limit is not reached, irreversible plastic strains increase until the displacement reaches its maximum value u_u at the time t_u , and then the response becomes purely elastic.

The closed-form solution of the displacement during the elastic discharge phase writes:

$$u(t) = \frac{1}{\omega^2} \left(a_0 p_0 + b_0 - \left(a_0 p_0 + b_0 - u_u \omega^2 \right) \cos(\omega(t - t_u)) \right) \quad (4.42)$$

where $b_0 = \frac{u_u E_*}{\rho r^2} - \frac{\sigma_Y}{\rho r}$.

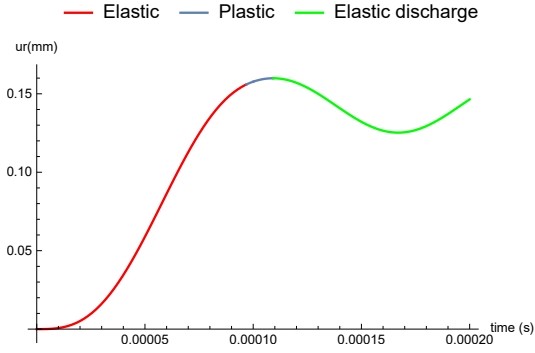


Figure 4.5: Thin tube / TCS analytical solution of the radial displacement for $p_0 = 3.2$ MPa.

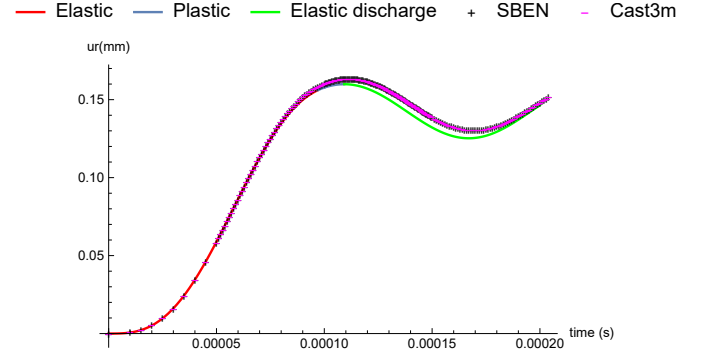


Figure 4.6: Thin tube / Comparison between TCS analytical and numerical results for $p_0 = 3.2$ MPa with $n_e = 1$, $n_t = 270$.

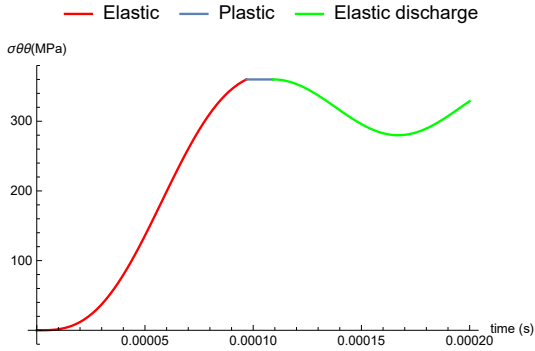


Figure 4.7: Thin tube / TCS analytical evolution of the hoop stress for $p_0 = 3.2$ MPa.

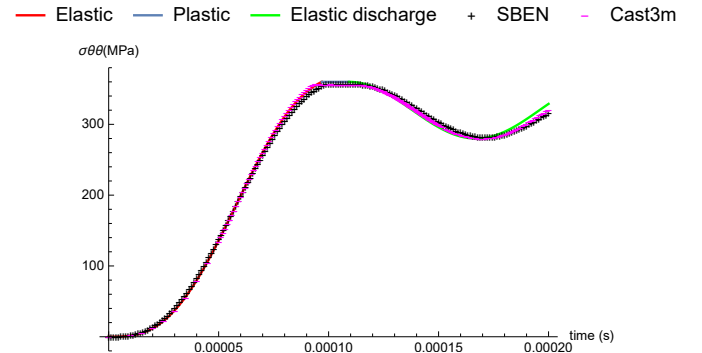


Figure 4.8: Thin tube / Comparison between TCS analytical and numerical results for $p_0 = 3.2$ MPa with $n_e = 1$, $n_t = 270$.

Figures 4.5 to 4.8 depict the thin shell analytical evolution of the radial displacement and the hoop stress versus time and compare them with the numerical results obtained by the SBEN principle and incremental procedure for an internal pressure $p_0 = 3.2$ MPa. It can be seen that the ductility limit is not reached and a shakedown-like response occurs. It is noted in the figures that the SBEN solution agrees very well with predictions provided by the incremental procedure. Moreover, a good concordance between the numerical simulations and the analytical thin shell solution is observed. A slight difference for the displacement field within the range of the plastic and elastic discharge phases is observed. Noticeable difference appears for a higher internal pressure $p_0 = 3.4$ MPa as shown in Figs.4.9 and 4.10. This can be explained by that in the

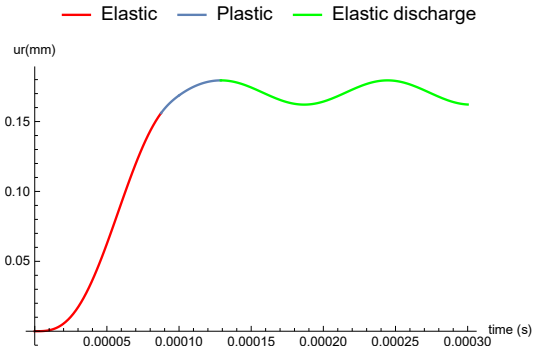


Figure 4.9: Thin tube / TCS analytical solution of the radial displacement for $p_0 = 3.4$ MPa.

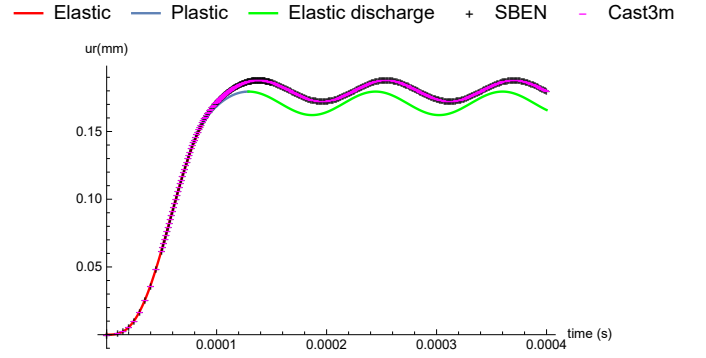


Figure 4.10: Thin tube / Comparison between TCS analytical and numerical results for $p_0 = 3.4$ MPa with $n_e = 1$, $n_t = 90$.

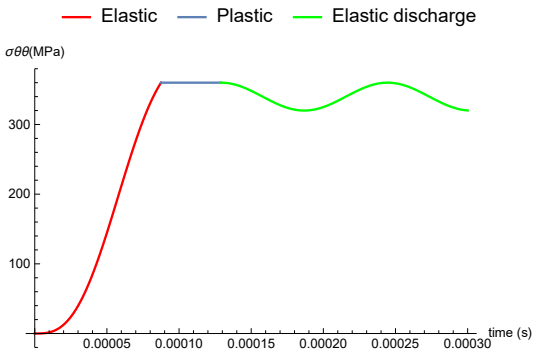


Figure 4.11: Thin tube / TCS analytical evolution of the hoop stress theory for $p_0 = 3.4$ MPa.

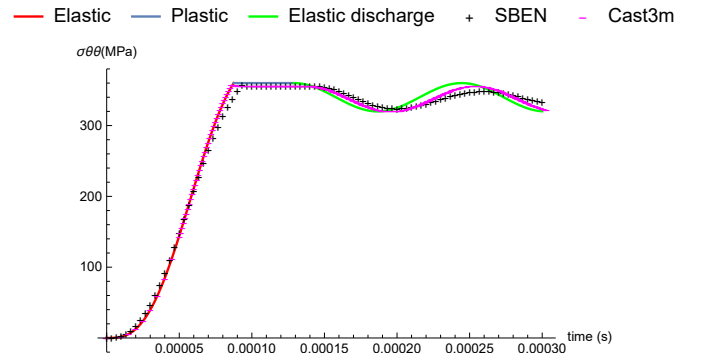


Figure 4.12: Thin tube / Comparison between TCS analytical and numerical results for $p_0 = 3.4$ MPa with $n_e = 1$, $n_t = 90$.

thin theory cylindrical shell, the radial stress σ_r is neglected. However, numerical experiences show that the contribution of σ_r in Tresca criterion is not negligible even if its value is very small compared to the stress component σ_θ . Regarding, the hoop stress time-evolution, a good agreement is illustrated in Figs. 4.11 and 4.12.

Eventually, in Figs. 4.13 to 4.16, the stress components computed by the SBEN variational principle are plotted together with the thin shell analytical solution when the displacement is unbounded and the ductility limit is reached. This response is obtained for the prescribed pressure $p_0 = 3.6$ MPa. Again, a very good agreement is observed.

4.3.2 The thick-walled tube

In this subsection, the SBEN variational principle is applied to address the dynamic response of the pressurized thick-walled tube with inner radius $a = 100$ mm and outer radius $b = 120$ mm. The material parameters are chosen like in section 4.3.1: $E = 210$ MPa, $\nu = 0.3$, $\sigma_Y = 360$ MPa and $\rho = 7800$ kg/m³. The prescribed internal pressure is given by equation (4.36) and plotted

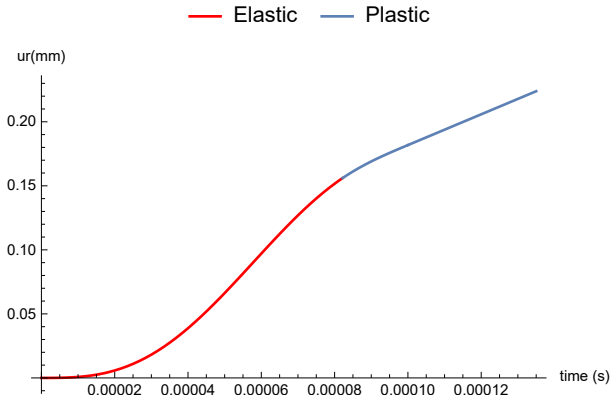


Figure 4.13: Thin tube / TCS analytical solution of the radial displacement for $p_0 = 3.6$ MPa.

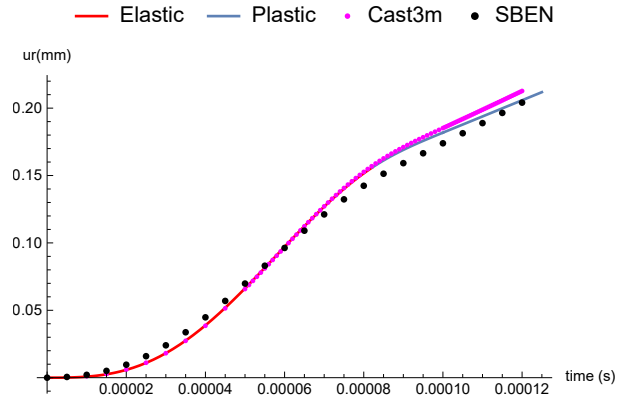


Figure 4.14: Thin tube / Comparison between TCS analytical and numerical results for $p_0 = 3.6$ MPa with $n_e = 1$, $n_t = 60$.

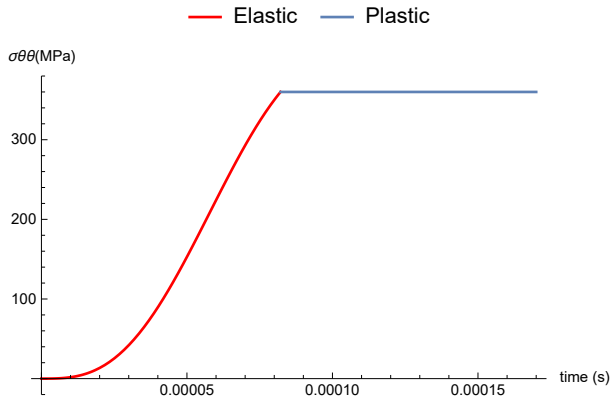


Figure 4.15: Thin tube / TCS analytical evolution of the hoop stress for $p_0 = 3.6$ MPa.

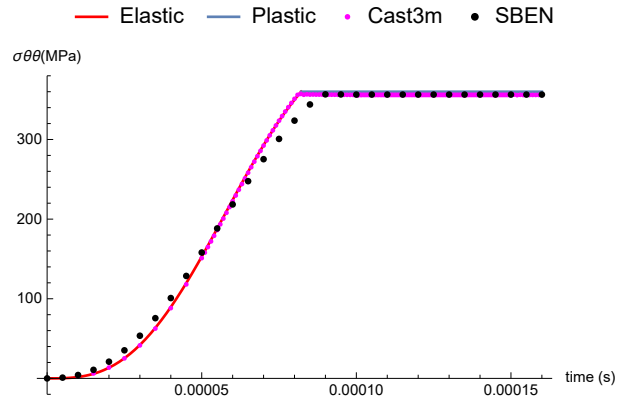


Figure 4.16: Thin tube / Comparison between TCS analytical and numerical results for $p_0 = 3.6$ MPa with $n_e = 1$, $n_t = 60$.

in Fig. 4.3.

Unfortunately, the analytical solution of the considered problem is not available neither for elastic nor elastoplastic ranges.

First, consider the elastic response under an internal pressure $p_0 = 40$ MPa. In Figs. 4.17(a) and 4.17(b), we plot the time evolution of the radial displacement and the hoop stress at the inner surface ($r = a$) computed by the SBEN method and the incremental procedure. The results relating to the external wall ($r = b$) are depicted in Figs. 4.18(a) and 4.18(b). By inspection of these figures we conclude that prediction of both procedures are very close which confirms that the SBEN principle works in elasticity.

Consider now the response of the tube under a given pressure $p_0 = 60$ MPa. The comparison between the SBEN and Cast3M predictions are depicted in Fig. 4.19(a) and 4.19(b) which show the radial displacement and the hoop stress for the node located on the internal wall ($r = a$) and in Figs. 4.20(a) and 4.20(b) for the external boundary ($r = b$). These figures are similar to

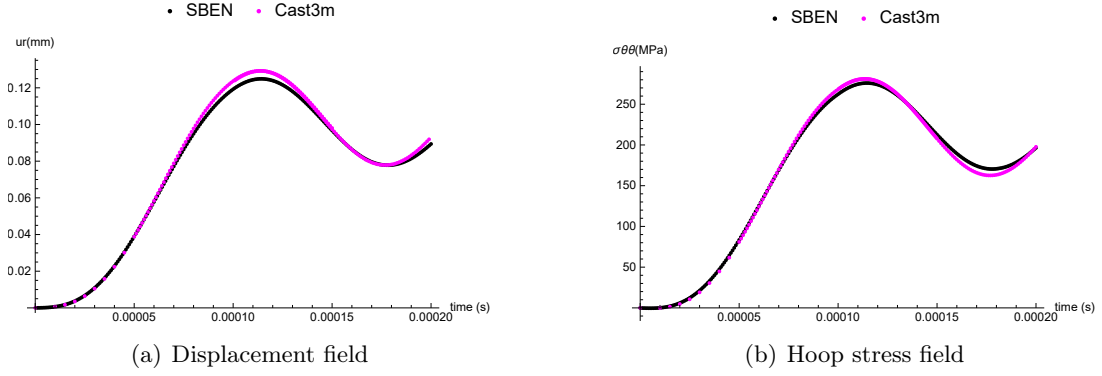


Figure 4.17: Thick tube / Elastic solution - Comparison of (a) displacement (b) hoop stress field between SBEN's results and step-by-step numerical predictions for $p_0 = 40$ MPa on the **internal** wall $r = a$ with $n_e = 1$, $n_t = 240$.

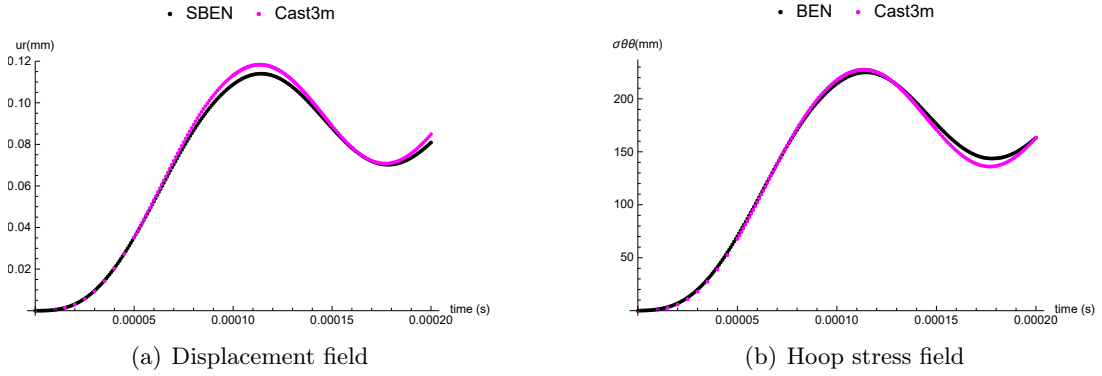


Figure 4.18: Thick tube / Elastic solution - Comparison of (a) displacement (b) hoop stress field between SBEN's results and step-by-step numerical predictions for $p_0 = 40$ MPa on the **external** wall $r = b$ with $n_e = 1$, $n_t = 240$.

the ones for the thin tube under $p = 3.2$ MPa and confirm that the response is first elastic then plastic strains develop until the displacement reaches a maximum and then the response becomes elastic again. In other words, under this pressure, the ductility limit is not reached. A difference between the numerical procedures is observed for the radial displacement simulations within the plastic range. Because the dynamic problem has not a closed-form solution, one cannot conclude on the relevance of the SBEN method or the step-by-step procedure.

Attention is focused now on the elastoplastic behavior under a higher pressure p_0 for which the ductility limit is reached and a mechanism is observed. For example, under the pressure $p_0 = 65$ MPa, Figs. 4.21(a) and 4.21(b) present the variation of the radial displacement and the hoop stress versus time on the inner boundary ($r = a$). The numerical comparison between SBEN's predictions and incremental simulations for the external surface ($r = b$) is presented in Figs. 4.22(a) and 4.22(b). It is worth noting that these figures are similar to the ones 4.13 and 4.16 related to the thin tube in the sense that the radial displacement is unbounded for the

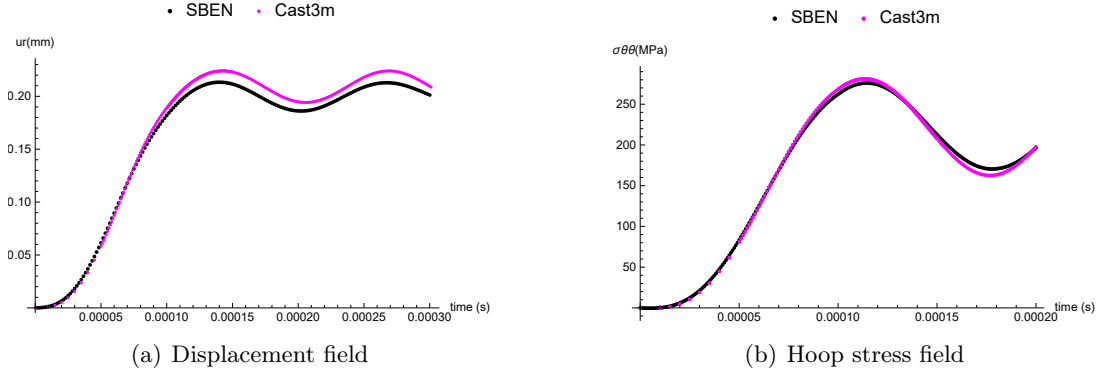


Figure 4.19: Thick tube - Comparison of (a) displacement (b) hoop stress field between SBEN's results and step-by-step numerical predictions for $p_0 = 60$ MPa on the *internal* wall $r = a$ with $n_e = 1$, $n_t = 180$.

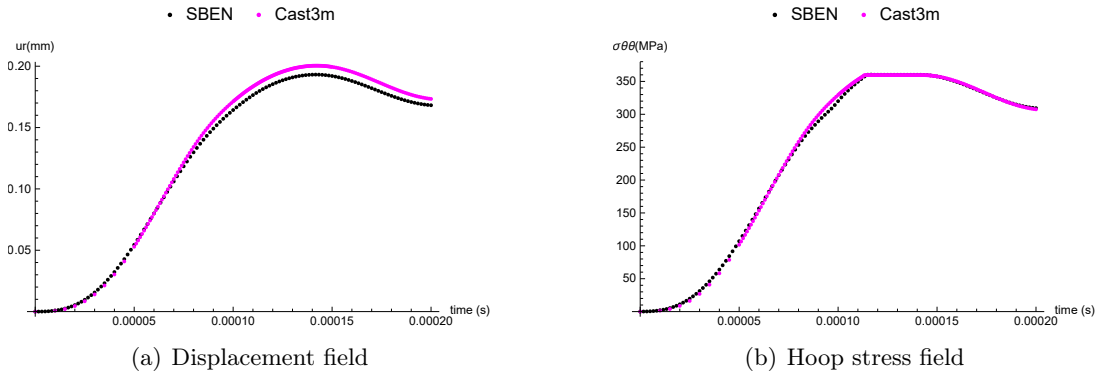


Figure 4.20: Thick tube - Comparison of (a) displacement (b) hoop stress field between SBEN's results and step-by-step numerical predictions for $p_0 = 60$ MPa on the *external* wall $r = b$ with $n_e = 1$, $n_t = 180$.

plastic regime. Moreover, a good agreement between the SBEN predictions and Cast3M results is observed.

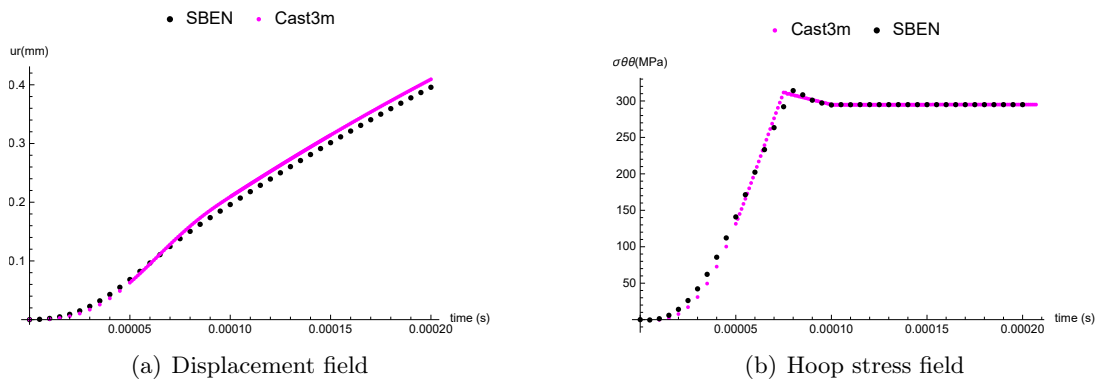


Figure 4.21: Thick tube - Comparison of (a) displacement (b) hoop stress field between SBEN's results and step-by-step numerical predictions for $p_0 = 65$ MPa on the *internal* wall $r = a$ with $n_e = 1$, $n_t = 40$.

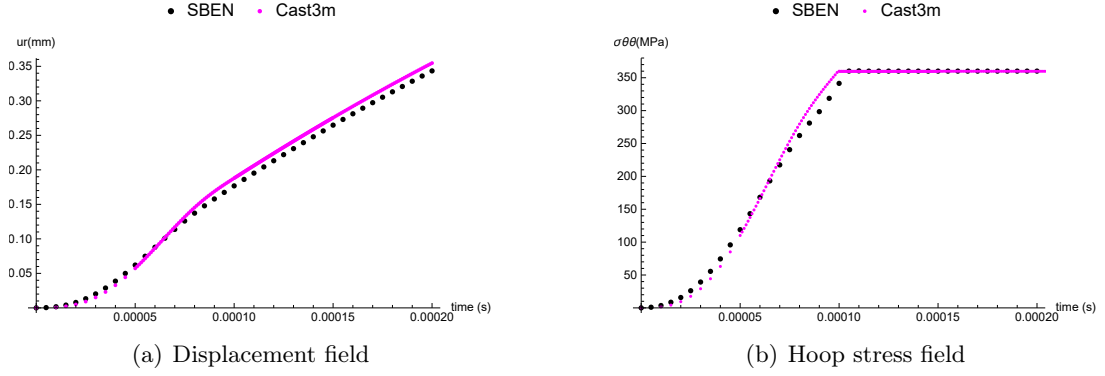


Figure 4.22: Thick tube - Comparison of (a) displacement (b) hoop stress field between SBEN's results and step-by-step numerical predictions for $p_0 = 65$ MPa on the *external* wall $r = b$ with $n_e = 1$, $n_t = 40$.

4.3.3 Comparison between the methods A and B

For completeness, as regards to the comparison between the methods A and B for treating the balance of momentum equation, we display in Figs. 4.23 and 4.24 the SBEN results for the thin tube subjected to the prescribed pressures $p = 3.4$ MPa and $p = 3.6$ MPa respectively (elastoplastic response). Furthermore, figures 4.25 and 4.26 showed the comparison for the pressurized thick tube. The presented results concern the radial displacement and the hoop stresses for the internal and external walls. From these figures, it is shown that, for the considered problems, there is no noticeable difference between the two methods. This observation is also valid for the tubes in the elastic range. However, from a numerical point of view, method A is more expensive since it requires more degrees of freedom to deliver accurate results. Furthermore, it is reasonable to think that method B is more accurate than the one A for elastoplastic simulations because the balance of momentum equation is satisfied exactly, which is more efficient to enforce the plastic criterion. On the other hand, method B benefits from the linear feature of the balance of linear momentum equation and it is not workable in large strains.

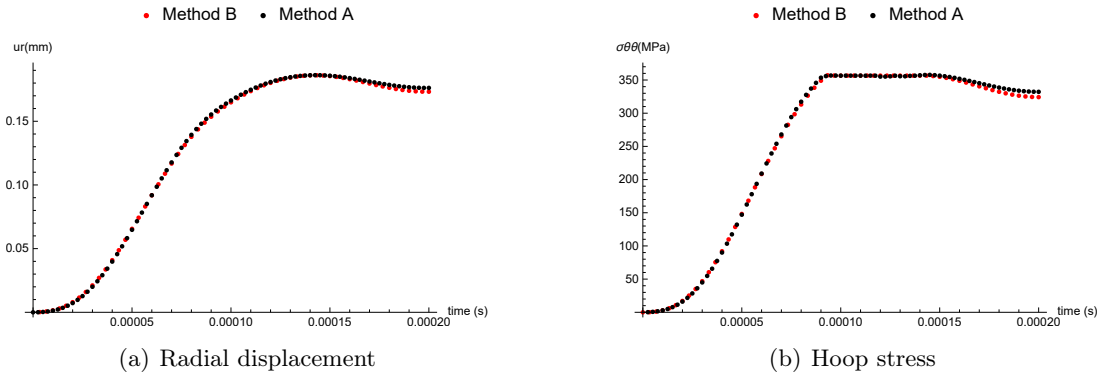


Figure 4.23: Thin tube - Comparison of numerical results provided by the methods A and B for an internal pressure $p_0 = 3.4$ MPa.

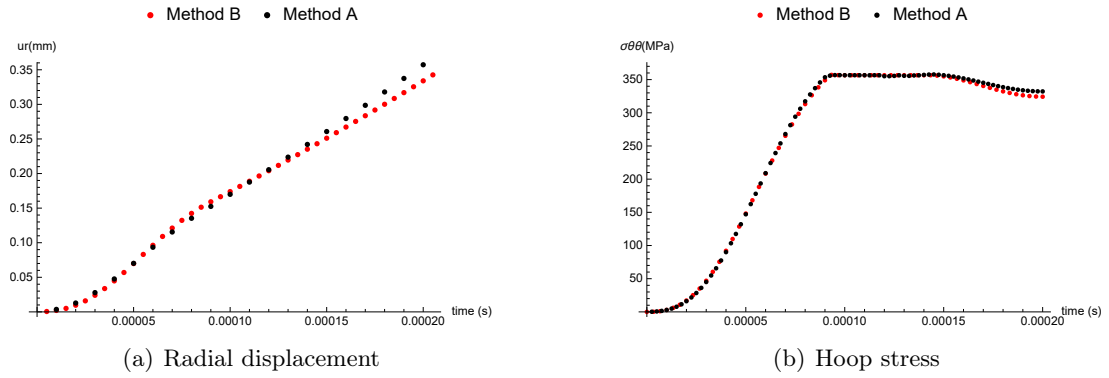


Figure 4.24: Thin tube - Comparison of numerical results provided by the methods A and B for an internal pressure $p_0 = 3.6$ MPa.

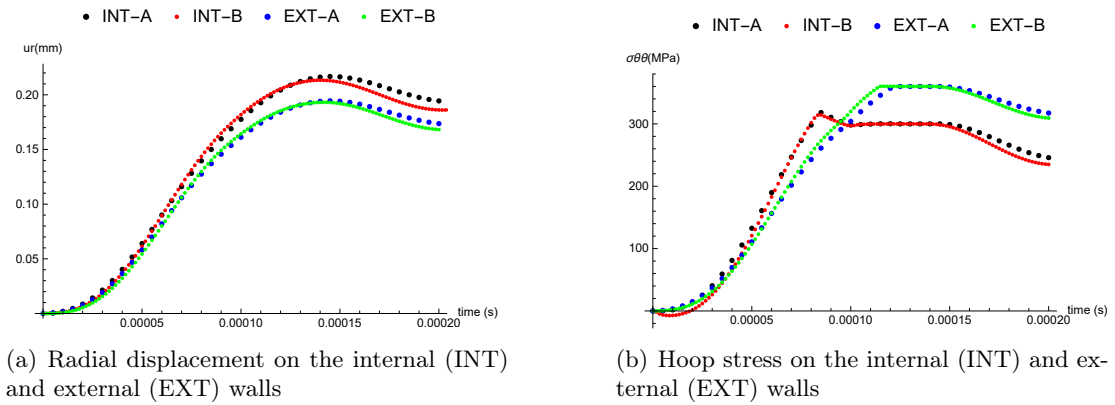


Figure 4.25: Thick tube - Comparison of numerical results provided by the methods A and B for an internal pressure $p_0 = 60$ MPa.

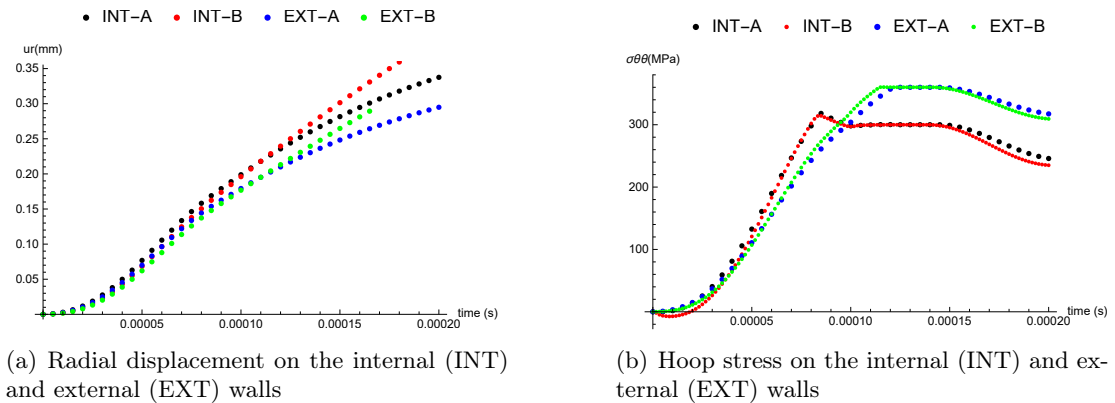


Figure 4.26: Thick tube - Comparison of numerical results provided by the methods A and B for an internal pressure $p_0 = 65$ MPa.

4.4 Conclusion and outlook

A new procedure based on the SBEN principle for the computation of the entire dynamic elastoplastic response of deformable solids at once is presented in this work. This principle relies on the energy dissipation and leads to a constrained minimization problem for which the objective function depends on the stress and displacement fields. As illustration, the thin and thick elastic-perfectly plastic tubes subjected to an internal pressure are successfully studied numerically by using the SBEN principle. The analysis has been performed within the framework of the mixed finite element method, which is quite natural given the mathematical structure of the problem. A very good agreement between the SBEN numerical results compared with analytical solutions for the thin cylindrical shell and step-by-step FEM predictions is observed. It is relevant to mention that, unlike the traditional incremental procedures, the SBEN formulation offers the advantage to tackle easily complex nonlinear constitutive laws (hardening plasticity, non-local models, damage under shock-waves, etc.) involving inertia effects without additional computational efforts.

A symplectic Brezis-Ekeland-Nayroles
principle for dynamic plasticity in finite
strains

5.1	Notations and definitions	116
5.2	Lagrangian formalism	117
5.3	Hamiltonian formalism	120
5.4	Symplectic BEN principle for dynamic plasticity	122
5.5	Conclusion	127

In the previous chapters, we applied the BEN principle to simulate the quasi-static or the dynamic elastoplastic problems in small deformations. In this chapter, we generalize the previous formalism to dissipative media in finite strains. This aim is reached in three steps. Firstly, we develop a Lagrangian formalism for the reversible media based on the calculus of variation. Next, we propose a corresponding Hamiltonian formalism for such media. Finally, we deduce from it a symplectic minimum principle for dissipative media and we show how to get a minimum principle for plasticity in finite strains.

5.1 Notations and definitions

For any convex and closed subset A of a topological real vector space V , the indicatory function χ_A is defined by

$$\chi_A(\mathbf{x}) = \left\{ \begin{array}{ll} 0 & \text{if } \mathbf{x} \in A \\ +\infty & \text{otherwise} \end{array} \right\} .$$

The characteristic function is convex and lower semi continuous. If the set A contains only one element $A = \{\mathbf{a}\}$ then we shall use the notation $\chi_{\mathbf{a}}$ for the characteristic function of A .

Besides, if V is equipped with a symplectic form ω , the symplectic subdifferential of a convex lower semi continuous function $F : V \rightarrow \mathbb{R} \cup \{+\infty\}$ is the function which associates to any $\mathbf{z} \in V$ such that $F(\mathbf{z}) < +\infty$ the set:

$$\partial^\omega F(\mathbf{z}) = \{ \mathbf{z}' \in V : \forall \mathbf{z}'' \in V \quad F(\mathbf{z} + \mathbf{z}'') \geq F(\mathbf{z}) + \omega(\mathbf{z}', \mathbf{z}'') \} .$$

If F is also differentiable, the subdifferential is reduced to a unique element, its symplectic gradient (or Hamiltonian vector field). The symplectic polar or symplectic Fenchel transform of F is the function:

$$F^{*\omega}(\mathbf{z}') = \sup \{ \omega(\mathbf{z}', \mathbf{z}) - F(\mathbf{z}) : \mathbf{z} \in V \} .$$

The derivative of a scalar field defined on an open domain of \mathbb{R}^n is the n -row :

$$\frac{\partial f}{\partial \mathbf{x}} = \left(\frac{\partial f}{\partial x^1} \quad \frac{\partial f}{\partial x^2} \quad \dots \quad \frac{\partial f}{\partial x^n} \right) .$$

Its gradient is the n -column:

$$\text{grad}_{\mathbf{x}} f = \left(\frac{\partial f}{\partial \mathbf{x}} \right)^T .$$

Let $\mathbf{v} \in \mathbb{R}^p$ be a vector field. Its derivative is the $p \times n$ matrix:

$$\frac{\partial \mathbf{v}}{\partial \mathbf{x}} = \begin{pmatrix} \frac{\partial \mathbf{v}}{\partial x^1} & \frac{\partial \mathbf{v}}{\partial x^2} & \cdots & \frac{\partial \mathbf{v}}{\partial x^n} \end{pmatrix}.$$

Let \mathbf{A} be an $n \times p$ matrix field. Its divergence is the field $div_{\mathbf{x}} \mathbf{A}$ of p -columns such that for every constant vector \mathbf{k} of \mathbb{R}^p :

$$(div_{\mathbf{x}} \mathbf{A}) \cdot \mathbf{k} = div_{\mathbf{x}} (\mathbf{A} \mathbf{k}).$$

Alternatively, $\mathbf{A}_1, \dots, \mathbf{A}_p$ being the columns of \mathbf{A} , we have:

$$div_{\mathbf{x}} (\mathbf{A}_1, \dots, \mathbf{A}_p) = \begin{pmatrix} div_{\mathbf{x}} \mathbf{A}_1 \\ \vdots \\ div_{\mathbf{x}} \mathbf{A}_p \end{pmatrix}.$$

For any vector fields $\mathbf{v} \in \mathbb{R}^p$, and any $n \times p$ matrix field \mathbf{A} , it holds:

$$div_{\mathbf{x}} (\mathbf{A} \mathbf{v}) = (div_{\mathbf{x}} \mathbf{A}) \cdot \mathbf{v} + Tr \left(\mathbf{A} \frac{\partial \mathbf{v}}{\partial \mathbf{x}} \right) \quad (5.1)$$

where Tr is the trace operator.

For any open domain \mathcal{V} of \mathbb{R}^n with suitable regularity assumptions and any C^1 square matrix field \mathbf{A} , we have the divergence formula:

$$\int_{\mathcal{V}} div_{\mathbf{x}} \mathbf{A} d\mathcal{V} = \int_{\partial \mathcal{V}} \mathbf{A}^T \mathbf{n} dS \quad (5.2)$$

the column \mathbf{n} representing the outward unit normal vector to $\partial \mathcal{V}$, pointing away from \mathcal{V} .

The derivative of a scalar f function of an $n \times p$ matrix \mathbf{M} is a $p \times n$ matrix $\partial f / \partial \mathbf{M}$ such that its directional derivative in the direction $d\mathbf{M}$ is:

$$Tr \left(d\mathbf{M} \frac{\partial f}{\partial \mathbf{M}} \right).$$

5.2 Lagrangian formalism

To begin with, we consider in this Section and the next one only reversible continuous system. For the target applications, we shall be working in the material representation. Let \mathcal{V}_0 be the initial (or undeformed) configuration, that is an open domain of \mathbb{R}^3 occupied by a solid at the

initial time t_0 . Its motion is described by a smooth map:

$$\varphi : \Omega_0 = [t_0, t_1] \times \mathcal{V}_0 \rightarrow \mathbb{R}^3 : \mathbf{X}_0 = (t, \mathbf{x}_0) \mapsto \mathbf{x} = \varphi(t, \mathbf{x}_0)$$

where \mathbf{x} is the current position at time t of the material particle \mathbf{x}_0 , then $\varphi(t_0, \cdot)$ is the identity.

Its space-time gradient is the 3×4 matrix:

$$\frac{\partial \mathbf{x}}{\partial \mathbf{X}_0} = \left(\frac{\partial \mathbf{x}}{\partial t}, \frac{\partial \mathbf{x}}{\partial \mathbf{x}_0} \right) = (\mathbf{v}, \mathbf{F}) \quad (5.3)$$

where \mathbf{v} is the velocity at time t of the particle \mathbf{x}_0 , tangent to the trajectory $t \mapsto \varphi(t, \mathbf{x}_0)$, and \mathbf{F} is the deformation gradient, whose determinant (Jacobian) is denoted by $J = \det \mathbf{F}$.

Our goal now is deducing the balance of linear momentum from a variational action principle of the form:

$$\alpha[\mathbf{x}] = \int_{\Omega_0} L_0 \left(\mathbf{X}_0, \mathbf{x}, \frac{\partial \mathbf{x}}{\partial \mathbf{X}_0} \right) d^4 \mathbf{X}_0 \quad (5.4)$$

where the Lagrangian L_0 depends on the field \mathbf{x}_0 and its first derivative. As we are only interested in what follows by the variational equations in the interior of Ω_0 , we consider simple boundary conditions with the value of \mathbf{x} imposed on $\partial\Omega_0$. For sake of easiness, we introduce the 3-column:

$$\mathbf{f}_0 = \text{grad}_{\mathbf{x}} L_0$$

and the 4×3 matrix:

$$\mathbf{P}_0 = \frac{\partial L_0}{\partial \left(\frac{\partial \mathbf{x}}{\partial \mathbf{X}_0} \right)} .$$

The variation of the action reads:

$$\delta\alpha = \int_{\Omega_0} \left[\text{Tr} \left(\mathbf{P}_0 \frac{\partial}{\partial \mathbf{X}_0} (\delta \mathbf{x}) \right) + \mathbf{f}_0 \cdot \delta \mathbf{x} \right] d^4 \mathbf{X}_0 = 0 .$$

Owing to (5.1) and (5.2) and taking into account the fact that the values of \mathbf{x} are imposed on the boundary, the integration by part gives:

$$\delta\alpha = - \int_{\Omega_0} (\text{div}_{\mathbf{X}_0} \mathbf{P}_0 - \mathbf{f}_0) \cdot \delta \mathbf{x} d^4 \mathbf{X}_0 = 0$$

where the divergence is calculated with respect to the coordinates \mathbf{X}_0 . The variation of \mathbf{x} being arbitrary, we obtain Euler-Lagrange equations of variation:

$$\text{div}_{\mathbf{X}_0} \mathbf{P}_0 - \mathbf{f}_0 = \mathbf{0} . \quad (5.5)$$

According to the principle of material indifference, the Lagrangian is depending on the deformation gradient through the Green-Lagrange strain measure:

$$\mathbf{E} = \frac{1}{2} (\mathbf{F}^T \mathbf{F} - \mathbf{1}_{\mathbb{R}^3}) \quad (5.6)$$

then, owing to (5.3):

$$L_0 \left(\mathbf{X}_0, \mathbf{x}, \frac{\partial \mathbf{x}}{\partial \mathbf{X}_0} \right) = \mathcal{L}_0 (\mathbf{X}_0, \mathbf{x}, \mathbf{v}, \mathbf{E}) .$$

Its differential with respect to \mathbf{v} and \mathbf{F} is:

$$\delta \mathcal{L}_0 = Tr \left(\frac{\partial \mathcal{L}_0}{\partial \mathbf{E}} \delta \mathbf{E} \right) + \frac{\partial \mathcal{L}_0}{\partial \mathbf{v}} \delta \mathbf{v} = Tr \left(\frac{\partial \mathcal{L}_0}{\partial \mathbf{E}} \mathbf{F}^T \delta \mathbf{F} \right) + grad_{\mathbf{v}} \mathcal{L}_0 \delta \mathbf{v} .$$

Hence:

$$div_{\mathbf{x}_0} \mathbf{P}_0 - \mathbf{f}_0 = \frac{\partial}{\partial t} (grad_{\mathbf{v}} \mathcal{L}_0) + div_{\mathbf{x}_0} \left(\frac{\partial \mathcal{L}_0}{\partial \mathbf{E}} \mathbf{F}^T \right) - \mathbf{f}_0 = \mathbf{0} .$$

The initial value ρ_0 of the mass density is a function of \mathbf{x}_0 . Its current value at the date t :

$$\rho = \frac{\rho_0}{J} \quad (5.7)$$

satisfies the balance of mass (de Saxce and Vallée, 2016):

$$\frac{\partial \rho}{\partial t} + div_{\mathbf{x}} (\rho \mathbf{v}) = 0 .$$

From now on, we consider a standard Lagrangian of the form:

$$\mathcal{L}_0 (\mathbf{X}_0, \mathbf{x}, \mathbf{v}, \mathbf{E}) = \rho_0 \left(\frac{1}{2} \|\mathbf{v}\|^2 - \psi(\mathbf{x}_0, \mathbf{E}) \right) + \mathbf{f}_0(t) \cdot \mathbf{x} \quad (5.8)$$

where ψ is the specific free energy, responsible of the reversible elastic behaviour. Introducing the second Piola-Kirchhoff stresses:

$$\mathbf{S} = \rho_0 \frac{\partial \psi}{\partial \mathbf{E}} \quad (5.9)$$

the variation equation (5.5) reads:

$$\rho_0 \frac{\partial \mathbf{v}}{\partial t} = div_{\mathbf{x}_0} (\mathbf{S} \mathbf{F}^T) + \mathbf{f}_0 \quad (5.10)$$

which can be interpreted as the balance of linear momentum in the Lagrangian specification.

Indeed, transforming the former term as in (de Saxcé, 2001), it holds:

$$\rho_0 \frac{\partial \mathbf{v}}{\partial t} = J (\operatorname{div}_{\mathbf{x}} \boldsymbol{\sigma} + \mathbf{f})$$

where :

$$\boldsymbol{\sigma} = \frac{1}{J} \mathbf{F} \mathbf{S} \mathbf{F}^T$$

are Cauchy stresses and $\mathbf{f} = \mathbf{f}_0/J$ are the volume forces in the spatial representation. Then, taking into account of (5.7), one obtains the balance of linear momentum in the Eulerian specification:

$$\rho \frac{\partial \mathbf{v}}{\partial t} = \operatorname{div}_{\mathbf{x}} \boldsymbol{\sigma} + \mathbf{f} .$$

5.3 Hamiltonian formalism

In (Buliga and de Saxcé, 2017), the last author proposed with Buliga a generalisation of the Brezis-Ekeland-Nayroles principle in a symplectic version called SBEN, able to treat the dynamical dissipative systems.

In the material representation, let us introduce the linear momentum:

$$\mathbf{p}_0 = \operatorname{grad}_{\mathbf{v}} \mathcal{L}_0 = \rho_0 \mathbf{v} \tag{5.11}$$

and the Hamiltonian density:

$$\mathcal{H}_0 = \operatorname{grad}_{\mathbf{v}} \mathcal{L}_0 \cdot \mathbf{v} - \mathcal{L}_0 . \tag{5.12}$$

Eliminating the velocity \mathbf{v} between (5.11) and (5.12) gives the Hamiltonian density as function of the linear momentum :

$$\mathcal{H}_0 = \frac{1}{2\rho_0} \|\mathbf{p}_0\|^2 + \rho_0 \psi - \mathbf{f}_0 \cdot \mathbf{x} \tag{5.13}$$

we recover (5.11) by:

$$\mathbf{v} = \operatorname{grad}_{\mathbf{p}_0} \mathcal{H}_0 = \frac{\mathbf{p}_0}{\rho_0} . \tag{5.14}$$

The total energy at time t is represented by the Hamiltonian:

$$H_t = \int_{\mathcal{V}_0} \mathcal{H}_0(\mathbf{X}_0, \mathbf{x}, \mathbf{E}, \mathbf{p}_0) d^3 \mathbf{x}_0 ,$$

Then the value of the Hamiltonian density depends on \mathbf{F} thanks to 5.6:

$$\mathcal{H}_0(\mathbf{X}_0, \mathbf{x}, \mathbf{E}, \mathbf{p}_0) = H_0(\mathbf{X}_0, \mathbf{x}, \mathbf{F}, \mathbf{p}_0) .$$

For sake of easiness, we introduce the 3-columns:

$$\mathbf{V} = \text{grad}_{\mathbf{p}_0} \mathcal{H}_0, \quad \mathbf{f}_0^* = \text{grad}_{\mathbf{x}} \mathcal{H}_0$$

and the 3×3 matrix:

$$\mathbf{P}_0^* = \frac{\partial H_0}{\partial \mathbf{F}}. \quad (5.15)$$

The variation of the Hamiltonian with respect to the canonical variables \mathbf{x} and \mathbf{p}_0 reads:

$$\delta H_t = \int_{\mathcal{V}_0} \left[\text{Tr} \left(\mathbf{P}_0^* \frac{\partial}{\partial \mathbf{x}_0} (\delta \mathbf{x}) \right) + \mathbf{f}_0^* \cdot \delta \mathbf{x} + \mathbf{V} \cdot \delta \mathbf{p}_0 \right] d^3 \mathbf{x}_0.$$

Taking into account the fact that the values of \mathbf{x} are imposed on the boundary, the integration by part gives:

$$\delta H_t = \int_{\mathcal{V}_0} [-(\text{div}_{\mathbf{x}_0} \mathbf{P}_0^* - \mathbf{f}_0^*) \cdot \delta \mathbf{x} + \mathbf{V} \cdot \delta \mathbf{p}_0] d^3 \mathbf{x}_0. \quad (5.16)$$

Let \mathcal{V}_t be the deformed configuration at date t , that is the image of \mathcal{V}_0 by $\mathbf{x}_0 \mapsto \varphi(t, \mathbf{x}_0)$. The phase space is the cotangent bundle $T^* \mathcal{V}_t$ of which the elements are represented in a local chart by a couple $\mathbf{z} = (\mathbf{x}, \mathbf{p}_0)$. It is equipped with a symplectic structure by giving a field of non degenerated 2-forms $\mathbf{z} \mapsto \varpi_{\mathbf{z}} \in \bigwedge^2(T^* \mathcal{V}_t)$. The value of the symplectic form for two tangent vectors $\mathbf{Z} = (d\mathbf{x}, d\mathbf{p}_0)$ and $\mathbf{Z}' = (d\mathbf{x}', d\mathbf{p}_0')$ is defined in a local chart by:

$$\varpi(\mathbf{Z}, \mathbf{Z}') = d\mathbf{x} \cdot d\mathbf{p}_0' - d\mathbf{p}_0 \cdot d\mathbf{x}'. \quad (5.17)$$

The evolution of the matter is modeled by a map $t \mapsto \mathbf{z}(t)$ where $\mathbf{z}(t)$ is a smooth section of the vector bundle:

$$\mathbf{z}(t) : \mathcal{V}_0 \rightarrow T^* \mathcal{V}_t : \mathbf{x}_0 \mapsto (\mathbf{z}(t))(\mathbf{x}_0)$$

of which the value is represented in a local chart by $(\mathbf{z}(t))(\mathbf{x}_0) = (\mathbf{x}, \mathbf{p}_0)$.

Remark 5.3.1. Before going further, it is worth to observe that in (Buliga and de Saxcé, 2017), dedicated to a simpler theory for discrete systems, $\mathbf{z}(t)$ is an element of a manifold and $\dot{\mathbf{z}}(t)$ is perfectly defined as the tangent vector to the evolution curve $t \mapsto \mathbf{z}(t)$. In the present approach for continua, $\mathbf{z}(t)$ is replaced by a section of a vector bundle but there is no canonical way to define $\dot{\mathbf{z}}(t)$. The most natural choice is to replace it by:

$$\mathbf{x}_0 \mapsto \left(\frac{\partial \mathbf{x}}{\partial t}(t, \mathbf{x}_0), \frac{\partial \mathbf{p}_0}{\partial t}(t, \mathbf{x}_0) \right) \quad (5.18)$$

that we shall denote by $\partial \mathbf{z} / \partial t$.

Hence $\mathbf{z}(t)$ belongs to a manifold of infinite dimension $\Gamma(T^*\mathcal{V}_t)$ which is equipped with a 2-form:

$$\omega(\mathbf{Z}, \mathbf{Z}') = \int_{\mathcal{V}_0} \varpi(\mathbf{Z}(t, \mathbf{x}_0), \mathbf{Z}'(t, \mathbf{x}_0)) d^3 \mathbf{x}_0 . \quad (5.19)$$

Definition 5.3.2. The **symplectic gradient** of the Hamiltonian $\frac{\partial \mathbf{z}}{\partial t} = X H$ is the section of $T^*\mathcal{V}_t$ such that for all variation $\delta \mathbf{z}$:

$$\omega\left(\frac{\partial \mathbf{z}}{\partial t}, \delta \mathbf{z}\right) = \delta H_t . \quad (5.20)$$

Combining (5.17), (5.18) and (5.19), one has:

$$\omega\left(\frac{\partial \mathbf{z}}{\partial t}, \delta \mathbf{z}\right) = \int_{\mathcal{V}_0} \left[\frac{\partial \mathbf{x}}{\partial t} \cdot \delta \mathbf{p}_0 - \frac{\partial \mathbf{p}_0}{\partial t} \cdot \delta \mathbf{x} \right] d^3 \mathbf{x}_0$$

and, owing to (5.16), (5.20) leads to the **canonical equations**:

$$\frac{\partial \mathbf{x}}{\partial t} = \mathbf{V}, \quad \frac{\partial \mathbf{p}_0}{\partial t} = -\mathbf{f}_0^* + \operatorname{div}_{\mathbf{x}_0} \mathbf{P}_0^* \quad (5.21)$$

or, explicitly with respect to the Hamiltonian density:

$$\frac{\partial \mathbf{x}}{\partial t} = \operatorname{grad}_{\mathbf{p}_0} \mathcal{H}_0, \quad \frac{\partial \mathbf{p}_0}{\partial t} = -\operatorname{grad}_{\mathbf{x}} \mathcal{H}_0 - \operatorname{div}_{\mathbf{x}_0} \left(\frac{\partial \mathcal{H}_0}{\partial \left(\frac{\partial \mathbf{x}}{\partial \mathbf{x}_0} \right)} \right) . \quad (5.22)$$

For the particular form (5.13) of the Hamiltonian, one has:

$$\mathbf{V} = \frac{\mathbf{p}_0}{\rho_0}, \quad \mathbf{P}_0^* = \frac{\partial \mathcal{H}_0}{\partial \mathbf{F}} = \rho_0 \frac{\partial \psi}{\partial \mathbf{E}} \mathbf{F}^T$$

which allows to recover the balance of linear momentum (5.10). Taking into account (5.9), \mathbf{P}_0^* can be interpreted as the nominal stresses (transpose of the first Piola-Kirchhoff stresses):

$$\mathbf{P}_0^* = \mathbf{S} \mathbf{F}^T .$$

5.4 Symplectic BEN principle for dynamic plasticity

Having set on the backdrop of the Hamiltonian formalism for continuous media, we tackle now the modeling of the dissipative systems. To make it more concrete, we develop our approach in the framework of plasticity but the ideas are general and can be adapted easily to other

constitutive laws deriving of a free energy and a convex potential characteristic of the so-called Generalized Standard Materials (Halphen and Nguyen, 1975).

From there, we assume that \mathcal{V}_0 has a piecewise smooth boundary $\partial\mathcal{V}_0$. As usual, it is divided into two disjoint parts, S_x (called support) where the positions are imposed and S_f where the surface forces are imposed. The elements of the space X are couples $(\mathbf{x}, \mathbf{E}^{in}) \in U \times E$ where \mathbf{E}^{in} is the inelastic strain field and \mathbf{x} is an initial position field on the initial configuration \mathcal{V}_0 with trace $\gamma\mathbf{x}$ on $\partial\mathcal{V}_0$. The elements of the corresponding dual space Y are of the form $(\mathbf{p}_0, \boldsymbol{\pi}_0)$. Unlike \mathbf{p}_0 which is clearly the linear momentum, we do not know at this stage the physical meaning of $\boldsymbol{\pi}_0$. Our phase space is now the set of elements $\mathbf{z} = ((\mathbf{x}, \mathbf{E}^{in}), (\mathbf{p}_0, \boldsymbol{\pi}_0))$.

To build a minimum principle, we adapt the scheme proposed in (Buliga and de Saxcé, 2017) to continuous media. We start with the decomposition of $\frac{\partial\mathbf{z}}{\partial t}$ into reversible and irreversible parts:

$$\frac{\partial\mathbf{z}}{\partial t} = \zeta_R + \zeta_I, \quad \zeta_R = X H, \quad \zeta_I = \frac{\partial\mathbf{z}}{\partial t} - X H . \quad (5.23)$$

We claim the dissipative process is governed by the phenomenological law:

$$\zeta_I \in \partial^\omega \Phi \left(\frac{\partial\mathbf{z}}{\partial t} \right)$$

where Φ is a convex semi lowercontinuous function called **dissipation potential** and ∂^ω is the symplectic subdifferential operator (Buliga and de Saxcé, 2017). From there, we consider problems in which the fields satisfy *a priori* the initial conditions:

$$\mathbf{z}(0) = \mathbf{z}_0 \quad (5.24)$$

and boundary conditions on supports:

$$\mathbf{x} = \bar{\mathbf{x}} \quad \text{on } S_x \quad (5.25)$$

where $\bar{\mathbf{x}}$ are imposed positions. Next, we generalize the **symplectic BEN principle** of ((Buliga and de Saxcé, 2017), Definition 4.1):

Definition 5.4.1. An evolution curve $t \mapsto \mathbf{z}(t)$ satisfies the symplectic BEN principle for the Hamiltonian H_t and dissipation potential Φ if for almost any $t \in [t_0, t_1]$ we have:

$$\Phi \left(\frac{\partial\mathbf{z}}{\partial t} \right) + \Phi^{*\omega} \left(\frac{\partial\mathbf{z}}{\partial t} - X H \right) - \omega \left(\frac{\partial\mathbf{z}}{\partial t} - X H, \frac{\partial\mathbf{z}}{\partial t} \right) = 0 . \quad (5.26)$$

In integral form, this becomes a variational principle which claims that:

Definition 5.4.2. An evolution curve $t \mapsto \mathbf{z}(t)$ satisfies the symplectic BEN principle for the Hamiltonian H_t and dissipation potential Φ , the initial conditions (5.24) and the boundary conditions (5.25) if and only if it minimizes the functional:

$$\begin{aligned} \Pi[\mathbf{z}] = & \int_{t_0}^{t_1} \left\{ \Phi \left(\frac{\partial \mathbf{z}}{\partial t} \right) + \Phi^{*\omega} \left(\frac{\partial \mathbf{z}}{\partial t} - X H \right) \right. \\ & \left. - \omega \left(\frac{\partial \mathbf{z}}{\partial t} - X H, \frac{\partial \mathbf{z}}{\partial t} \right) \right\} dt, \end{aligned} \quad (5.27)$$

and the minimum is zero.

Integrating by part as in (Buliga and de Saxcé, 2017), we have also:

$$\begin{aligned} \Pi[\mathbf{z}] = & \int_{t_0}^{t_1} \left\{ \Phi \left(\frac{\partial \mathbf{z}}{\partial t} \right) + \Phi^{*\omega} \left(\frac{\partial \mathbf{z}}{\partial t} - X H \right) - \frac{\partial H_t}{\partial t} \right\} dt \\ & + H_{t_1} - H_{t_0} \end{aligned} \quad (5.28)$$

but we shall not continue any longer with this unnecessary more complicated version. In the new phase space, the symplectic form reads:

$$\omega \left(\frac{\partial \mathbf{z}}{\partial t}, \delta \mathbf{z} \right) = \int_{\mathcal{V}_0} \left[\frac{\partial \mathbf{x}}{\partial t} \cdot \delta \mathbf{p}_0 - \frac{\partial \mathbf{p}_0}{\partial t} \cdot \delta \mathbf{x} + Tr \left(\frac{\partial \mathbf{E}^{in}}{\partial t} \delta \boldsymbol{\pi}_0 - \frac{\partial \boldsymbol{\pi}_0}{\partial t} \delta \mathbf{E}^{in} \right) \right] d^3 \mathbf{x}_0. \quad (5.29)$$

The Hamiltonian is taken of the form:

$$H_t = \int_{\mathcal{V}_0} \left\{ \frac{1}{2\rho_0} \|\mathbf{p}_0\|^2 + \rho_0 \psi(\mathbf{E} - \mathbf{E}^{in}) - \mathbf{f}_0(t) \cdot \mathbf{x} \right\} d^3 \mathbf{x}_0 - \int_{S_f} \bar{\mathbf{f}}_0(t) \cdot \mathbf{x} dS_f \quad (5.30)$$

where $\bar{\mathbf{f}}_0$ is the imposed surface force on the part S_f of the boundary. Its variation is:

$$\begin{aligned} \delta H_t = & \int_{\mathcal{V}_0} \left\{ \frac{\mathbf{p}_0}{\rho_0} \cdot \delta \mathbf{p}_0 + Tr \left(\mathbf{S} \left(\mathbf{F}^T \frac{\partial}{\partial \mathbf{x}_0} (\delta \mathbf{x}) - \delta \mathbf{E}^{in} \right) \right) - \mathbf{f}_0 \cdot \delta \mathbf{x} \right\} d^3 \mathbf{x}_0 \\ & - \int_{S_f} \bar{\mathbf{f}}_0(t) \cdot \delta \mathbf{x} dS_f \end{aligned} \quad (5.31)$$

$$(5.32)$$

where the second Piola-Kirchhoff stresses \mathbf{S} is given by (5.9). Integrating by part and taking

into account (5.2) and the boundary conditions (5.25), we obtain:

$$\begin{aligned} \delta H_t &= \int_{\mathcal{V}_0} \left\{ \frac{\mathbf{p}_0}{\rho_0} \cdot \delta \mathbf{p}_0 - (\operatorname{div}_{\mathbf{x}_0} (\mathbf{S} \mathbf{F}^T) + \mathbf{f}_0) \cdot \delta \mathbf{x} - \operatorname{Tr} (\mathbf{S} \delta \mathbf{E}^{in}) \right\} d^3 \mathbf{x}_0 \\ &\quad + \int_{S_f} (\mathbf{F} \mathbf{S} \mathbf{n}_0 - \bar{\mathbf{f}}_0) \cdot \delta \mathbf{x} dS_f, \end{aligned} \quad (5.33)$$

$$(5.34)$$

where \mathbf{n}_0 is the outward unit normal vector to $\partial \mathcal{V}_0$. Denoting the symplectic gradient by:

$$X H = ((D_{\mathbf{p}_0} H, D_{\pi_0} H), (-D_{\mathbf{x}} H, D_{\mathbf{E}^{in}} H))$$

where the variational gradients are denoted by D . Owing to (5.29) and (5.34), (5.20) leads to:

$$D_{\mathbf{p}_0} H = \frac{\mathbf{p}_0}{\rho_0}, \quad D_{\pi_0} H = \mathbf{0}, \quad -D_{\mathbf{x}} H = \operatorname{div}_{\mathbf{x}_0} (\mathbf{S} \mathbf{F}^T) + \mathbf{f}_0, \quad -D_{\mathbf{E}^{in}} H = \mathbf{S}.$$

On the boundary, the variational gradient with respect to the position is:

$$D_{\gamma \mathbf{x}} H = \mathbf{F} \mathbf{S} \mathbf{n}_0 - \bar{\mathbf{f}}_0. \quad (5.35)$$

Taking into account the decomposition (5.23), the irreversible part is:

$$\zeta_I = \left(\left(\frac{\partial \mathbf{x}}{\partial t} - \frac{\mathbf{p}_0}{\rho_0}, \frac{\partial \mathbf{E}^{in}}{\partial t} \right), \left(\frac{\partial \mathbf{p}_0}{\partial t} - (\operatorname{div}_{\mathbf{x}_0} (\mathbf{S} \mathbf{F}^T) + \mathbf{f}_0), \frac{\partial \pi_0}{\partial t} - \mathbf{S} \right) \right). \quad (5.36)$$

We shall use a dissipation potential which has an integral form:

$$\Phi \left(\frac{\partial \mathbf{z}}{\partial t} \right) = \int_{\mathcal{V}_0} \phi \left(\frac{\partial \mathbf{x}}{\partial t}, \frac{\partial \mathbf{E}^{in}}{\partial t}, \frac{\partial \mathbf{p}_0}{\partial t}, \frac{\partial \pi_0}{\partial t} \right) d^3 \mathbf{x}_0$$

and we shall assume that the symplectic Fenchel transform of Φ expresses as the integral of the symplectic Fenchel transform of the dissipation potential density ϕ .

The symplectic Fenchel transform of the function ϕ reads

$$\begin{aligned} \phi^{*\omega}(\delta \mathbf{z}) &= \sup \{ \delta \mathbf{x} \cdot \delta' \mathbf{p}_0 - \delta \mathbf{p}_0 \cdot \delta' \mathbf{x} + \operatorname{Tr} (\delta \mathbf{E}^{in} \delta' \pi_0 - \delta \pi_0 \delta' \mathbf{E}^{in}) \\ &\quad - \phi(\dot{\mathbf{z}}') : \delta' \mathbf{z} \in X \times Y \} \end{aligned} \quad (5.37)$$

where δ and δ' are arbitrary variations, independent one of each other. To recover the standard

plasticity, we suppose that ϕ is depending explicitly only on $\partial\boldsymbol{\pi}_0/\partial t$

$$\phi\left(\frac{\partial\mathbf{z}}{\partial t}\right) = \bar{\phi}\left(\frac{\partial\boldsymbol{\pi}_0}{\partial t}\right) \quad (5.38)$$

then we obtain

$$\phi^{*\omega}(\delta\mathbf{z}) = \chi_0(\delta\mathbf{x}) + \chi_0(\delta\mathbf{p}_0) + \chi_0(\delta\boldsymbol{\pi}_0) + \bar{\phi}^*(\delta\mathbf{E}^{in})$$

where $\bar{\phi}^*$ is the usual Fenchel transform of $\bar{\phi}$. In other words, owing to (5.35) and (5.36), the quantity $\phi^{*\omega}(\boldsymbol{\zeta}_I)$ is finite if and only if all of the following are true:

(a) $\phi^{*\omega}(\boldsymbol{\zeta}_I) = \bar{\phi}^*\left(\frac{\partial\mathbf{E}^{in}}{\partial t}\right),$

(b) \mathbf{p} is the linear momentum in the material representation

$$\mathbf{p}_0 = \rho_0 \frac{\partial\mathbf{x}}{\partial t} \quad (5.39)$$

(c) the balance of linear momentum is satisfied

$$\operatorname{div}_{\mathbf{x}_0}(\mathbf{S}\mathbf{F}^T) + \mathbf{f}_0 = \frac{\partial\mathbf{p}_0}{\partial t} \quad \text{on } \mathcal{V}_0, \quad \mathbf{F}\mathbf{S}\mathbf{n}_0 = \bar{\mathbf{f}}_0 \quad \text{on } S_f \quad (5.40)$$

(d) and an equality which reveals the meaning of the variable $\boldsymbol{\pi}_0$:

$$\frac{\partial\boldsymbol{\pi}_0}{\partial t} = \mathbf{S}. \quad (5.41)$$

In integral form, we put:

$$\bar{\Phi}\left(\frac{\partial\boldsymbol{\pi}_0}{\partial t}\right) = \int_{\mathcal{V}_0} \bar{\phi}\left(\frac{\partial\boldsymbol{\pi}_0}{\partial t}\right) d^3\mathbf{x}_0, \quad \bar{\Phi}^*\left(\frac{\partial\mathbf{E}^{in}}{\partial t}\right) = \int_{\mathcal{V}_0} \bar{\phi}^*\left(\frac{\partial\mathbf{E}^{in}}{\partial t}\right) d^3\mathbf{x}_0.$$

Definition 5.4.3. The symplectic BEN principle applied to standard plasticity in finite strain states that the evolution curve minimizes:

$$\begin{aligned} \Pi[\mathbf{z}] = & \int_{t_0}^{t_1} \left\{ \bar{\Phi}(\mathbf{S}) + \bar{\Phi}^*\left(\frac{\partial\mathbf{E}^{in}}{\partial t}\right) \right. \\ & \left. - \omega\left(\frac{\partial\mathbf{z}}{\partial t} - X H, \frac{\partial\mathbf{z}}{\partial t}\right) \right\} dt \end{aligned} \quad (5.42)$$

among all curves \mathbf{z} such that (5.24), (5.25), (5.39) and (5.40) are satisfied and the minimum is zero.

5.5 Conclusion

In this chapter, we extended to the finite strains in the Lagrangian specification the symplectic BEN principle proposed in (Buliga and de Saxcé, 2017) to the dynamic plasticity in small strains, using tools of differential geometry. The phase space is the cotangent bundle to the deformed configuration, equipped with a symplectic structure. The crux of the matter is to replace $\dot{\mathbf{z}}$ by the partial derivative $\frac{\partial \mathbf{z}}{\partial t}$ with respect to the time at constant \mathbf{x}_0 .

The aim is reached in three steps. Firstly, a Lagrangian formalism is developed for the reversible media based on the calculus of variation. Next, a corresponding Hamiltonian formalism is proposed for such media. Finally, a symplectic minimum principle is deduced from it for dissipative media and we show how to get a minimum principle for plasticity and viscoplasticity in finite strains.

General conclusion and perspectives

The main objective of this thesis was to investigate the numerical feasibility of the Symplectic Brezis-Ekeland-Nayroles (SBEN) variational principle. By transforming an elastoplastic evolution problem into a constrained minimization procedure, the SBEN principle avoids the accumulation of computation errors in each iteration. It provides more accurate solutions comparing to a classical step-by-step method.

Although the SBEN principle was designed for the dynamics of dissipative systems, we started with the limit case of the statics, considering first a simple structure, the axisymmetric tube. The linear and nonlinear behaviors of a thick wall tube under internal pressure are examined. A perfect agreement is provided by the SBEN principle comparing to the analytical solution or classical incremental ones for elastic perfectly plastic and viscoplastic materials.

Besides, another mechanical model is investigated numerically by the SBEN principle in statics. For circular axisymmetric plates under distributed loads, the elastic and elastoplastic behaviors were analyzed. Two plate hypotheses are implemented. The Love-Kirchhoff plate theory is applied for thin plate and Mindlin hypothesis is designed for thick one. Comparing to reference analytical or numerical solutions, the SBEN principle provides a good agreement both in elastic and elastoplastic regimes.

Furthermore, the SBEN principle was applied to the dissipative system in dynamics. For thin and thick tubes subjected to internal pressure, two methods have been implemented to treat the balance of momentum equation. It can be satisfied *a priori*, as in statics, or be enforced only at Gauss points, which leads to additional constraints in the optimization problem. The SBEN principle provides satisfactory numerical results.

The numerical experiences with different kinds of structures and constitutive laws show that the SBEN principle allows obtaining a global view for all time steps simultaneously within a loading history problem. Moreover, we find that the SBEN principle provides a better conver-

gence of the stress field values thanks to a mixed finite element method. Unlike the classical displacement finite element method for which the stress field is deduced from the displacement one, the SBEN principle results have an important advantage in plasticity because the plastic yield condition is directly expressed in terms of stresses.

The results of these implementations are promising and suggest that the SBEN variational formulation provides a rigorous framework for modeling dynamic dissipative, leading to powerful non-incremental numerical methods.

In the last chapter, the SBEN principle applied in previous chapters is generalized to finite strains in the Lagrangian specification, using differential geometry tools. The phase space is the cotangent bundle to the deformed configuration, equipped with a symplectic structure.

Several interesting and challenging research directions are worthy of further exploration in future works:

- In the near term, particular attention and interest should be focused on the choice of an appropriate optimization procedure in the case of large and complex problems, especially regarding the management of the (many) non-linear inequality constraints arising from the formulation. In such cases, an efficient optimization solver is crucial for the performance of the SBEN principle. Numerical simulations of realistic and industrial structures with complex geometry involving more sophisticated models are being considered.
- For continuous systems, the SBEN principle is a variational space-time principle. Considering the techniques of model order reduction, a possible numerical strategy is to combine it with the Proper Generalized Decomposition (PGD) (Chinesta et al., 2011), based on the method of separation of variables coupled to successive enrichment strategy. For more details, one can refer to (Chinesta and Ladevèze, 2014; Chinesta et al., 2013) and the references therein.
- Another interesting aspect of the SBEN principle lies in its strong link with the symplectic form that encodes the structure of the canonical equations. In the recent literature, another model order reduction is the so-called Proper Symplectic Decomposition (PSD), a variant of the Proper Orthogonal Decomposition (POD) adapted to the dynamics that could also be naturally combined with the SBEN principle.
- In the footsteps of the last chapter, it would be worth to perform the numerical implementation of the extended SBEN principle in finite strains. This is an interesting feature of the

SBEN principle that it can be naturally generalized to the large deformation framework.

- Another important and natural extension of the SBEN principle concerns atypical constitutive laws such as Coulomb's friction law or numerous flow rules of geomaterials for which the normality rule fails. Indeed, it is worth knowing that many realistic dissipative laws, called non-associated, cannot be cast in the mold of the standard ones deriving of a dissipation potential. To skirt this pitfall, the theoretical framework of the bipotential allows extending the classical calculus of variation and building robust numerical algorithms.

Bibliography

- Aubin, J.-P. (2003). Boundary-value problems for systems of hamilton-jacobi-bellman inclusions with constraints. In *Evolution Equations: Applications to Physics, Industry, Life Sciences and Economics*, pages 25–60. Springer.
- Aubin, J.-P., Cellina, A., and Nohel, J. (1977). Monotone trajectories of multivalued dynamical systems. *Annali di Matematica pura ed applicata*, 115(1):99–117.
- Belytschko, T. and Velebit, M. (1972). Finite element method for elastic plastic plates. *Journal of the Engineering Mechanics Division*, 98(1):227–242.
- Brézis, H. and Ekeland, I. (1976a). Un principe variationnel associé à certaines équations paraboliques. le cas dépendant du temps. *CR Acad. Sci. Paris Sér. A*, 282:1197–1198.
- Brézis, H. and Ekeland, I. (1976b). Un principe variationnel associé à certaines équations paraboliques. le cas indépendant du temps. *CR Acad. Sci. Paris Sér. A*, 282:971–974.
- Bui, H. D. (1969). *Etude de l'évolution de la frontière du domaine élastique avec l'écroutissage et relations de comportement élasto-plastique des métaux cubiques*. PhD thesis, Paris VI.
- Buliga, M. (2008). Hamiltonian inclusions with convex dissipation with a view towards applications. *arXiv preprint arXiv:0810.1419*.
- Buliga, M. and de Saxcé, G. (2017). A symplectic brezis–ekeland–nayroles principle. *Mathematics and Mechanics of Solids*, 22(6):1288–1302.
- Cao, X., Oueslati, A., and de Saxcé, G. (2020a). Analytical study of the dynamic elastoplastic response of the pressurized thin and long tube. *submitted*.

- Cao, X., Oueslati, A., Nguyen, A. D., and de Saxcé, G. (2020b). Numerical simulation of elastoplastic problems by brezis–ekeland–nayroles non-incremental variational principle. *Computational Mechanics*, pages 1–14.
- Cast3M (2019). Finite element code developed by the CEA(French atomic energy commission). <http://www-cast3m.cea.fr>.
- Chinesta, F., Keunings, R., and Leygue, A. (2013). *The proper generalized decomposition for advanced numerical simulations: a primer*. Springer Science & Business Media.
- Chinesta, F. and Ladevèze, P. (2014). Separated representations and pgd-based model reduction. *Fundamentals and Applications, International Centre for Mechanical Sciences, Courses and Lectures*, 554:24.
- Chinesta, F., Ladevèze, P., and Cueto, E. (2011). A short review on model order reduction based on proper generalized decomposition. *Archives of Computational Methods in Engineering*, 18(4):395.
- Clarke, F. H. (1990). *Optimization and nonsmooth analysis*. SIAM.
- Comi, C. and Corigliano, A. (1991). Dynamic shakedown in elastoplastic structures with general internal variable constitutive laws. *International journal of plasticity*, 7(7):679–692.
- Comte, F., Maitournam, H., Burry, P., and Nguyen, T. M. L. (2006). A direct method for the solution of evolution problems. *Comptes Rendus Mécanique*, 334(5):317–322.
- Cristfield, M. (1998). Non-linear finite element analysis of solids and structures-volume 2: Advanced topics. *Chichester: John Wiley and Sons*.
- Dal Maso, G. and Scala, R. (2014). Quasistatic evolution in perfect plasticity as limit of dynamic processes. *Journal of Dynamics and Differential Equations*, 26(4):915–954.
- Davoli, E. and Stefanelli, U. (2019). Dynamic perfect plasticity as convex minimization. *SIAM Journal on Mathematical Analysis*, 51(2):672–730.
- De Giorgi, E., Marino, A., and Tosques, M. (1980). Problems of evolution in metric spaces and maximal decreasing curve. *Atti Accad. Naz. Lincei Rend. Cl. Sci. Fis. Mat. Natur.(8)*, 68(3):180–187.
- de Saxcé, G. (2001). Divergence and curl of a product of linear mapping fields and applications to the large deformations. *International Journal of Engineering Science*, 39(5):555–561.

- de Saxce, G. and Vallée, C. (2016). *Galilean mechanics and thermodynamics of continua*. Wiley Online Library.
- Donnell, L. H. (1976). Beams, plates, and shells(book). *New York, McGraw-Hill Book Co., 1976. 563 p.*
- Ghoussoub, N. and Moameni, A. (2007). Selfdual variational principles for periodic solutions of hamiltonian and other dynamical systems. *Communications in Partial Differential Equations*, 32(5):771–795.
- Greenberg, H. J. (1949). Complementary minimum principles for an elastic-plastic material. *Quarterly of Applied Mathematics*, 7(1):85–95.
- Gurtin, M. (1972). The linear theory of elasticity, mechanics of solids ii, encyclopedia of physics.
- Halphen, B. and Nguyen, Q. S. (1975). Sur les matériaux standard généralisés. *Journal de Mécanique*, 13:39–63.
- Hasbroucq, S., Oueslati, A., and de Saxcé, G. (2010). Inelastic responses of a two-bar system with temperature-dependent elastic modulus under cyclic thermomechanical loadings. *International Journal of Solids and Structures*, 47(14-15):1924–1932.
- Hasbroucq, S., Oueslati, A., and de Saxcé, G. (2012). Analytical study of the asymptotic behavior of a thin plate with temperature-dependent elastic modulus under cyclic thermomechanical loadings. *International journal of mechanical sciences*, 54(1):95–104.
- Hibbett, Karlsson, and Sorensen (1998). *ABAQUS/standard: User's Manual*, volume 1. Hibbitt, Karlsson & Sorensen.
- Hill, R. (1998). *The mathematical theory of plasticity*, volume 11. Oxford university press.
- Ibrahimbegovic, A. (2009). *Nonlinear solid mechanics: theoretical formulations and finite element solution methods*, volume 160. Springer Science & Business Media.
- Koiter, W. T. (1960). General theorems for elastic plastic solids. *Progress of Solid Mechanics*, pages 167–221.
- Krantz, S. G. (2015). *Differential Equations: Theory, Technique and Practice with Boundary Value Problems*, volume 30. CRC Press.
- Ladevèze, P. (1985a). Nouveaux algorithmes: cadre mécanique et développements. Technical report, Report.

- Ladevèze, P. (1985b). On a family of algorithms for structural mechanics. *Comptes Rendus Académie des Sciences Paris*, 300(2):41–44.
- Ladevèze, P. (1989). Large time increment method for the analysis of structures with non-linear behavior caused by internal variables (la méthode à grand incrément de temps pour l'analyse de structures à comportement non linéaire décrite par variables internes). *Académie des Sciences, (Paris), Comptes Rendus, Serie II-Mécanique, Physique, Chimie, Sciences de l'Univers, Sciences de la Terre*, 309(11):1095–1099.
- Ladevèze, P. (1991). New advances in the large time increment method. *New advances in computational structural mechanics*. Elsevier, Amsterdam, pages 3–21.
- Ladevèze, P. (2012). *Nonlinear computational structural mechanics: new approaches and non-incremental methods of calculation*. Springer Science & Business Media.
- Love, A. (1887). The small free vibrations and deformation of a thin elastic shell. *RSPS*, 43:352–353.
- Lubliner, J. (2008). *Plasticity theory*. Courier Corporation.
- Maitournam, H. (2013). *Mécanique des structures anélastiques*. Les éditions de l'École polytechnique.
- Melan, E. (1938). Zur Plastizität des räumlichen Kontinuums. *Ingenieur-Archiv*, 9(2):116–126.
- Mielke, A. (2005). Evolution of rate-independent systems. *Evolutionary equations*, 2:461–559.
- Mielke, A. and Stefanelli, U. (2008). A discrete variational principle for rate-independent evolution. *Advances in Calculus of Variations*, 1(4):399–431.
- Mindlin, R. (1951). Influence of rotary inertia and shear on flexural motions of isotropic, elastic plates. *J. appl. Mech.*, 18:31–38.
- Nayroles, B. et al. (1976). Deux théorèmes de minimum pour certains systèmes dissipatifs. *C R Acad Sci Paris, Sér AB* 282(17):A1035–1038.
- Nguyen, Q.-S. (2000). Stabilité et mécanique non linéaire. *Revue Française de Génie Civil*, 4(1):149–149.
- Oden, J. T. (2006). *Finite elements of nonlinear continua*. Courier Corporation.

- Oñate, E. (2013). *Structural analysis with the finite element method. Linear statics: volume 2: beams, plates and shells*. Springer Science & Business Media.
- Peigney, M. and Stolz, C. (2001). Approche par contrôle optimal des structures élastoviscoplastiques sous chargement cyclique. *Comptes Rendus de l'Académie des Sciences-Series IIB-Mechanics*, 329(9):643–648.
- Peigney, M. and Stolz, C. (2003). An optimal control approach to the analysis of inelastic structures under cyclic loading. *Journal of the Mechanics and Physics of Solids*, 51(4):575–605.
- Polizzotto, C. (1984a). Dynamic shakedown by modal analysis. *Meccanica*, 19(2):133–144.
- Polizzotto, C. (1984b). Dynamic shakedown of elastic-plastic solids for a set of alternative loading histories. *International journal of non-linear mechanics*, 19(4):363–371.
- Prager, W. and Hodge, P. G. (1968). *Theory of perfectly plastic solids*. Dover Publications.
- Rockafellar, R. (1970a). Generalized hamiltonian equations for convex problems of lagrange. *Pacific Journal of Mathematics*, 33(2):411–427.
- Rockafellar, R. T. (1970b). *Convex Analysis*. Citeseer.
- Save, M. A., Massonnet, C. E., and de Saxcé, G. (1997). *Plastic limit analysis of plates, shells and disks*. Elsevier.
- Schaefer, H. (1953). Die spannungsfunktionen des dreidimensionalen kontinuums und des elastischen körpers. *ZAMM-Journal of Applied Mathematics and Mechanics/Zeitschrift für Angewandte Mathematik und Mechanik*, 33(10-11):356–362.
- Seitz, A., Popp, A., and Wall, W. A. (2015). A semi-smooth newton method for orthotropic plasticity and frictional contact at finite strains. *Computer Methods in Applied Mechanics and Engineering*, 285:228–254.
- Simo, J. and Hughes, T. (2000). *Computational Inelasticity*. Springer.
- Son, N. Q. (1977). On the elastic plastic initial-boundary value problem and its numerical integration. *International Journal for Numerical Methods in Engineering*, 11(5):817–832.
- Suquet, P.-M. (1981). Sur les équations de la plasticité: existence et régularité des solutions. *J. Mécanique*, 20(1):3–39.

- Temam, R. (2018). *Mathematical problems in plasticity*. Courier Dover Publications.
- Tresca, H. E. (1864). *Sur l'écoulement des corps solides soumis a de fortes pressions*. Imprimerie de Gauthier-Villars, successeur de Mallet-Bachelier.
- von Mises, R. (1928). Mechanik der plastischen formänderung von kristallen. *ZAMM-Journal of Applied Mathematics and Mechanics/Zeitschrift für Angewandte Mathematik und Mechanik*, 8(3):161–185.
- Zienkiewicz, O. (1971). The finite element method in engineering science mcgraw-hill. *London. zbMATH*.
- Zienkiewicz, O., Valliappan, S., and King, I. (1969). Elasto-plastic solutions of engineering problems 'initial stress', finite element approach. *International Journal for Numerical Methods in Engineering*, 1(1):75–100.